NTNU
Norwegian University of Science and Technology
Department of Marine Technology

M.Sc.THESIS

Title:	Delivered:
DESIGN OF TENSION LEG ANCHOR SYSTEMS FOR FLOATING WINDMILLS	08.06.2011
	Availability: Open
Student: Rolf Åge Vågen	**Number of pages:** 84

Abstract:

Renewable energy is likely to be of great importance in decades to come due to increased energy consumption. Kinetic energy from wind is expected to cover a part of this need, and wind farms are so far built onshore or at shallow water. On the other hand wind turbines are not always wanted close to land due to both the visual aspects and bird life. An alternative may therefore be to place wind turbines offshore. However, large water depths are causing problems for existing bottom fixed structures and floating wind turbines may therefore be a solution.

In this thesis feasibility of tension leg anchor systems for floating wind turbines is investigated. A literature study including tension leg principles, relevant load parameters and methods for calculating motions on tension leg structures are looked into. Preliminary calculations of motion based on a one degree of freedom model are coded and executed in Matlab. Finally, a model in scale 1:100 has been built and further exposed to regular waves in a laboratory test. Numerical and experimental results are investigated and compared for different wave parameters in order to reveal potential weaknesses of the concept.

Numerical and experimental results coincide quite well for structure motion in the wave direction, and in most cases the structure get small motion amplitudes which generate negligible vertical motions in form of set down. The overturning moment calculations also coincide well, and show that there are limitations in the mooring feasibility when exposed to large waves. The pretension is proven to be a very important parameter for the concept. Measurement of tendon forces from laboratory test show that the model is loaded differently and in larger order of magnitude than expected. For the scaled model a simplified tendon attachment arrangement in form of a steel plate is used. The strange force distribution may therefore represent loading on this plate. The results however show that tension leg anchoring can be a relevant alternative type of anchor system for floating wind turbines if sufficient system pretension is obtained. In addition, if also a reasonable magnitude and distribution of mass are obtained, the structure is expected to handle quite large waves.

The design presented in this thesis is far from optimized. For further work it is therefore advised to model the structure in software where structural analysis can be executed in order to decide upon an optimized structural weight, seeing this as an important parameter.

Keyword:

Floating Wind Turbine
Tension leg
Motion analysis

Advisor:

Prof. Carl M. Larsen

Address:
NTNU
Department of Marine Technology
N-7491 Trondheim

Location
Marinteknisk Senter
O. Nielsens vei 10

Tel. +47 73 595501
Fax +47 73 595697

NTNU Trondheim
Norwegian University of Science and Technology
Faculty of Engineering Science and Technology
Department of MarineTechnology

M.Sc. thesis 2011

for

Stud.tech. Rolf Vågen

DESIGN OF TENSION LEG ANCHOR SYSTEMS FOR FLOATING WINDMILLS

Renewable energy is considered to be the only sustainable way for future energy supply. Norway is blessed with topography and sufficient rainfall that makes it possible to produce electricity from hydropower at a very large scale. However, future growth in domestic and industrial energy demand and export will require unwanted encroachments on rivers and lakes. Alternative energy production is therefore encouraged. Wind energy is an obvious alternative, but wind turbines are not always wanted on land. Offshore windmills have therefore been proposed. For several reasons one would prefer to have such installations at some distance from the coast, but the water depth on the Norwegian continental shelf is too large for the use of bottom fixes turbines. It is therefore proposed to have floating windmills, and the design of cheap but reliable mooring systems for such structures will hence crucial for the economy of this concept.

Tension leg platforms (TLPs) have long been used for petroleum production on moderate and deep waters. This anchor system type may also be a good choice for floating wind turbines. The purpose of this project is to investigate the feasibility of tension leg wind turbine through use of simplified analysis models, advanced analyses and model tests. The MSc project is a continuation of the pre-project that was carried out during the fall semester.

The work should be carried out in steps as follows:

1. Literature study, which should include principles for design of TLPs, use of scaled models, and advanced theoretical methods for calculation of TLP motions and tendon forces
2. Establish a simple linear model for calculation of surge motions, set-down and tendon forces in regular waves, and make a Matlab code for such calculations
3. Use the simple model to design a scaled model of a floating wind turbine for testing in the MC lab at Tyholt, make the model and carry out a set of tests
4. If time allows some analysis with software like RIFLEX, SIMO or DeepC should be carried out and results should be compared to model tests

The work may show to be more extensive than anticipated. Some topics may therefore be left out after discussion with the supervisor without any negative influence on the grading.

The candidate should in her/his report give a personal contribution to the solution of the problem formulated in this text. All assumptions and conclusions must be supported by mathematical models and/or references to physical effects in a logical manner.
The candidate should apply all available sources to find relevant literature and information on the actual problem.

The report should be well organised and give a clear presentation of the work and all conclusions. It is important that the text is well written and that tables and figures are used to support the verbal presentation. The report should be complete, but still as short as possible.

The final report must contain this text, an acknowledgement, summary, main body, conclusions and suggestions for further work, symbol list, references and appendices. All figures, tables and equations must be identified by numbers. References should be given by author name and year in the text, and presented alphabetically by name in the reference list. The report must be submitted in two copies unless otherwise has been agreed with the supervisor.

The supervisor may require that the candidate should give a written plan that describes the progress of the work after having received this text. The plan may contain a table of content for the report and also assumed use of computer resources.

From the report it should be possible to identify the work carried out by the candidate and what has been found in the available literature. It is important to give references to the original source for theories and experimental results.

The report must be signed by the candidate, include this text, appear as a paperback, and - if needed - have a separate enclosure (binder, DVD/ CD) with additional material.

Supervisor at NTNU is professor Carl M. Larsen

Trondheim, 24 January 2011-01-23

Carl M. Larsen

Submitted: January 2011
Deadline: June 2011

Preface

This report is the result of the Master Thesis conducted by Stud. Techn. Rolf Åge Vågen spring 2011 at the Norwegian University of Science and Technology (NTNU). The thesis count as 30 credits and the intention with the report is to check the feasibility of tension leg anchoring systems on floating wind turbines. The introductory work started with a project fall 2010.

During this thesis one week was purposed for executing experiment with a scaled model in the Marine Cybernetics laboratory at NTNU. The model was built by Marintek, and completed within testing date. However after several runs testing the model, it was concluded that the model was built with tendons making it overly stiff. Therefore it was necessary to replace the tendons in order to get results that could represent the motion of a tension leg structure. This delay was inconvenient in an already tight time schedule, and therefore not all planned tests could be carried out.

Due to large workload the fourth point in the problem description is left out in agreement with supervisor.

I would like to thank my supervisor, Professor Carl Martin Larsen for his guidance with the thesis. He has been very available for counseling throughout the whole process, and his great experience within the field of Marine structures has been very helpful. Torgeir Wahl at NTNU should also be acknowledged for all help with the Laboratory test, where especially his instrumentation skills were invaluable.

Trondheim 08.06.2011

Rolf Åge Vågen

Abstract

Renewable energy is likely to be of great importance in decades to come due to increased energy consumption. Kinetic energy from wind is expected to cover a part of this need, and wind farms are so far built onshore or at shallow water. On the other hand wind turbines are not always wanted close to land due to both the visual aspects and bird life. An alternative may therefore be to place wind turbines offshore. However, large water depths are causing problems for existing bottom fixed structures and floating wind turbines may therefore be a solution.

In this thesis feasibility of tension leg anchor systems for floating wind turbines is investigated. A literature study including tension leg principles, relevant load parameters and methods for calculating motions on tension leg structures are looked into. Preliminary calculations of motion based on a one degree of freedom model are coded and executed in Matlab. Finally, a model in scale 1:100 has been built and further exposed to regular waves in a laboratory test. Numerical and experimental results are investigated and compared for different wave parameters in order to reveal potential weaknesses of the concept.

Numerical and experimental results coincide quite well for structure motion in the wave direction, and in most cases the structure get small motion amplitudes which generate negligible vertical motions in form of set down. The overturning moment calculations also coincide well, and show that there are limitations in the mooring feasibility when exposed to large waves. The pretension is proven to be a very important parameter for the concept. Measurement of tendon forces from laboratory test show that the model is loaded differently and in larger order of magnitude than expected. For the scaled model a simplified tendon attachment arrangement in form of a steel plate is used. The strange force distribution may therefore represent loading on this plate. The results however show that tension leg anchoring can be a relevant alternative type of anchor system for floating wind turbines if sufficient system pretension is obtained. In addition, if also a reasonable magnitude and distribution of mass are obtained, the structure is expected to handle quite large waves.

The design presented in this thesis is far from optimized. For further work it is therefore advised to model the structure in software where structural analysis can be executed in order to decide upon an optimized structural weight, seeing this as an important parameter.

Table of contents

Table of figures

List of tables

Nomenclature

Equivocal symbols and abbreviations are in general explained as given in the text. Some of the symbols listed will however not be presented or repeated any further.

Abbreviations

DAF	-	Dynamic amplification
DNV	-	Det Norske Veritas
Dof	-	Degree of freedom
FFT	-	Fast Fourier Transform
MC lab	-	Marine Cybernetics laboratory
RP	-	Recommended Practice
TLP	-	Tension Leg Platform
ULS	-	Ultimate Limit State
VCG	-	Vertical Center of Gravity
VIM	-	Vortex Induced Motion
VIV	-	Vortex Induced Vibrations
2D	-	Two dimensional

Roman letters

A	-	Projected area [m^2]
A_{jk}	-	Added mass forces/moments
B_{jk}	-	Damping forces/moments
C_{jk}	-	Restoring forces/moments
C_d	-	Drag coefficient
C_m	-	Mass coefficient
C_w	-	Shape coefficient, wind force
D	-	Diameter [m]
f_n	-	Eigenfrequency [Hz]
f_v	-	Vortex shedding frequency [Hz]

g	-	Gravity acceleration [m/s^2]
H	-	Wave height [m]
H_s	-	Significant wave height [m]
k	-	Stiffness [N/m]
m	-	Mass [kg]
St	-	Strouhal number
T	-	Wave period [s]
T_p	-	Peak period [s]
u	-	Structure motion in horizontal direction [m]
$\dot{u}$	-	Structure velocity in horizontal direction [m/s]
$\ddot{u}$	-	Structure acceleration in horizontal direction [m/s^2]
U	-	Current velocity [m/s]

Greek symbols

β	-	Frequency ratio
η_k	-	Motion in direction k [m]
$\dot{\eta_k}$	-	Velocity in direction k [m/s]
$\ddot{\eta_k}$	-	Acceleration in direction k [m/s^2]
θ	-	Phase angle [rad]
λ	-	Wave length [m]
ξ	-	Damping ratio
ρ_A	-	Density of air [kg/m^3]
ρ_w	-	Density of water [kg/m^3]
ω	-	Frequency [rad/s]
ω_0	-	Eigenfrequency [rad/s]
ω_d	-	Damped eigenfrequency [rad/s]

1. Introduction

In this Master thesis an alternative type of anchoring system on floating wind turbines is investigated. This system is based on the tension leg principle, and consists of three parallel tendons. This is a new concept for floating wind turbines, and the main purpose of this work is to investigate the feasibility of this mooring design for floating wind turbines.

This concept study is divided into three parts. The first part involves a literature study where tension leg principles, relevant load parameters and methods for calculating TLP motions are looked into. The second part deals with preliminary calculations of motions based on a one-degree of freedom model. The model is coded in Matlab and used to calculate motions from waves with different heading in order to reveal possible unfavorable wave headings. To optimize the design, important parameters such as vertical position of tendon termination and draught are varied. The last part of the thesis elaborates on laboratory tests in a scale 1:100 executed in the Marine Cybernetics laboratory at NTNU. The scaled model is exposed to regular waves with different height, period and heading. Different draughts and hence also pretensions are investigated.

Some calculations are presented throughout the report in order to support assumptions and restrictions in the calculations. The final design parameters however are presented and discussed in the result chapter.

Figure 1 show a conceptual sketch of how a final design may look like. The design is shown from different headings with the side view on the upper part of the figure and vertical view of the mooring attachment arrangement on the lower part.

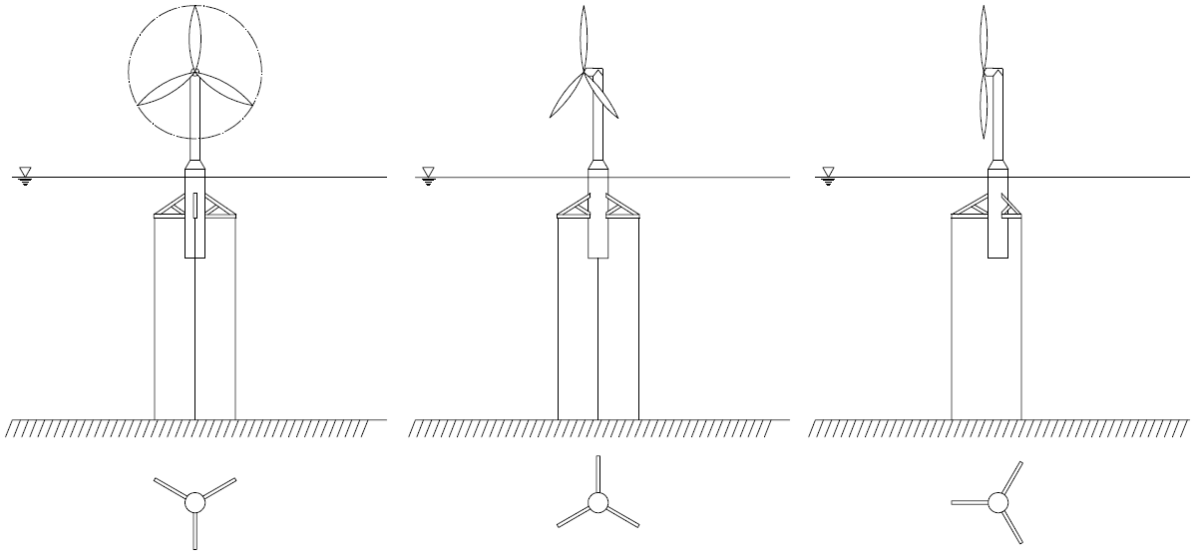

Figure 1: The system shown from different angles

2. Background

As need for energy constantly increases, the discussion regarding fossil energy is turning more relevant than ever before. In addition to the Greenhouse effect, problems with oil-spills are threatening the environment and animal life both on the coast and offshore.

In search of new oil- and gas fields, the oil companies have to look towards more vulnerable areas. Environmental groups and parts of the population are concerned that the search of energy will destroy the nature. An example of a frequently discussed area is Lofoten, in the northern part of Norway. This is one of the most important spawning grounds for cod in Norway, and might be in danger when new reservoirs are searched for and processed.

The coming years will most likely lead to an increased need for energy, see Figure 2. Renewable energy seems to be the only way to secure the energy need in the coming decades in an environmental friendly way. It is therefore necessary to improve the knowledge and use of renewable energy sources in the future.

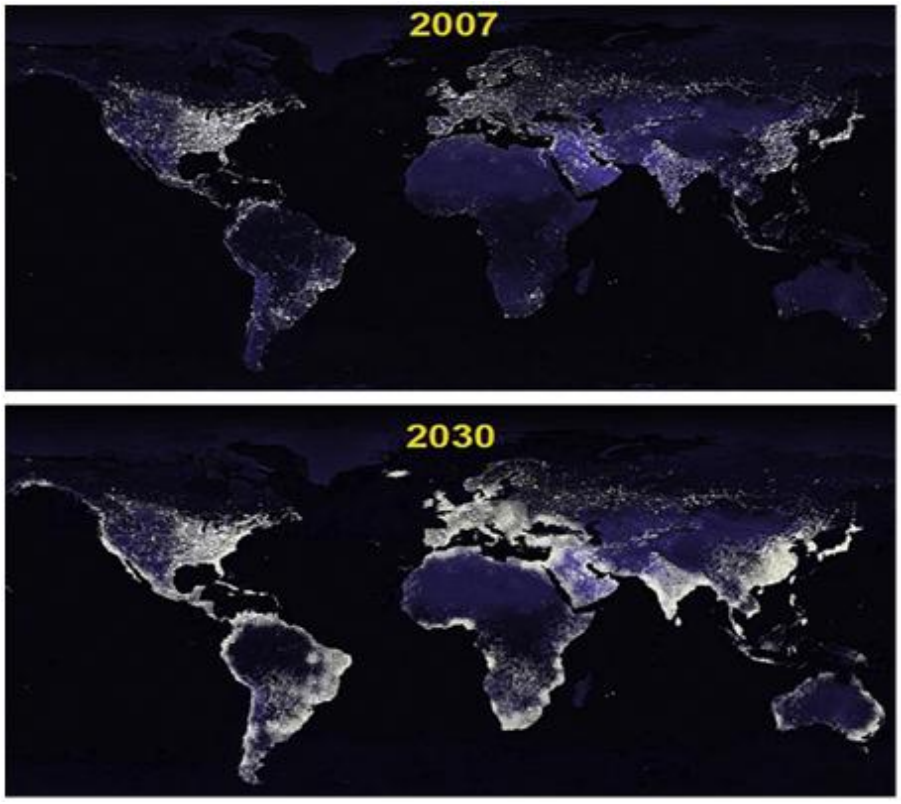

Figure 2: Energy demand around the world in the year 2007, compared with forcasted energy demand in 2030 (Estaban M.D. Et. Al 2010).

One of the renewable energy sources that may have a large potential is wind power. We know that wind turbines have been used for many years. Varying temperature around the world leads to atmospheric pressure differences, which again makes air move from one area to another. This creates huge amounts of kinetic energy which can be utilized with the right technology. The challenge is however to do this in a cost-effective and reliable way. In Norway, the oil industry has brought many challenges, thus a lot of knowledge that can be used to build cleaner energy sources, such as floating offshore wind turbines.

3. Theory

3.1 General

There is not much literature regarding tension leg wind turbines available at the moment. However is the principles from tension leg platforms (TLP) applicable and for this topic good literature are available.

TLPs are restrained from oscillating vertically by tendons, which are vertical anchor lines tensioned by the platform buoyancy. To make this concept operational is it therefore important that the buoyancy with good margin is larger than the total weight of the structure.

A tension leg system consists of tendons and connectors. Foundation templates at the sea floor need to be installed in order to keep the position of the tendons. For tension leg platforms with large distance between tendons, one template for each set of tension legs are most common (Demirbilek 1989). A typical installation can be seen on Figure 3. When it comes to wind turbines where distance between fastening points are smaller, a joint template can be relevant. This template can be restrained either by weight or by anchoring

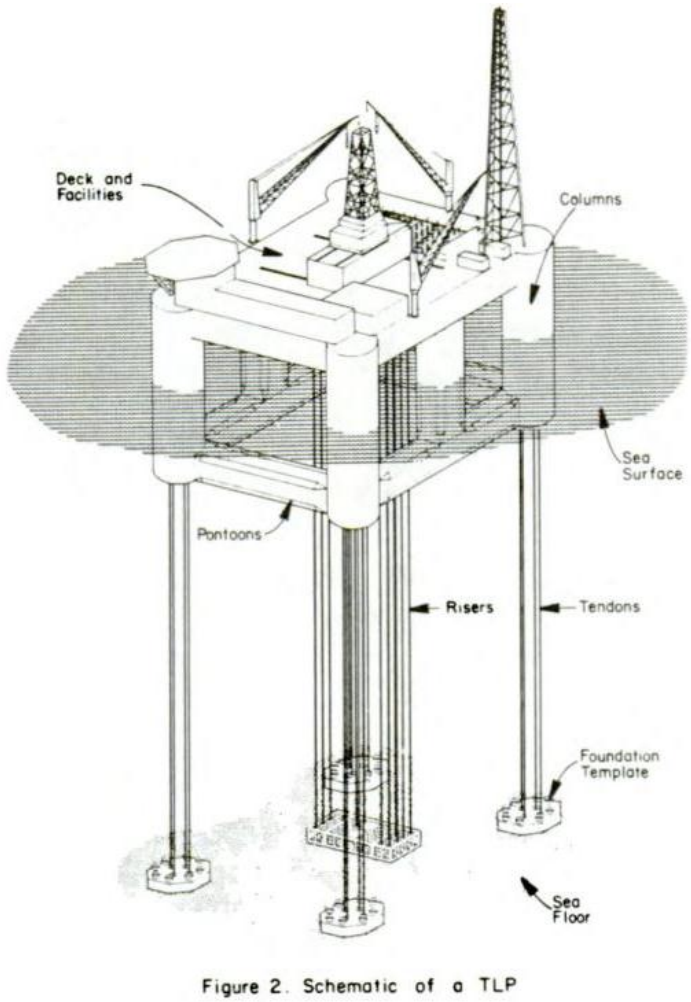

Figure 2. Schematic of a TLP

Figure 3: Tension leg platform (Demirbilek 1989)

3.1.1 Tendons

As tendons hollow pipes, wire ropes or high strength cables are most common to use. If thin-walled tubular tendons are used, special attention must be paid to the collapse and buckling problems, especially at deep waters.

Vertical tendons fixed to the bottom, will restrain the structure from oscillating in vertical direction. However, this is only possible if the buoyancy of the structure is larger than the weight. A tension legged structure are therefore sensitive to large increase in weight in form of payload. This is not a large problem for wind turbines, since they are not constructed to bear any payload. Added weight may yet be experienced if for instance defect equipment is replaced with heavier parts and marine growth.

3.1.2 Motion

A typical heave period for a tension leg platform according to Faltinsen (1990) will be in the range of 2 – 4 seconds in the first order wave force frequency range. When the water depth increases, hence the tendon length, stiffness of the tendons will decrease, and the eigenfrequencies of the system can then move into the wave loading frequency. In this case other types of tendons or alternative mooring type needs to be considered. The eigenperiod in heave will mainly depend on the elasticity of the tendons, while the eigenperiod in pitch and roll also depend on the distance between the tendons.

In the lateral motions (surge, sway and yaw) the eigenfrequencies will be more low-frequent, and inertia dominated in the same wave frequency range as for vertical motion. The long eigenperiods are due to low transverse stiffness in the tendons. The stiffness and hence the motion in these modes are controlled by the pretension in the mooring system and the water depth. It is also important to avoid a natural frequency that can coincide or get close to the typical wave loading frequency for the specific area. This will be explained further in section 3.2.1.

3.1.3 Design criteria for TLPs

For an offshore structure wind, waves and current are important parameters for the response of the structure. It is not likely that all these contribute with a maximum value at the same time, but it should anyhow be considered in the specification of metoccean design criteria. According to Demirbilek (1989) the metoccean design criteria falls into general classes of;

1. Extreme one-time storms
2. Storms expected during maintenance activities
3. Normal conditions affecting operations and fatigue
4. Conditions along the tow route

Stochastic analysis can be a good way to find a design value for both wind- and wave loading. The design value can for instance be taken as the ultimate limit state (ULS) criteria. The design loads may then be taken as the environmental loading with an annual exceeding probability of 10^{-2} (Haver 2009). Time domain analysis in an irregular sea state may also be applied in order to get information of how the structure behaves in different load frequencies, in terms of a transfer function.

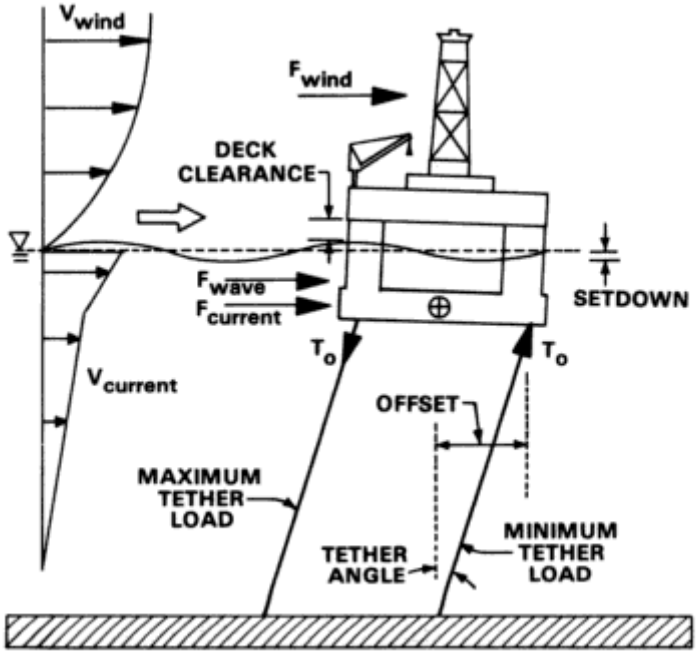

Figure 4: TLP design responses (Demirbilek 1989)

3.1.4 Environmental parameters in design

Figure 4 show primary TLP responses with forces acting on the structure. The effect from wind-, wave- and current forces can be resolved into a resultant force and an overturning moment. When the structure gets a horizontal offset from the resultant force, the tension will in turn increase uniformly in the tendons. This increased tension will yield a set down of the structure. According to Demirbilek (1989) the set down is not used as a design check itself, but it is a contributor to for instance tendon tension and tendon angle which are used as design checks. When it comes to overturning moment, it will cause differential tension between the up-weather and down-weather tendon. It is important that the tendons satisfy both the minimum and maximum tendon load for stress and buckling respectively. It is important to take into consideration that the tide increases and decreases the hull submergence; hence the buoyancy and tendon tension. The drag coefficients will be affected by the marine growth on the tendons. To determine the lifetime of a structure the occurrence of these different parameters need to be investigated. According to Demirbilek (1989) the specific environmental parameters important in design are;

- Wind
  - Mean wind speed profile
  - Mean wind direction
  - Wind turbulence spectrum
- Wave
  - Significant wave height, characteristic wave period (e.g. spectral peak period)
  - Wave spectral shape
  - Mean wave direction

  - Wave directional spreading function
- Current
  - Speed profile
  - Direction profile
- Tide
  - Astronomical tide
  - Storm surge
- Marine growth
  - Thickness profile
  - Roughness profile

3.1.5 Hydrodynamic analysis of TLP

Motions of floating structures according to Faltinsen (1990) can be divided into wave-frequency motion, high-frequency motion, slow drift motion and mean drift. The oscillatory rigid-body translatory motions are referred to as surge, sway and heave. The oscillatory angular motions are referred to as roll, pitch and yaw. High-frequency motion is significant for TLPs and is often referred to as "ringing" and "springing" and is due to resonance oscillations in heave, pitch and roll of the platform. The natural periods of these motions are excited by non-linear wave effects (Faltinsen 1990). For drilling platforms the heave motion is a limiting factor, since the riser motion need to be compensated. There are limits of how much the motion can be compensated. When it comes to wind turbines the heave, pitch and roll motion are also important factors. This high-frequency loading may lead to fatigue problems in rotor and nacelle.

3.1.6 Vortex induced vibrations

For a slender offshore structure exposed to current, vibrations may occur due to the vortex shedding on the downstream side of the structure. For tension leg anchored wind turbines, vortex shedding may be of importance both for tendon and structure motion. When talking about more low frequent motions on bodies caused by vortex shedding, the term Vortex Induced Motions (VIM) is used.

Alternating vortex shedding gives varying pressure and hence oscillatory forces. Under right circumstances, this vortex shedding can provoke large oscillations or motions that can lead to fatigue and fracture of the structure. In addition, the VIV may lead to a larger effective diameter; hence contribute to larger forces acting on the structure. An important parameter when calculating VIV, is the Strouhal number, given as

$$St = \frac{f_v D}{U} \tag{3.1}$$

Where

St – Strouhal number (taken as 0.2 for most practical cases (Fredsoe et. Al, 1997)

f_v – Vortex shedding frequency

D – Diameter

U – Current velocity

For the large motions to occur, the vortex shedding frequency needs to be close to the eigenfrequency of the structure. The vibration frequency will lock into the damped eigenfrequency and create resonance. Since the eigenfrequency will be affected by the added mass the lock-in will occur at the adjusted eigenfrequency. This is illustrated in Figure 5, and it can be seen that lock-in occurs somewhat over ratio, fv/fn = 1.

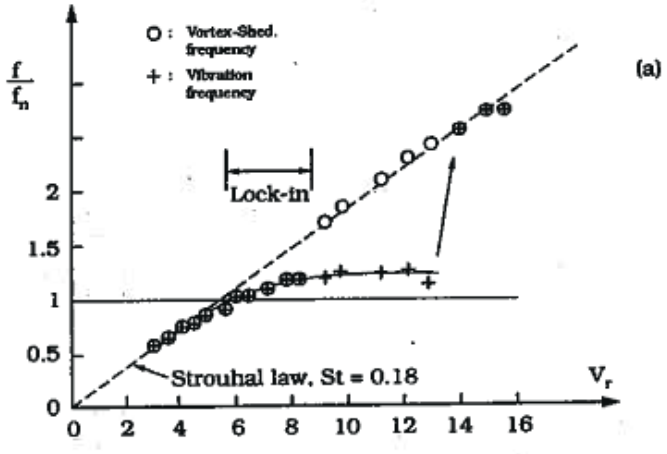

Figure 5: Lock-in for a cylinder exposed to current. Sumer & Fredsøe (1997)

A slender structure can have different eigenmodes, and in a uniform current the resonance will occur in the mode with the eigenfrequency closest to the vortex shedding frequency. In shear current, different modes can experience resonance at the same time, due to different current velocities, hence vortex shedding over the depth.

3.2 Motion of a structure

This section contain the basic theoretically parameters that are important in an early stage of a concept study for a tension legged wind turbine. The chapter contains structural properties, hydrodynamic loading and effects in addition to motion theory. The coordinate system used in the following is based on the standard coordinate system for a floater, shown in Figure 6

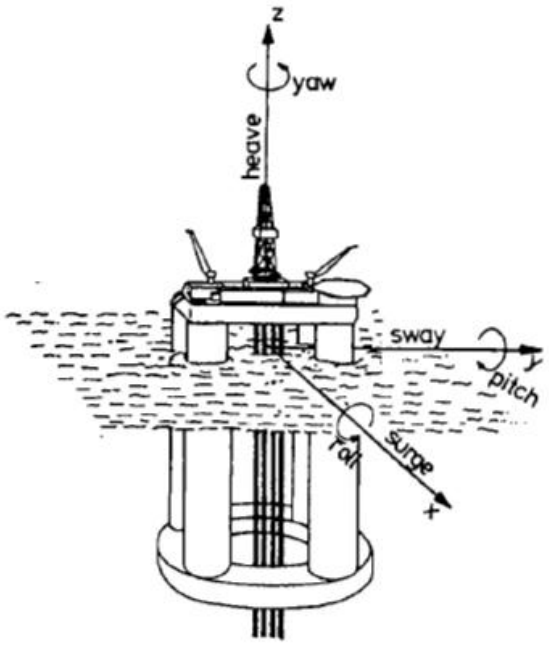

Figure 6: Coordinate system,with rigid body motions for a floater (Faltinsen 1990)

3.2.1 System characteristics

When designing a marine structure it is as mentioned important to make sure that the eigenfrequencies are outside the wave loading frequency for the specific area. In this section methods for finding the eigenfrequencies are presented.

To give an impression of the order of magnitude for wanted and unwanted eigenperiods, typical load- and eigenperiods for marine structures are shown in Figure 7.

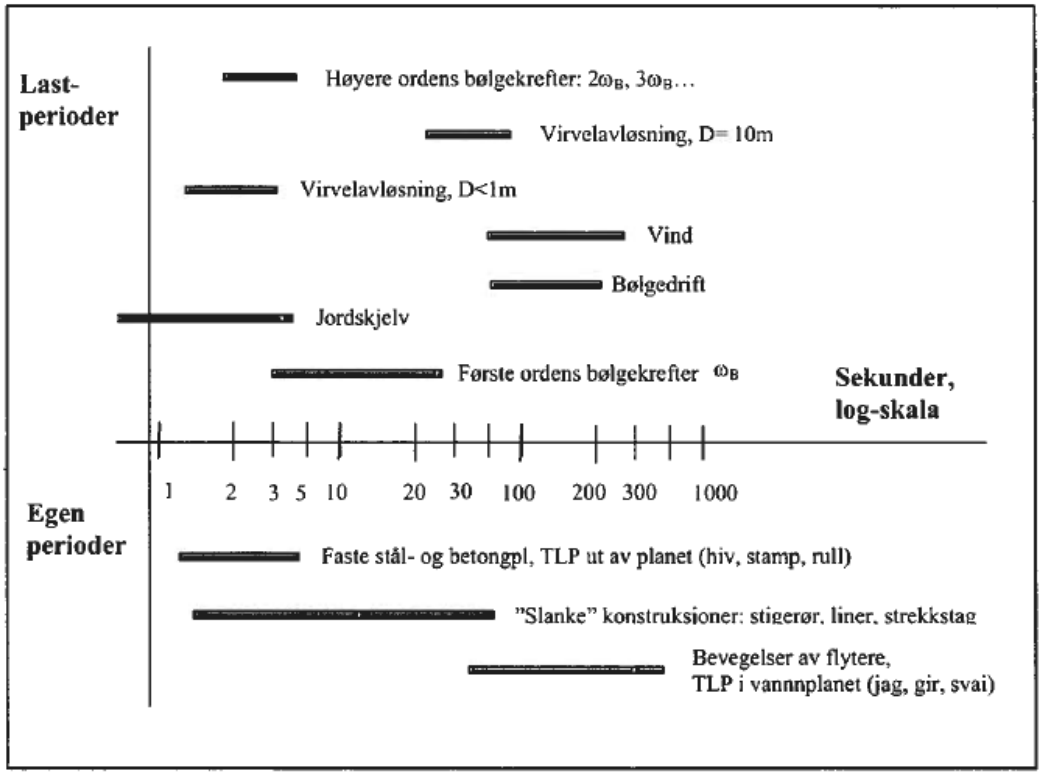

Figure 7: Typical load periods and eigenperiods for marine structures (Larsen 2009)

The eigenfrequency for a undamped system can according to Larsen (2009), be given as

$$\omega_0 = \sqrt{\frac{k}{m}} \tag{3.2}$$

Where *k* represents the system stiffness and *m* is the mass of the system. For an eigenfrequency with added mass and damping, these parameters need to be introduced in relevant degrees of freedom.

The added mass can be added to the mass while the damping can be introduced as damping ratio, and the eigenfrequency can then be expressed as

$$\omega_d = \omega_0\sqrt{1-\xi^2} \tag{3.3}$$

Where, ξ is the damping ratio given as;

$$\xi = \frac{C}{C_{Crit}} \tag{3.4}$$

Frequency ratio is a common concept in structural design, and gives us information about how close the eigenfrequency of the system is to the load frequency. Frequency ratio is given as

$$\beta = \frac{\omega}{\omega_0} \tag{3.5}$$

Where ω is the load frequency.

The dynamic amplification factor is another important term when calculating a dynamic response. If the eigenfrequency is close to the load frequency (frequency ratio close to one) the dynamic response will have a large amplification compared with the static response. DAF is given as

$$DAF = \left|\frac{U_{max}}{U_{stat}}\right| = \frac{1}{\sqrt{(1-\beta^2)^2 + (2\,\xi\,\beta)^2}} \tag{3.6}$$

For a structure the dynamic response can be divided into three ranges.

- Stiffness-dominated system
- Resonance
- Inertia-dominated system

For a stiffness dominated system the load frequency is clearly below the eigenfrequency, see Figure 8. The loads are therefore relatively slow, and no significant inertia forces occur.

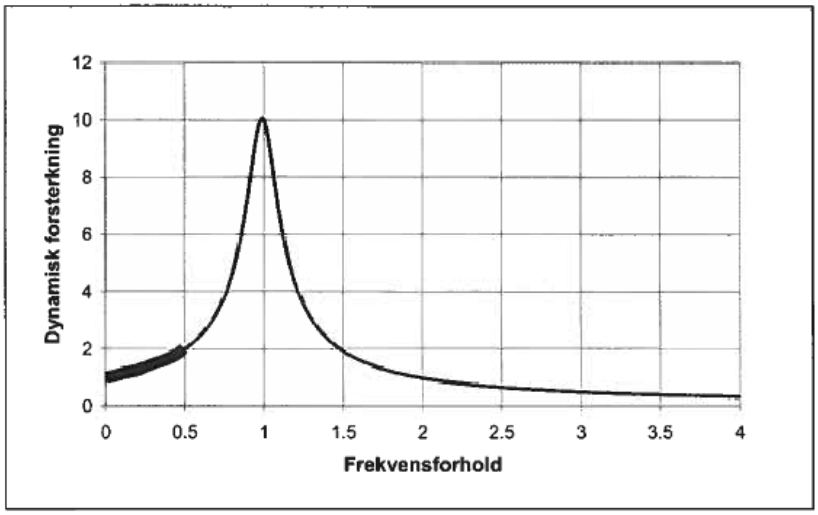

Figure 8: Stiffness-dominated system. Larsen (2009)

For a system in resonance the load frequency will be close or equal to the eigenfrequency, see Figure 9. This range should be avoided, since large motions and forces will occur for a structure in this range and the structures eigenfrequency should be increased or decreased.

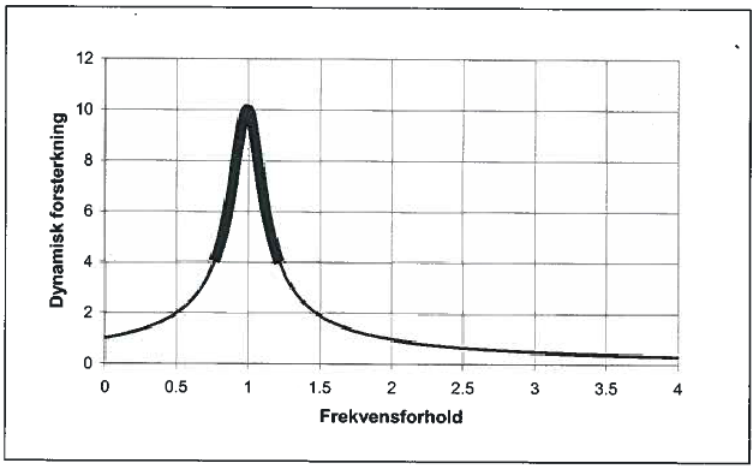

Figure 9: System in resonance. Larsen (2009)

For an inertia-dominated system the load frequency will be significantly higher than the systems eigenfrequency, see Figure 10. The system has large inertia and the stiffness forces will not be activated, hence equilibrium is obtained by the inertia forces.

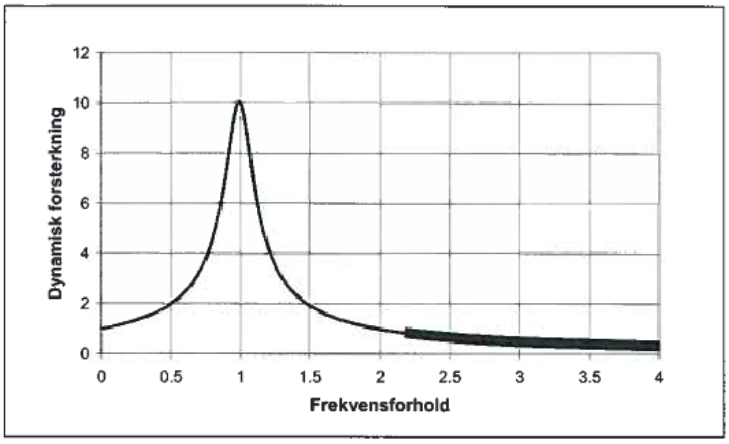

Figure 10: Inertia-dominated system. Larsen (2009)

3.2.2 Motion of a structure in waves

For a steady state sinusoidal motion we may write (Faltinsen 1990), (j = 1, 2 .., 6)

$$\sum_{k=1}^{6}[(M_{jk}+A_{jk})\,\ddot{\eta}_k + B_{jk}\dot{\eta}_k + C_{jk}\,\eta_k] = F_j e^{-\omega_e t} \tag{3.7}$$

Where

M_{jk} – Mass in dof *j* for motion in *k*

A_{jk} – Added mass in dof *j* due to motion in *k*

B_{jk} – Damping force/moment in dof *j* due to motion in *k*

C_{jk} – Restoring force/moment in dof *j* due to motion in *k*

F_j – Exciting force or moment

The equation of motion can give us information about the motion of the structure. However, we see that there are terms that need to be determined in order to get the motion characteristics.

A hydrodynamic problem in regular waves is according to Faltinsen (1990) normally dealt with as two sub problems. The two sub problems are illustrated in Figure 11.

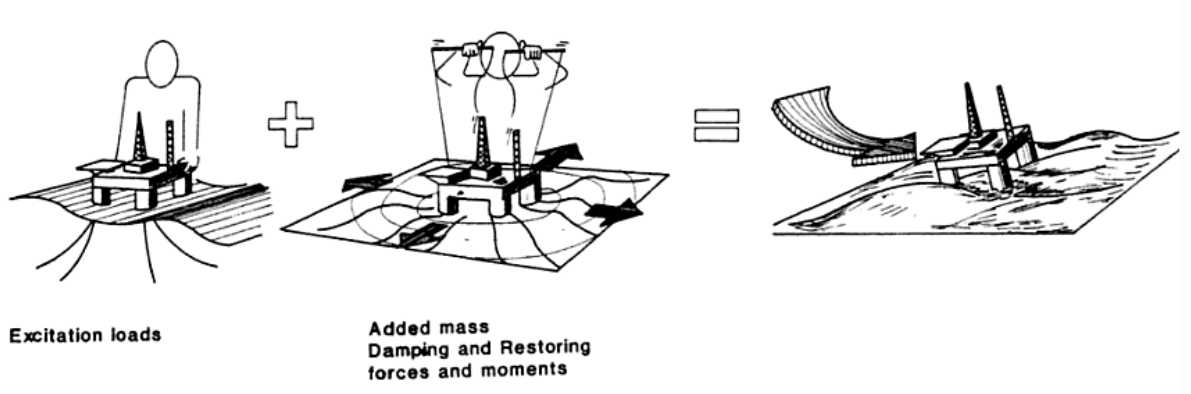

Figure 11: The two subproblems used to solve hydrodynamic problems (Faltinsen 1990).

Sub problem A – the wave excitation forces is composed of Froude-Kriloff and diffraction forces and moments. This is the forces and moments acting on the body when the structure is restrained from oscillating in incident regular waves.

Sub problem B – Contains the added mass, damping and restoring terms. These forces are found when the structure is forced to oscillate with the wave excitation frequency in any rigid-body motion, with no incident waves.

Due to linearity the forces found in sub problem A and B can be added to give the total hydrodynamic forces.

When we have forced harmonic rigid body motions, we get hydrodynamic forces which are called added mass and damping forces, or moments depending on in which degree of freedom they occur. The forced motion of the structure generates outgoing waves, and the forced motion results in oscillating fluid pressures on the body surface. Integration of the fluid pressure forces over the body surface gives resulting forces and moments on the body (Faltinsen 1990).

According to Karimirad et. al (2010), resonant motions of a spar type wind turbine can be damped by aerodynamic damping. This does not automatically mean that the same conclusion can be drawn for a tension legged turbine, but it is something to be aware of. For a floating wind turbine, we may also get additional damping due to the gyro-effect on the rotor (Fylling 2010). These two damping contributions will however not be investigated further in the present study.

For a freely floating body, restoring forces will be determined from hydrostatic and mass considerations. The only non-zero terms for a body with the x-y plane as a symmetry plane for the submerged body will be C_{33} , C_{35} , C_{45} , and C_{55} (Faltinsen 1990).

3.2.3 One degree of freedom system

For a one-degree of freedom system with a harmonic loading and damping, the equation of motion can be expressed as

$$m\ddot{u} + c\dot{u} + ku = P_0 \sin(\omega t) \tag{3.8}$$

The homogenous solution of the differential equation is expressed as the damped eigenfrequency ω_d, while the particular solution of the equation can be given as

$$u_p = C_1 \sin(\omega t) + C_2 \cos(\omega t) \tag{3.9}$$

By inserting equation (3.8) into equation (3.9), and re-arranging, the system can be presented as

$$\begin{aligned} -m\omega^2 C_1 - c\omega C_2 + kC_1 &= P_0 \\ -m\omega^2 C_2 - c\omega C_1 + kC_2 &= 0 \end{aligned} \tag{3.10}$$

Solved for the integration constants, gives;

$$\begin{aligned} C_1 &= \frac{P_0}{k} \frac{1-\beta^2}{(1-\beta^2)^2 + 2(\xi\,\beta)^2} \\ C_1 &= \frac{P_0}{k} \frac{2\,\xi\,\beta}{(1-\beta^2)^2 + 2(\xi\,\beta)^2} \end{aligned} \tag{3.11}$$

Hence, the particular solution is (Larsen 2009);

$$u_p = \frac{P_0}{k} \frac{1}{(1-\beta^2)^2 + 2(\xi\,\beta)^2} \left[(1-\beta^2)\sin(\omega t) - 2\,\xi\,\beta\cos(\omega t)\right] \tag{3.12}$$

The homogenous solution of the equation will decay, and the particular solution will be governing. We can present the response as one single harmonic function

$$u_p = R\sin(\omega t - \theta) \tag{3.13}$$

Where;

$$\begin{aligned} R &= (C_1^2 + C_2^2)^{\frac{1}{2}} \\ \theta &= \arctan(-\frac{C_2}{C_1}) \end{aligned} \tag{3.14}$$

This method includes the concepts that are presented under section 3.2.1, and is a good way to do simplified motion analysis of a system. Later in the report this method will be used to find motions of the floating wind turbine.

3.3 Forces on a structure

3.3.1 Large- and small volume structures

The wave forces are important parameters when calculating loads on Marine structures. From a hydrodynamic point of view it is desirable to classify the structures as large volume or small volume. For a large volume structure the structures wave-generation is important when forces are calculated, but this is not important for a small volume structure (Pettersen 2007). In Figure 12 is the relation illustrated. It can be seen from the figure that for a large wavelength relative to the structure, mass and viscous forces are most relevant. For the other way round, a small wavelength compared with the structure, will lead to governing diffraction forces.

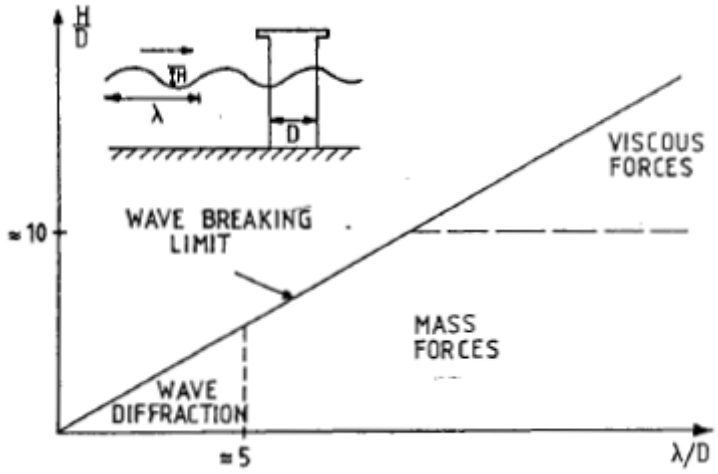

Figure 12: Relative importance of forces on marinte structures (Faltinsen 1990)

The small volume structures can further be divided into drag force-, and mass force-dominated, depending on the wave height over diameter ratio. This criterion will however change as the environmental parameters change, and there is therefore no clear border between the mass dominated structure and a viscous force dominated structure.

A common way to calculate forces on a small-volume structure is to use the Morison equation. This equation is often used to calculate wave-forces on cylindrical structures, and a force dF, see Figure 13, on a strip with length dz is according to Pettersen (2007) given as

$$dF = \rho \frac{\pi D^2}{4} C_M a_x dz + \frac{1}{2} \rho C_D D \, u|u| dz \tag{3.15}$$

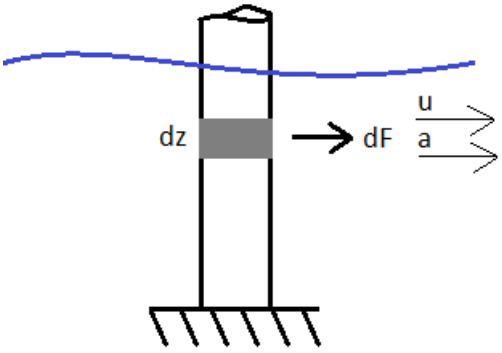

Figure 13: Drag force on a strip

Where ρ_w is the density of water, a is the particle acceleration, u is the particle velocity. C_M and C_D is the mass and drag coefficients respectively.

When the structure is large compared with the wave length, Morison equation is no longer applicable. A typical limit for use of Morison equation is given in Pettersen (2007):

- The wavelength need to be more than or equal to 5 times the diameter on the cylinder in order to use Morison equation.

In that case it is necessary to use another method to decide the wave forces. MacCamy and Fuchs theory can then be introduced. These methods are analytical and relate to sinusoidal waves from a bottom fixed cylindrical structure, and use the potential theory. When the total potential are known, we can estimate the pressure around the cylinder, thus the horizontal force per length dF (Pettersen 2007).

$$dF = \frac{2\rho g H}{k}\frac{\cosh k(z+h)}{\cosh kh}A(ka)\cos(\omega t - \alpha) \tag{3.16}$$

3.4 Environmental loading

Environmental loads are according to Moan (2004) due to wind, current, waves, ice-loading and earthquake motions. In the following loads from ice and earthquake will not be further investigated.

3.4.1 Wind Loads

Wind is according to Haver (2010) experienced essential at two different time scales:

1: A slowly varying mean wind level; V_M. This component can often be considered as constant for a short term period, say 3 hours.

2: A "rapidly" fluctuating wind component; $V_{t,}$ riding on the mean wind speed. The period of fluctuations will be from some second to a few minutes.

In design, it is important to take both components in consideration when checking for dynamic amplification. For tension legged wind turbines the fluctuating wind components can for example coincide with the stiffness-dominated degrees of freedom, and generate ringing.

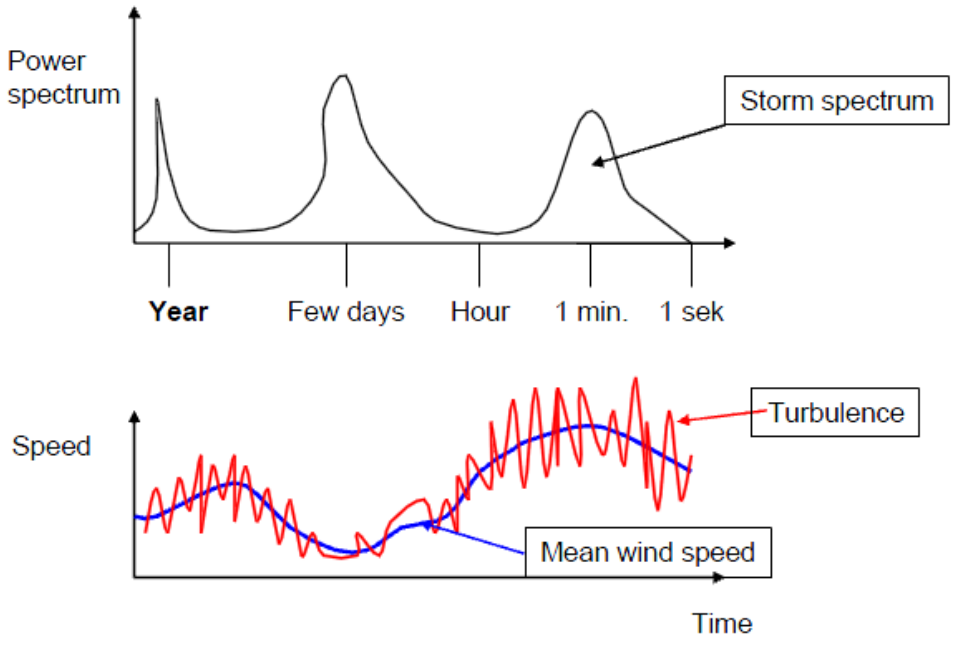

Figure 14: Storm spectrum together with a long term variation of wind speed. Haver S. (2010)

At a given point, the resulting wind speed can be written:

$$V(t) = V_M(t) + V_t(t)$$

The wind speed may be directly measured by an anemometer. But it is also possible to predict the wind speed based of information about the meteorological conditions, e.g. pressure, temperature etc., which is called hindcast predictions (Moan 2004). In areas where direct wind speed measurements are lacking, hindcast predictions are useful. Hindcast techniques are calibrated to directed measured wind speeds.

The wind speed will also vary with the height above sea surface, and to find the wind speed at the wanted height, one can use

$$u(z,t) = U(z) \cdot [1 - 0.41 \cdot I_u(z) \cdot \ln(\frac{t}{t_0})] \quad (3.17)$$

Where the 1 hour mean wind speed *U(z)* (m/s) is given by:

$$U(z) = U_0 \cdot \left[1 + C \cdot \ln\left(\frac{1}{10}\right)\right] \quad (3.18)$$

With

$$C = 5.73 \cdot 10^{-2} \cdot [1 + 0.15 \cdot U_0]^{\frac{1}{2}} \quad (3.19)$$

And the turbulence intensity $I_u(z)$ is given by

$$I_u(z) = 0.06 \cdot [1 + 0.043 \cdot U_0] \cdot \left(\frac{z}{10}\right)^{-0.22} \quad (3.20)$$

The static wind force on a structural member or surface acting normal to the member or surface is for practical problems given by:

$$F_W = \frac{1}{2}\rho_A C_w A V^2 \sin\alpha \quad (3.21)$$

Where

ρ_A – Density of air

C_w – Shape coefficient, can for example be found in DNV-RP-C205 (2007)

A – Projected are of the member normal to force direction

α – Angle between wind and axis of the exposed member

A considerable suction force can also occur on structural sides not facing the wind, but this will not be described more in this thesis.

3.4.2 Current loads

The current velocity is in general composed of wind- and tide driven components. In addition, coastal and ocean currents may occur. Also eddy currents, current generated over steep slopes, currents caused by storm surge, internal waves, should be considered (Moan 2004).

There is not much information available about the surface velocity and velocity distribution for the different contributions. According to Moan (2010), the wind current is commonly put equal to 1.0 –

2.0 % of the "sustained" wind velocity 10 m above the sea surface. Typical design current velocity profiles, assumed for the North Sea are given in Figure 15. The reference depth for wind driven currents, respectively, d_0 is often taken to be 30 - 60 m. The reference value for the tidal current, v_{cto} is assumed to be in the range 0.2 – 0.5 m/s on the Norwegian shelf (Moan 2004). The current velocities are summarized, and the force can be determined using Morison equation (3.15).

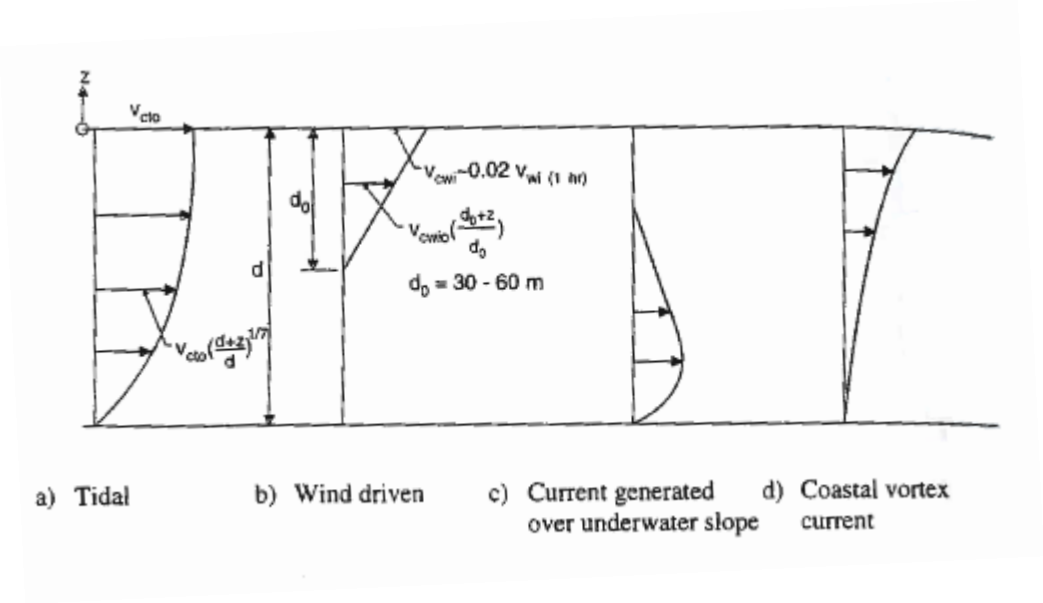

Figure 15: Current velocity profiles (Moan 2004)

3.4.3 Wave loads

The surface elevation is affected by (Moan 2004):

- Tide
- Storm surge
- Water waves

Also the presence of a structure may count.

There are different types of waves, and basically they can be divided into two types (Moan 2004):

- Translatory waves, such as solitary waves caused by tidal bores, moving hydraulic jumps, or earthquakes ("tsunami"-waves), with progressive deformation of the water surface and a considerable mass transfer in the direction of propagation.
- Oscillatory waves, progressive or standing, where mass transport is equal to zero or negligible, with water particles moving in closed or nearly closed orbital paths.

The main focus at this stage of the design will be on the latter case of waves caused by wind.

If we look at the sea surface on a day with lot of wind, a quite complex behavior can be observed. It is easy to understand that the sea surface cannot be described by a single regular wave. When representing a sea state like that, a number of regular waves with different period, amplitude and direction are combined. This is illustrated in Figure 16.

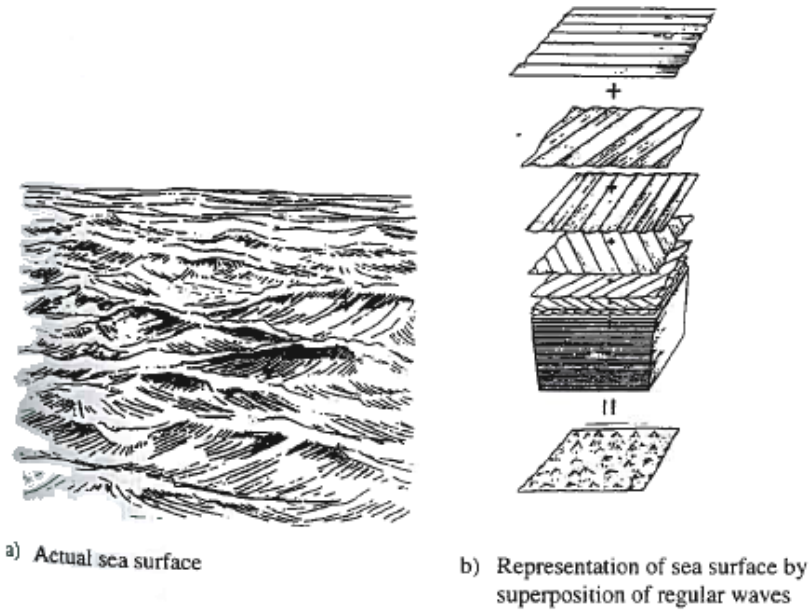

Figure 16: Representation of an actual sea surface (Moan 2004)

This sum of regular waves leads to the wave spectra, which are used in design for a structure. It can often be difficult to get a spectrum for a specific area and standardized spectra as Jonswap or Pierson-Moskowitz (PM) can be used.

For simple calculations, like the ones performed in this thesis, a regular wave can be used to find forces acting on a structure. Wave amplitude and wave period are then decided. And using regular wave theory, information about dynamic pressure, velocity and accelerations of particles can be found, and used with the proper formula for obtaining a force from relevant methods presented in section 3.3.

4. Numerical calculations

Preliminary calculations are as mentioned performed in MatLab, and in the following a thorough explanation of what the calculations are based on will be presented. The script used in the calculations is found in appendix A. The water depth in the calculations is 150 m, which represent a large part of the northern part of the North Sea.

4.1 The model

The model used is a simplification of the final design. The introductory work carried out the fall 2010, was used to decide upon the basic parameters since there was no design to start with. The model in this thesis consists of two columns with different diameter in addition to the mooring system. The nacelle and rotor are defined as a point mass at the top of the upper column. Masses in the system are defined as point masses in the center of gravity for the different parts of the structure.

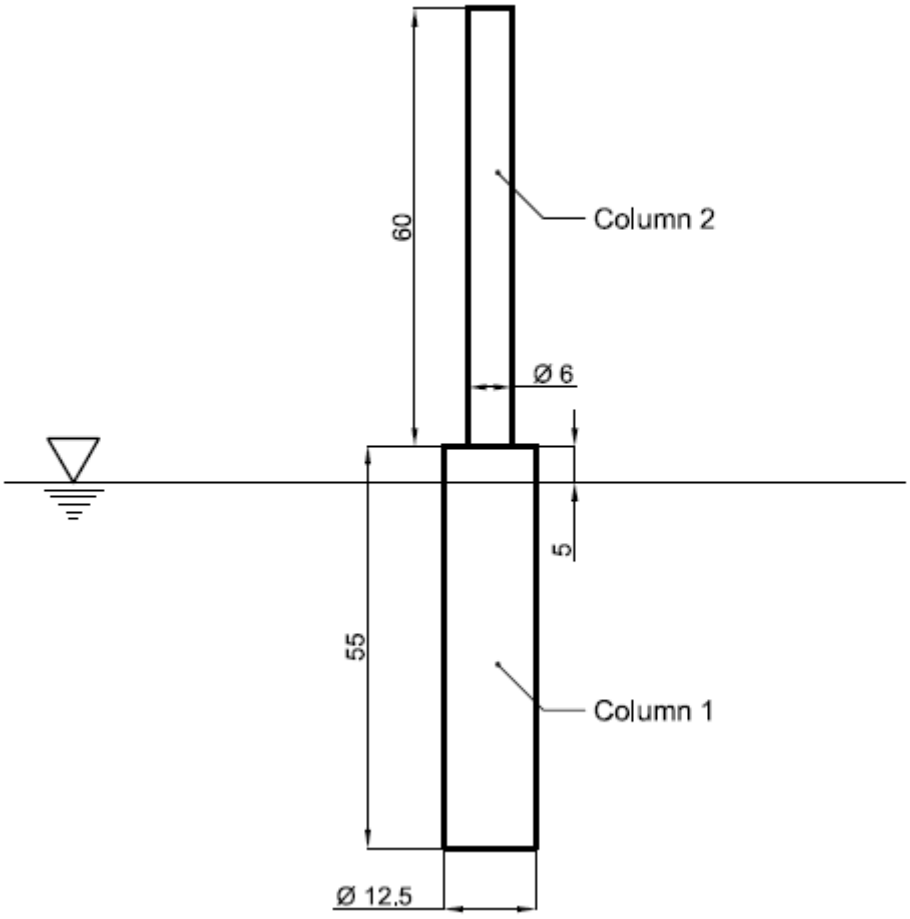

Figure 17: Dimensions of numerical model. (All dimension are in [m])

The wind turbine-body is defined using two cylindrical columns. The lowest part of the structure is the column with largest diameter and represents the part of the structure that gives sufficient buoyancy. The column with smallest diameter is intended to hold the nacelle and rotor above water. If the draught is increased the largest column is elongated while the distance to the nacelle, hence the length of the smallest column is kept constant. Details and dimensions can be seen on Figure 17 and Table 1.

Main dimensions	
Parameter	**Value**
Outer diameter column 1	12.5 m
Inner diameter column 1	12.2 m
Outer diameter column 2	6 m
Inner diameter column 2	5.7 m
Draught	50 m
Height above sea level	65 m

Table 1: Main dimensions of numerical model

The mass distribution of the structure can be seen in Figure 18 and Table 2. The total mass of the structure is taken as the mass of the two columns in addition to the mass of the turbine, which is taken from the Hywind-project (Offshorewind.net, 2011). Masses of the columns are taken as the total weight of the steel in the cylindrical columns. A wall thickness of 0.15 m is used, together with a density for steel on 7850 kg/m^3.

Added mass for surge and sway motion is taken as the weight of the displaced water and has center of gravity at half the draught.

It should be noted that the weight of the mooring system is not included in the Matlab model.

After the experimental model was built, it was clear that the model had a different mass distribution than explained in this chapter. The scaled model mass turned out to be too large compared with the numerical model. Additional mass is therefore added to the total weight, and in addition the vertical center of gravity is adjusted to represent the model. The VCG from the laboratory test is taken as the dry center of gravity without the added mass. When the added mass is included, a new total center of gravity is calculated.

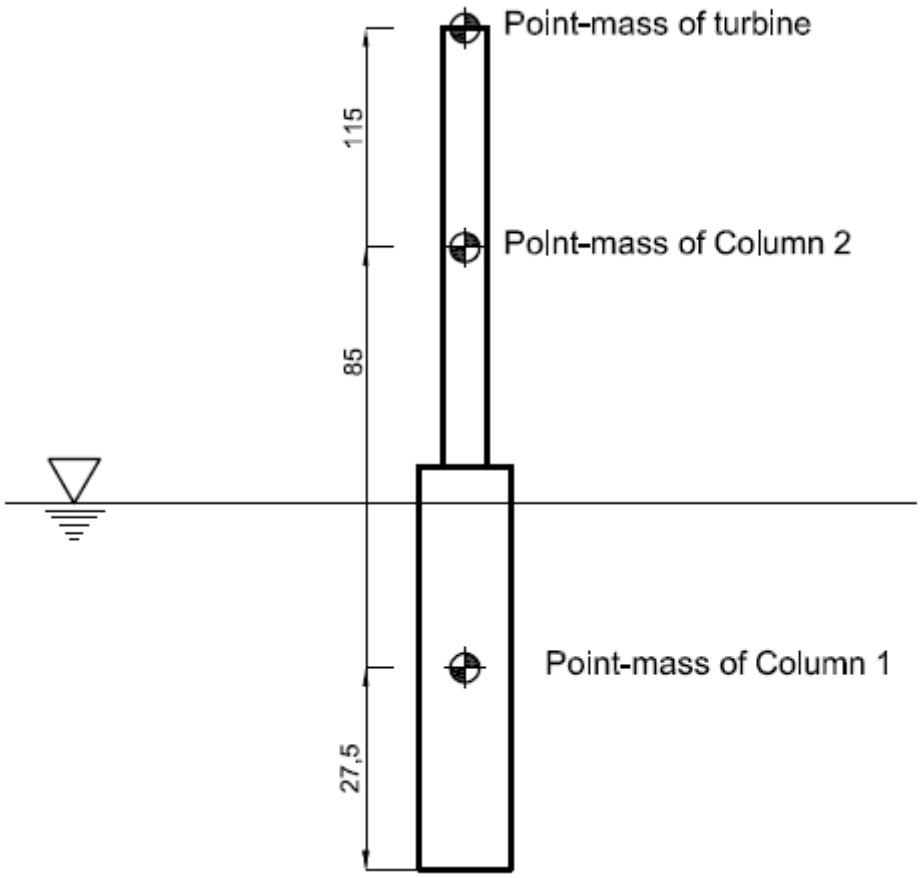

Figure 18: Mass distribution of numerical model. (Values are in [m])

Masses	
Parameter	**Value**
Weight column 1 [kg]	2.51E+06
Weight column 2 [kg]	1.30E+06
Weight of turbine [kg]	0.138E+06
Additional weight [kg]	0.756E+06
Total dry weight [kg]	*4.704E+06*
Added mass in surge/sway [kg]	6.29E+06

Table 2: Masses used in numerical model

The mooring system is defined with three parallel tendons organized in an equilateral triangle. The tendons are organized such that all tendons have the same moment arm to the center of the column which is placed in the triangles center of gravity. The tendons vertical fastening point can be adjusted in the script. This is done in order to see how vulnerable the design is for this parameter. The tendons are defined as hollow cylinder and are made of steel. Tendon diameters are defined such that weight in water is equal to zero in order to avoid additional weight which leads to lower pretension of the system. The pretension in the tendons is determined by the net buoyancy of the system. In Figure 19 is the mooring system shown together with the body and in Table 3 is the most

important numerical values presented. The triangular plate is not modeled in the numerical model, but is shown to illustrate how the tendons are organized with respect to the column.

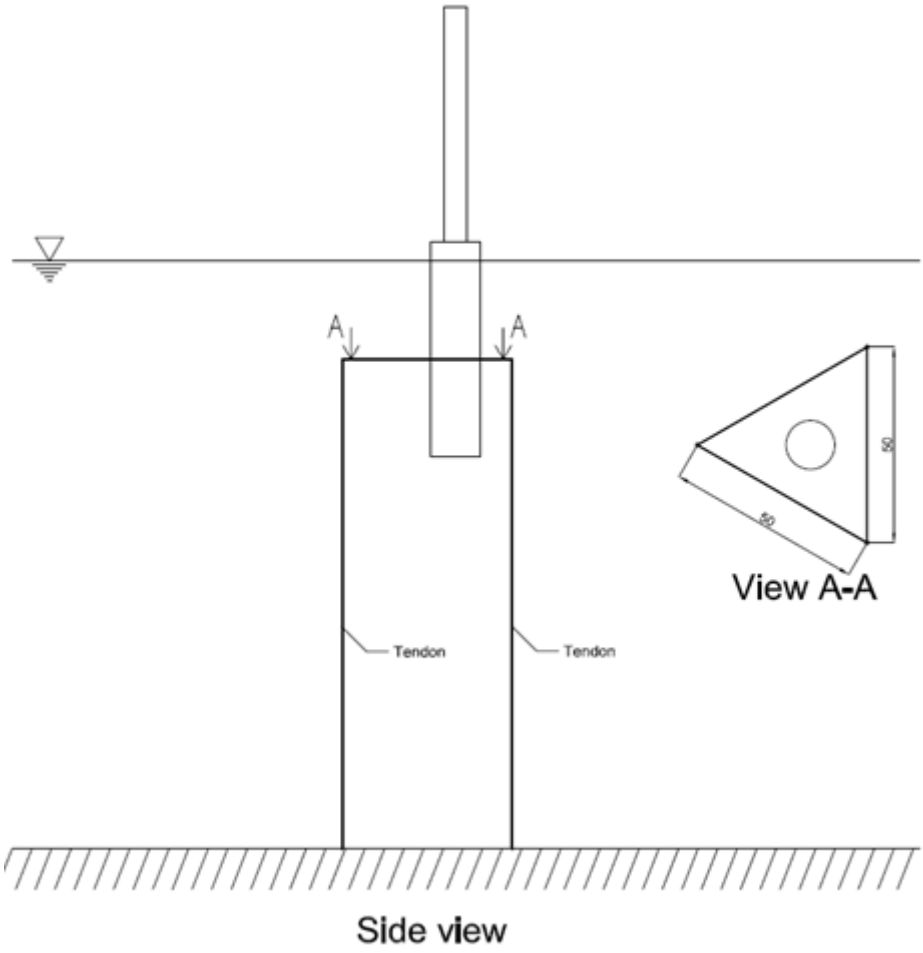

Figure 19: Overview of mooring system on numerical model.

Mooring system	
Parameter	**Value**
Number of tendons	3
Distance between tendons [m]	50
Tendon outer diameter [m]	0.6
Tendon inner diameter [m]	0.56
Tendon length at 50 m draught[m]	125
E-modulus [N/m^2]	2.10E+11
Density [kg/m^3]	7850

Table 3: Mooring system dimensions

4.1.1 Eigenfrequencies

The eigenfrequencies of the system are defined from the equations presented in 3.2.1. Since eigenfrequencies are dependent on main parameters of the system, frequencies in the different degrees of freedom have been used in order to decide upon dimension etc. Many variations have been done on the structure, and the main target of the final values is to keep the frequencies in

relevant degrees of freedom outside the wave-loading frequency range. The final eigenfrequencies for all degrees of freedom are presented in the result chapter.

4.2 Environment

4.2.1 Waves

The sea state in the calculations is defined by a sinusoidal regular wave with a total wave height H, and period T. In Matlab the time vector is defined with a step of 0.25 s, hence will the length of the time vector be four times the wave period. This is seen as sufficient in these calculations. The wave profile for a wave is shown in Figure 20. A wave with height 25 m and period 15 s is used to illustrate the different parameters.

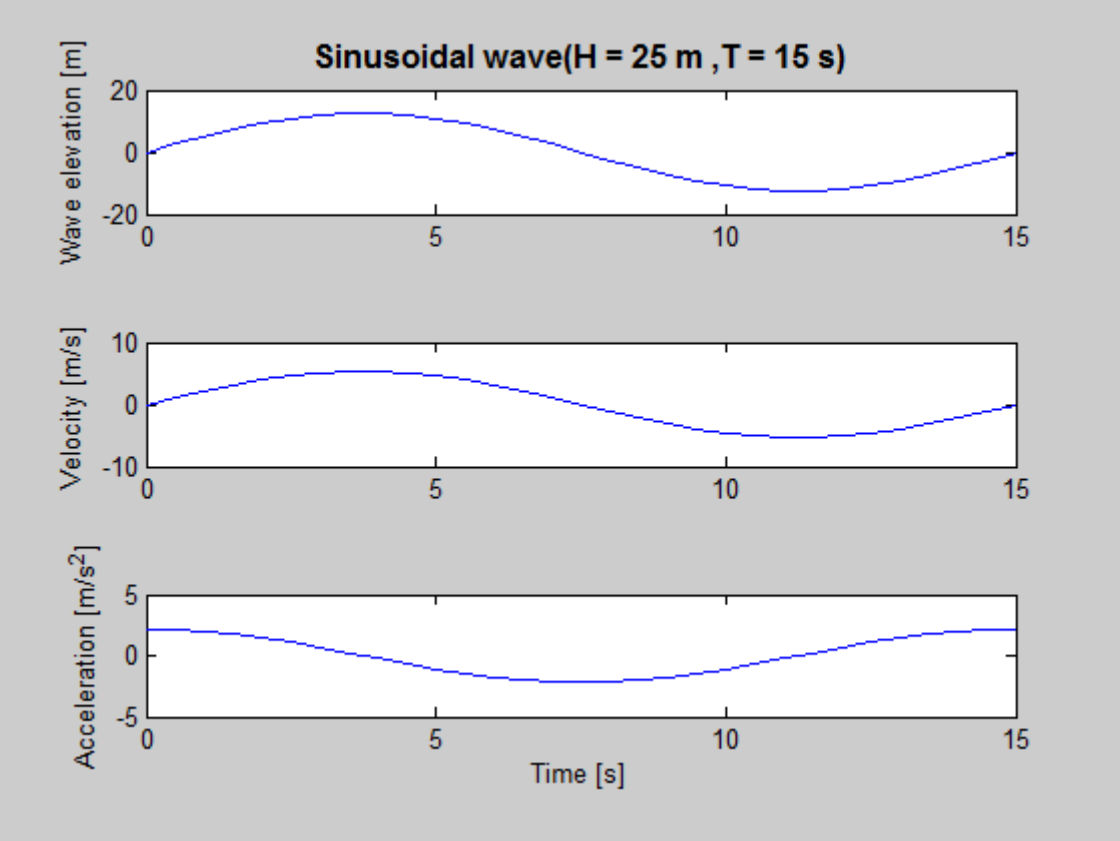

Figure 20: Sinusoidal wave with corresponding velocity and acceleration

When deciding the wave forces on a body the structure can as mentioned in section 3.3.1, be categorized in; Drag- and Mass dominated structures.

The mass- and drag force are illustrated for three different waves in Figure 21. It can be seen that for a wave with height 10 m and period 10 s, the mass force is by far governing. If the period is increased it is seen from the plot in the middle that the mass force is decreased while the drag force is almost the same. In the lowest plot the height is increased while the period is the same as in the upper plot. The drag force contribution is much larger than for lower waves but the mass force is still governing. This means that as the waves get higher the drag force will be of more interest, and as the period gets higher the drag force is of less interest. The forces' maximum will however not appear at the

same time, and the drag force will therefore not contribute to a larger maximum- or minimum value of the overturning moment.

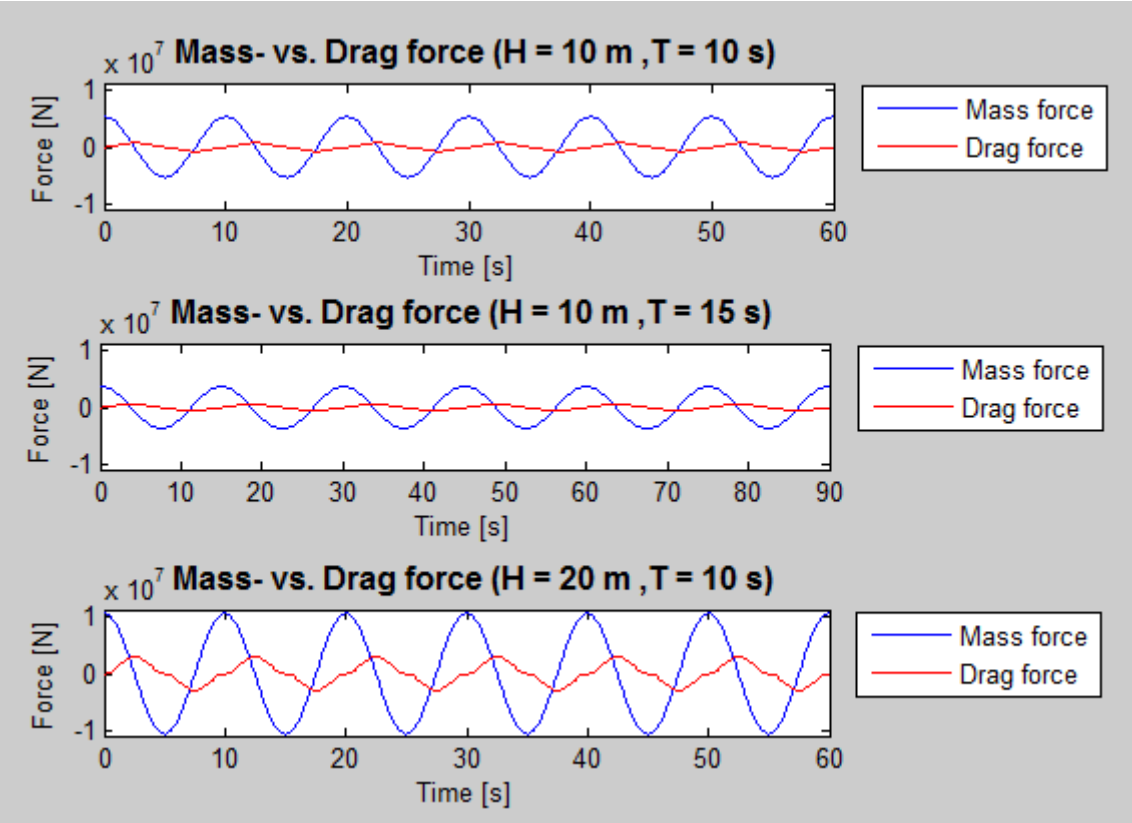

Figure 21: Mass- versus Drag force for three different waves

Due to the above mentioned effect from variation in wave parameters the total force on the structure is taken as the mass force. With a diameter of 12.5 m and a wave height of 20 m the structure is also in the mass-dominated area according to Figure 12.

The wave force in the calculation will therefore be in phase with the horizontal particle acceleration. Figure 22 show the profile of the acceleration over the depth.

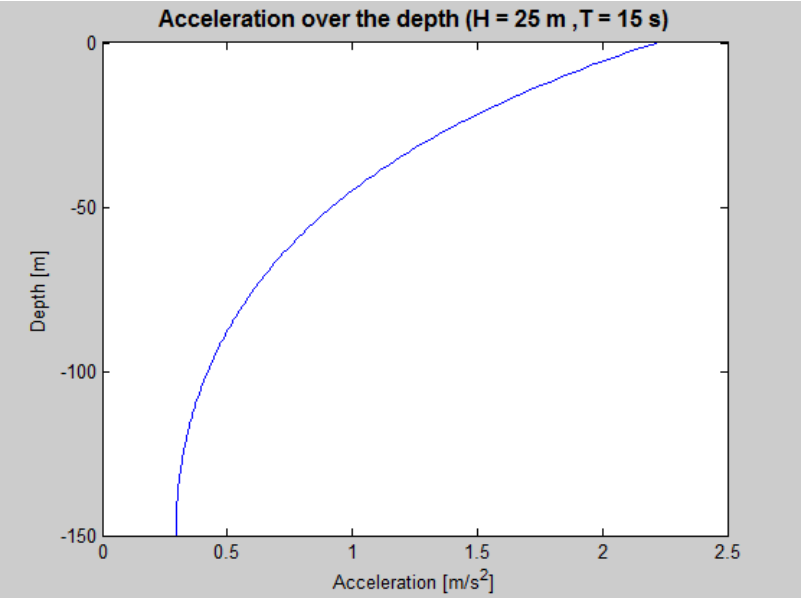

Figure 22: Maximum acceleration over the depth for a wave with H=25 m & T=15 s.

Due to the sinusoidal variation in the acceleration, the mass force will be a sinusoidal function in phase with the horizontal particle acceleration from the wave. The force is found, by doing a trapezoidal integration over the draught of the body with the corresponding acceleration. When the acceleration is at its maximum positive phase, the wave force over a wave-period will look like in Figure 23.

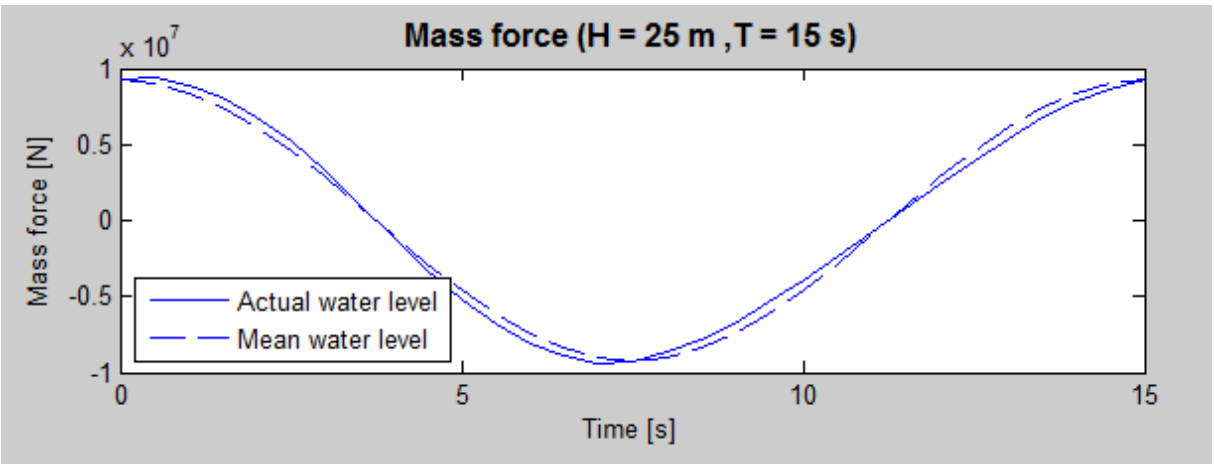

Figure 23: Total mass force over a period when integrating to mean water level

The force presented as a dashed line in the Figure 23 show the mass force when integration is done to the mean water level. This may seem like a simplification that can give limited results, especially for a large wave where the actual water level i.e. the submergence of the structure increases. When a structure is mass-dominated, the largest forces will however occur when the wave is at the zero-level (when the acceleration is at its maximum). The solid line illustrates the mass force when integration is done to the wave profile.

We see that there are small differences in the mass force when integrating to actual water level compared with mean water level. The simplification with zero-level integration is therefore used further in the calculations.

The wave load is calculated based on the largest column diameter regardless of the wave height. This column diameter will decrease 5 m above the mean water level. This means that if the wave amplitude exceeds 5 m above mean water level where the diameter is narrower, the wave loading will be conservative compared to the real case.

Similar comparison is not executed for the drag force since this force is not included in the calculations. The drag forces' maximum is at the wave crest and trough, and it is therefore likely that there is larger difference for that force contribution.

A scatter diagram with H_s and T_P values for the Statfjord area is investigated in order to see what sea states that can be expected as annual values in an area with 150 m water depth. According to Haver (2011), the data will from this diagram give 100 year values for Hs and Tp on 14.5 m and 16.5 s respectively. However, some calculations are performed to confirm these values. A Weibull distribution is used to obtain both significant wave height and maximum wave height. The significant wave height-values are obtained by plotting the cumulative probability with linear axis and further find a linear regression from the points. A plot of the regression can be seen in Figure 24. It should be noted that the lowest points in the regression is excluded to fit the higher values better seeing that these values are of the most interest.

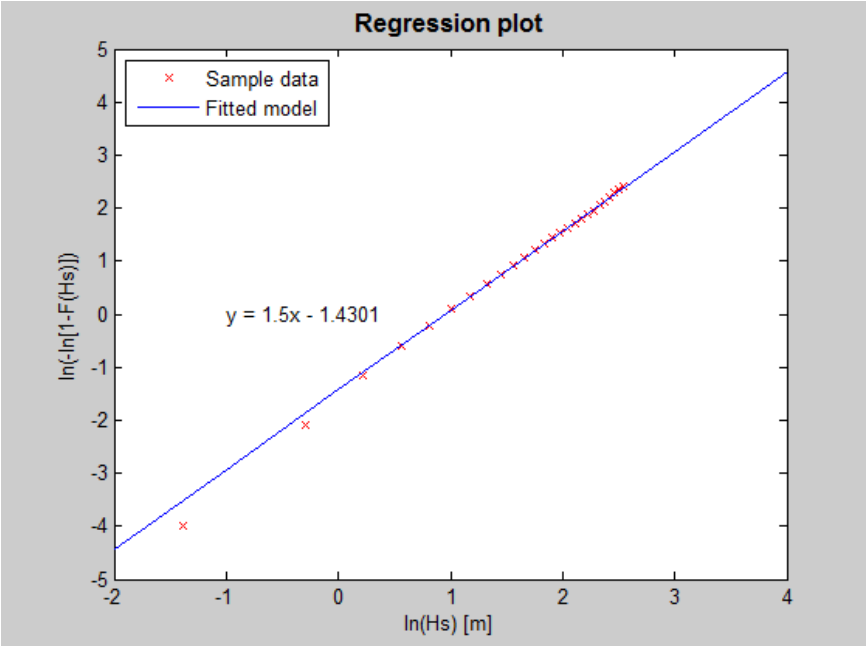

Figure 24: Linear regression of probability plot

The linear regression line has the following form;

$$y = ax + b \tag{4.1}$$

In Figure 24 we can see the distribution parameters in equation (4.1) to be;

$$a = 1.5 \qquad b = -1.43 \tag{4.2}$$

Further can the significant wave height be calculated with; Myrhaug (2007)

$$H_{m0,n} = \rho[\ln(N)]^{\frac{1}{a}} \tag{4.3}$$

Where;

$$\rho = e^{-\frac{b}{a}}$$

$$N = \frac{n \cdot 365 \cdot 24}{3} \qquad n = return\ period\ (years)$$

The most probable largest wave height during n years can be obtained by using the following relation, Myrhaug (2007.)

$$H_{max} = H_{m0}\sqrt{\frac{\ln N}{2}} \tag{4.4}$$

To obtain the peak period from the significant wave height values, a plot of the peak period as a function of significant wave height is used. A 90 percent confidence interval is also plotted together with the period. This can be seen in Figure 25.

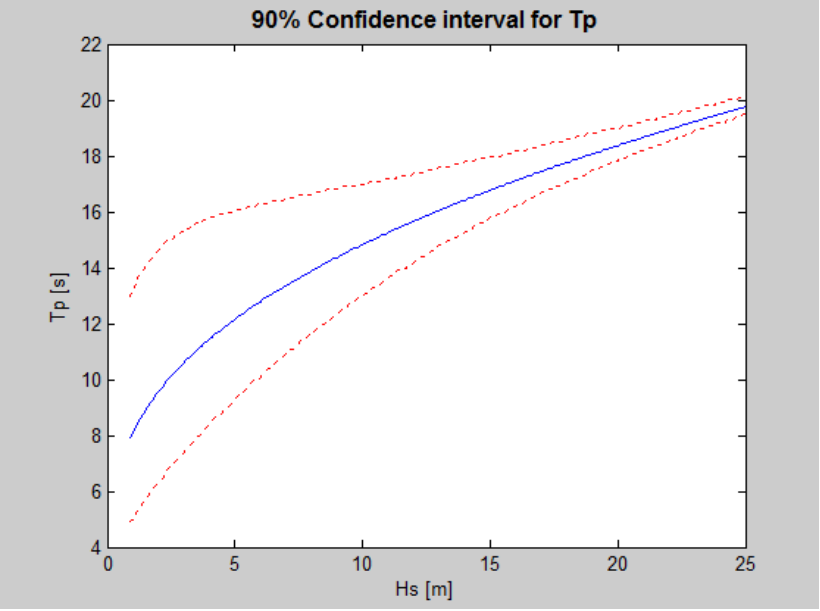

Figure 25: 90 percent confidence interval for peak period as a function of significant wave height

The period for the largest wave according to Myrhaug D & Kjeldsen S (1986) can be found by;

$$T_{Hmax} = 1.3 \cdot T_{m02} \tag{4.5}$$

According to Myrhaug (2007) is the ratio T_P/T_{m02} equal to 1.41 for spectra of PM type. For this purpose, when the values are meant basically for comparison this ratio is seen as satisfactorily when finding the zero crossing period (T_{m02}).

A summary of the annual wave values can be seen in Table 4.

Return period [years]	H_s [m]	T_P [s]	H_M [m]	T_{Hmax} [s]
10	12.3	15	27.9	13.8
100	14	16	30.9	14.8
1000	15.7	17	33.6	15.7

Table 4: Annual values for wave height and period

4.2.2 Aerodynamics

The Aerodynamic forces on the rotor blades consist of lift and drag. In this thesis where the main focus is the motion of the structure, the drag forces are of most interest.

The wind turbine blades are long and slender structures. And for wind turbine blades with a span wise velocity component much lower than the stream wise, 2D aero foil data can be applied (Hansen 2008).Figure 26 illustrates a transversal cut of one blade together with forces due to wind.

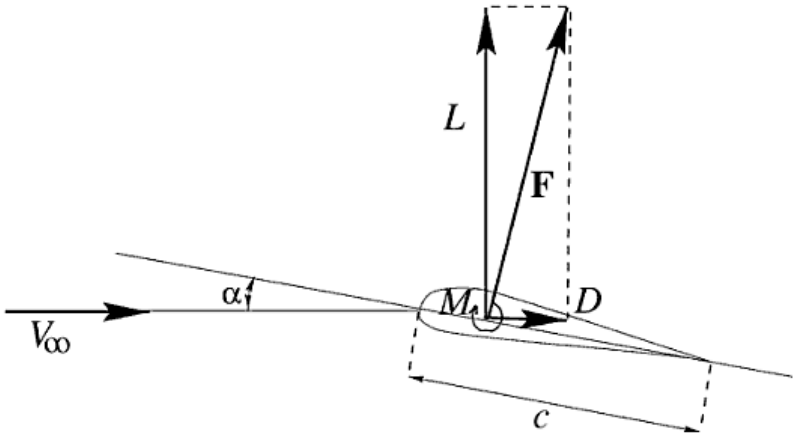

Figure 26: Definition of lift and drag (Hansen 2008)

Lift and drag coefficients per length unit, C_L and C_D are defined as;

$$C_L = \frac{L}{\frac{1}{2}\rho V_\infty^2 c} \tag{4.6}$$

And

$$C_D = \frac{D}{\frac{1}{2}\rho V_\infty^2 c} \tag{4.7}$$

The forces on the turbine blade will vary with different angles of attack. For a wind turbine it is not obvious that the highest lift coefficient is wanted since this may lead to a large rotational velocity which again can lead to damage on the turbine. In Figure 27 different coefficients are presented together with different angles of attack.

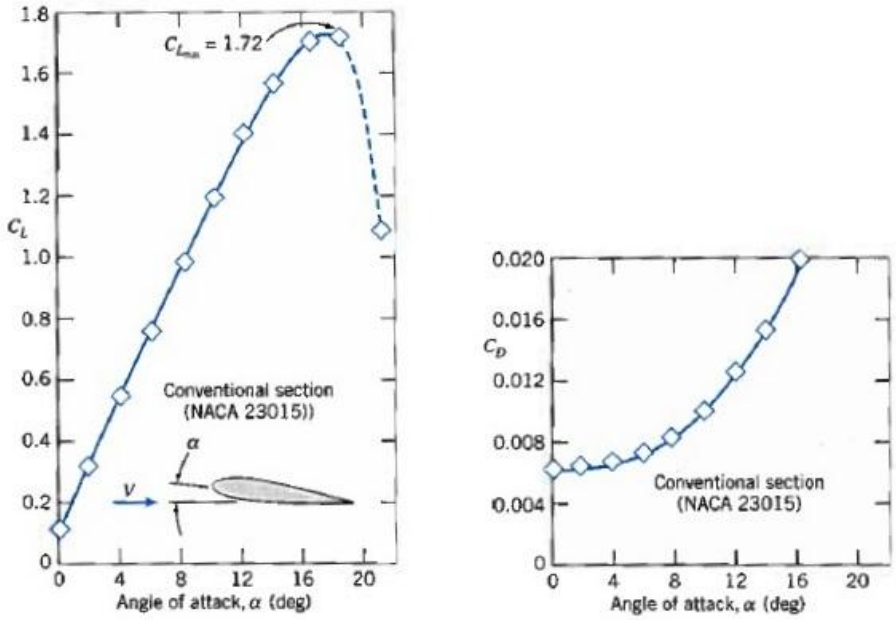

Figure 27: Lift- and drag coefficients for different angles of attack (Fox et. al 2004)

If a chord length and angle of attack is assumed, the lift- and drag forces acting on the rotor can be found. For a foil of the same type as above (NACA23015) 15 degree angle of attack is seen as a reasonable value to use since this will give a rather high lift coefficient. This leads to a lift coefficient of 1.6 and a drag coefficient of 0.016.

When it comes to chord length on typical blades, this parameter will probably vary over the blade length, thus is a parameter not easy to find. However, for these calculations a constant value assumed, and is intended to represent an average of the chord over the length of the blade. The chord length, c is taken as 3 m.

To get the force on the whole length of the blade it is necessary to rearrange and multiply equation (4.6) and (4.7) with the blade length l, and again multiply this with number of blades to obtain total force on the rotor.

The length of the blades, l is taken as half the rotor diameter (82.4/2 = 41.2 m).

Number of blades, n is 3.

Air density ρ_A, is taken as 1.204 kg/m^3

The forces are then given as;

$$D = \frac{1}{2} C_D \rho V_\infty^2 c l n \quad (4.8)$$

$$L = \frac{1}{2} C_L \rho V_\infty^2 c l n \quad (4.9)$$

Forces on rotor blades in different wind conditions			
Wind description (Acc. to Beaufort scale)	**Wind mean speed [m/s]**	**Total drag force [N]**	**Total lift force [N]**
Gentle breeze	4.4	69.2	6 914.5
Strong breeze	12.3	540.3	54 033.9
Gale	18.7	1248.9	124 893.4
Storm	26.45	2498.7	249 866.2

Table 5: Overview of forces on rotor in different wind conditions

As seen from Table 5 above the drag forces from wind acting on the rotor are quite small for the lower wind speeds. The higher speeds give larger contributions, but the relevance of these values can be discussed, since the blades often are pitched so that the rotation stops at high wind speeds. It is therefore decided that the wind forces on this stage of the motion analysis can be neglected.

4.3 Motion of structure

The motion characteristic in surge direction is calculated based on the solution of the differential equation presented in section 0. The motion together with velocity and acceleration of the system can be seen in Figure 28. The maximum wave amplitude is used as load value in the system, and a damping ratio of 10% is introduced to the system.

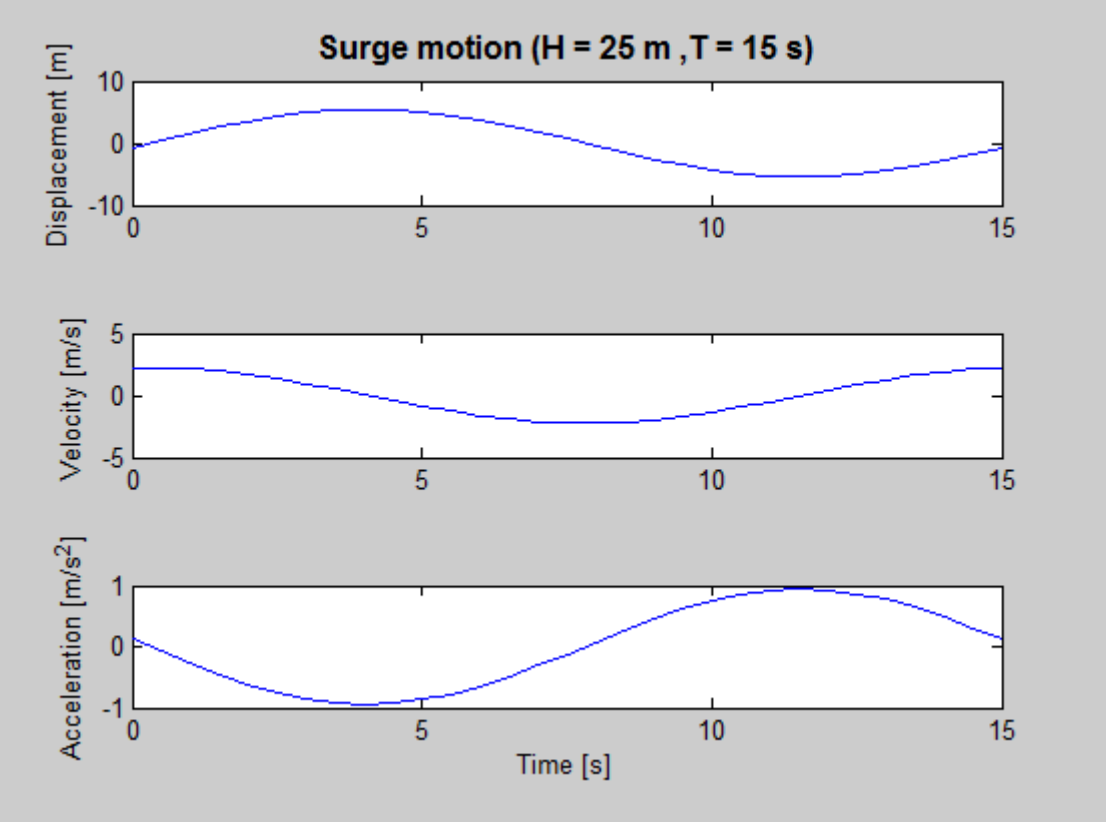

Figure 28: Surge motion for numerical model together with velocity and acceleration

From the figure we can see that the structure will oscillate around zero with the same motion amplitude both in positive and negative direction. The velocity has its maximum values as the structure passes the center, while the acceleration is largest at the motion extremes.

4.4 Tendon forces and overturning moment from wave loading

For the numerical model it is necessary to calculate the forces in the tendons from the motion of the structure and the environmental loading on the structure. The forces are found by calculating the total overturning moment on the structure, and further solve a moment consideration with respect to the tendons. The moment consideration and the overturning moment are explained in the coming section. In order to find the forces from the moment is it necessary to introduce some restrictions. For pitch motion one is that the tension in tendon 2 and tendon 3 are equal and in anti-phase with tendon 1. Another is that the tension in tendon 1 is twice the tension as in tendon 2 and tendon 3. For other motions and wave headings restrictions also will be introduced, but will not necessarily affect the same tendons in the way mentioned here. This method will however lead to some limited results, and may not necessarily represent the total tendon loading.

An important parameter in the design of tension legged structures is the overturning moment. The tendons can only resist a certain loading before they go slack. The capacity in the tendons for this study is defined by the pretension and the distance to the tendon from the rotation point of the body. If the moment from the environmental loading together with the inertia moment exceeds the capacity in the tendons, they may go slack and lead to large snatch-loads when they go back in tension. The moment consideration is defined as in Figure 29 for pitch motion, and the different contributions cause a moment around point M. For other headings than explained here, the method is the same but with different values for parameters such as moment arm etc.

Coupled forces from pitch/surge and roll/sway may also occur when the structure get a heel angle (Larsen 2011). In order to find the total contribution from coupled forces it is necessary to include another degree of freedom (pitch- or roll angle) in the model. This will make the calculations more advanced than intended at this stage of the analysis. As an alternative estimates of the effect with respect to the stiffness in the rotational degrees of freedom are investigated. The estimates show that the contributions from the weight and buoyancy at a pitch- or roll angle will affect stiffness and hence eigenperiods insignificantly. The coupled forces are therefore omitted at this stage.

The pretension in the tendons is taken as the net buoyancy divided on number of tendons in the system. When a wave pass the structure the actual submergence of the structure will also vary and lead to enhancement and reduction in the tension. This is not included in the calculations, but may be considerable for large waves since the submergence can decrease a lot if a large wave passes. For a mass dominated structure will however the largest environmental loading occur when the wave elevation is zero. This effective submergence is therefore not included in the analysis. It may however show to be important if other forces or effects are affecting the structure when the wave elevation is at its minimum.

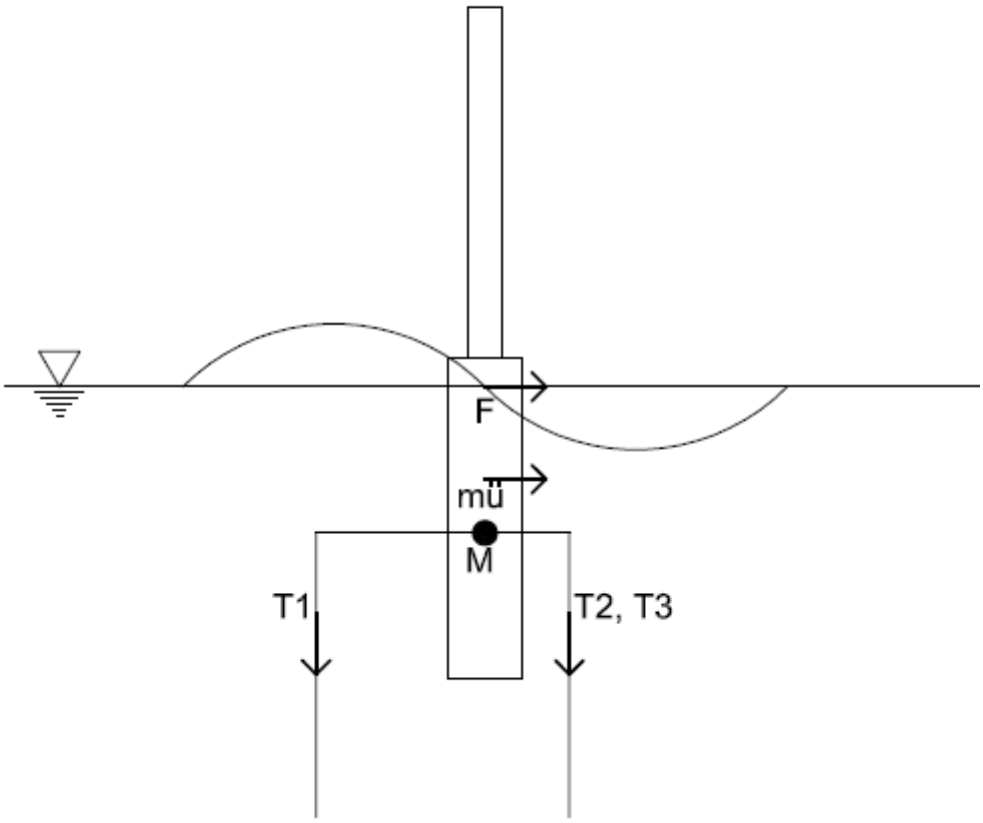

Figure 29: Definition of overturning moment in pitch motion

This gives the following simplified equation for pitch motion for the one degree of freedom system;

$$F_{wave} \cdot a_{wave} + m \cdot \ddot{u} \cdot a_{mass} = T_1 \cdot a_1 - 2 \cdot T_{2,3} \cdot a_{2,3} \quad (4.10)$$

Where

F_{wave} – Mass force from wave

a_{wave} – Distance from point M to point of attack for wave

m – Mass in surge motion including added mass

$\ddot{u}$ – Structure horizontal acceleration

a_{mass} – Distance from point M to center of gravity (added mass included)

T_1 – Tension in tendon 1

a_1 – Distance from point M to tendon 1

$T_{2,3}$ – Tension in tendon 2 and 3 (Assumed equal for pitch motion)

$a_{2,3}$ – Distance from point M to tendon 2 and 3

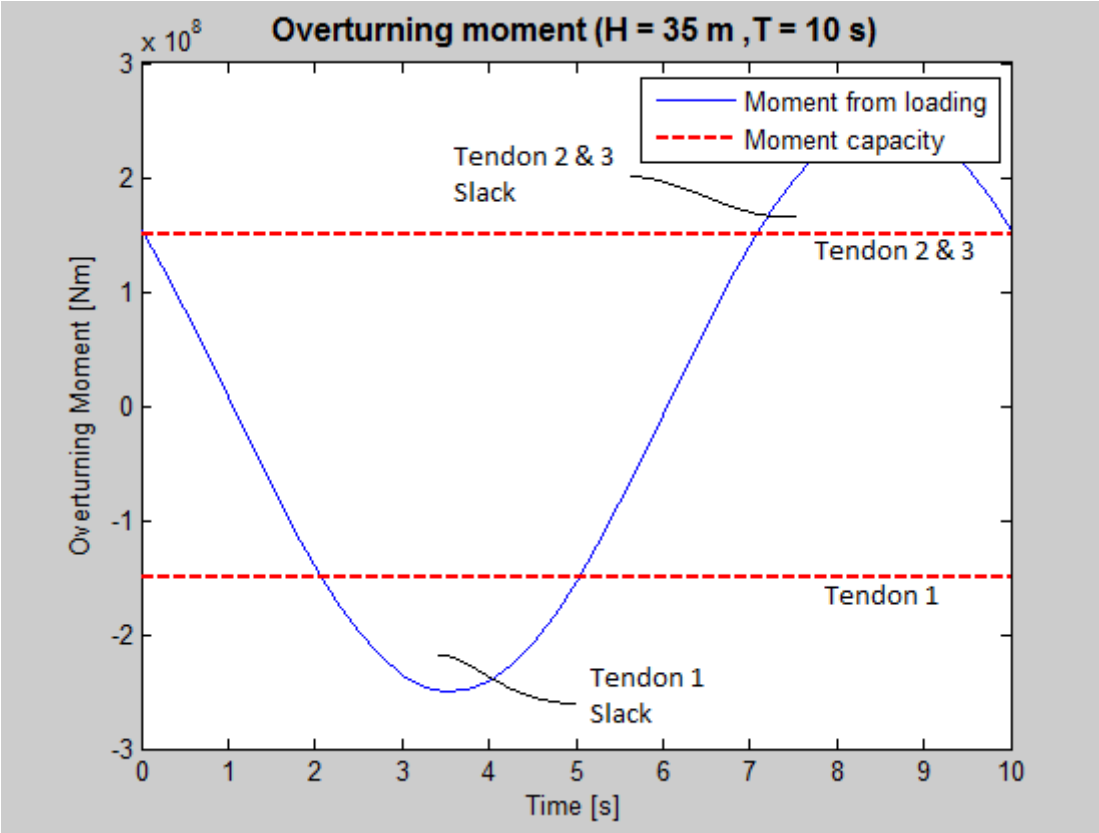

Figure 30: Overturning moment due to environmental loading and inertia forces

Figure 30 show the moment over a wave period for pitch motion. The blue line represents the left side of equation (4.10) with the wave loading and inertia moment, while the red lines illustrate the capacity in the tendons and the right side of the equation. The lower red line shows the moment capacity in tendon 1, while the upper represent tendon 2 and 3 together. The moment capacity will in theory be the same for tendon 1 as for tendon 2 and 3 together due to twice the moment arm in pitch motion. For a time instant, the distance between the moment capacity lines and the moment line will illustrate the remaining capacity in the tendons. A large distance is safe, but as the blue line gets closer to the red, the tension in the corresponding tendon approaches zero. The case illustrated in the figure above show that this wave is too large for the system to handle, and therefore all tendons will go slack during a wave period.

5. Laboratory test

In the laboratory test a 1:100 scale model is to be investigated. The water depth in the MC lab is limited to 1.5 m. This is a suitable depth for representing the full scale water depth of 150 m which is used in the one degree of freedom calculations. The model is to be fixed to the tank bottom and subjected to regular waves with varying height and period. A lab test specification written in advance of the experiment is enclosed in appendix B.

5.1 Scaling laws

The model should represent the full scale system as close as possible in a much smaller scale. To be able to represent the behavior in a model, we need to follow scaling laws.

In order to make the model test a satisfactorily representation of the full scale, three types of similarities are required (Steen et. Al. 2010):

- Geometrical similarity
- Kinematic similarity
- Dynamic similarity

Geometrical similarity involves that all model dimensions have the same proportions as the full scale structure. I.e. the relationships L/B, B/D etc. are equal in model scale and full scale. To fulfill this requirement, all geometrical details on the model must in principle have the same proportions as in full scale, and the requirement also applies to the surrounding environment. However, for practical reasons only the details of importance for the test are modeled. In this case, this means that the part of the structure that is above the sea surface is not of most importance as long as the vertical center of gravity etc. is modeled correctly.

The requirement is summarized in the length scale, which is the ratio between any dimension on the structure and the model:

$\lambda = \frac{L_F}{L_M}$, where L_F and L_M can be any dimensions of full- and model scale.

Kinematic similarity involves that ratios between velocities in model scale are equal to ratios between velocities in full scale. An example may be the ratio between the ship speed and the propeller rotational speed on a ship model. This requirement will not be of importance for our model.

Dynamic similarity is obtained through having the same ratio at model scale and full scale for the different force contributions present in the problem. In principle, this includes the following contributions (Steen et. Al. 2010):

1. Inertia forces
2. Viscous forces
3. Gravitational forces
4. Pressure forces
5. Elastic forces in the fluid
6. Surface forces

5.2 Test setup and test plan

The test is executed in the Mclab at NTNU. The Department of Marine Technology is the operator of the facility; hence the tank is mostly used in Master- and PhD-projects, but is also available for external users. The dimensions of the tank is 40 m x 6.45 m x 1.5 m (L x B x D), and contain a wave maker able to generate regular waves with maximal height of 0.25 m and wave periods between 0.3 and 3 seconds according to (NTNU, 2011). An overview of the tank, together with the coordinate system used in the laboratory test is shown in Figure 31.

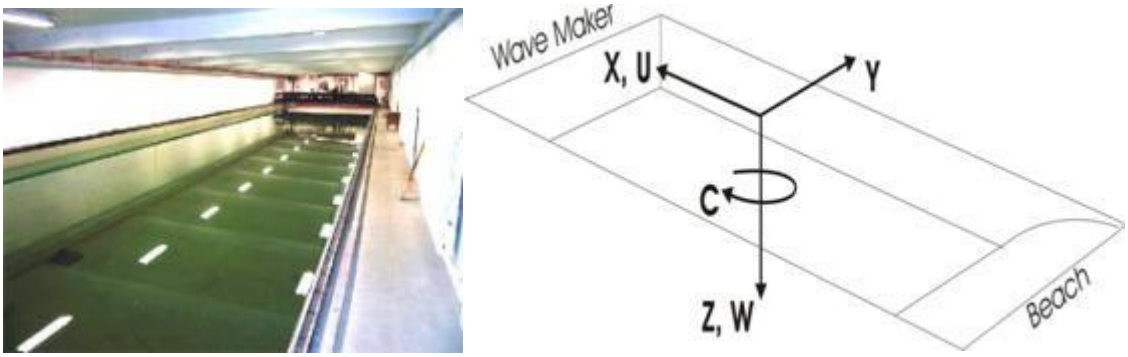

Figure 31: Overview of test facility together with coordinate system used (NTNU, 2011).

5.2.1 Model

The model is built by Marintek, and is a simplification of the final design. It consists of a 1.5 m high uniform column, a steel plate and tendons. The column is made in plastic, has a diameter of 0.125 m and is closed in the lower end. The steel plate is an equilateral triangle with sides of 0.50 m, a thickness of 6 mm and has a fastening point for the tendons in each corner. In the center of the triangle is a circular hole with diameter 0.125 m. The steel plate can be thread onto the column and adjusted to the wanted vertical position. The tendons are made of 5 mm steel bars.

After the model was tested in decay tests and exposed to regular waves it was clear that the steel bars used for tendons, was way too stiff to represent the tendons in the numerical model, and a potentially full scale structure. It was therefore decided to rebuild the model, and replace the steel bars with wire. The model was rebuilt by the undersigned, and the original model is shown in Figure 32 while the new and original tendons are shown in Figure 33. Additional pictures of model are enclosed in appendix C.

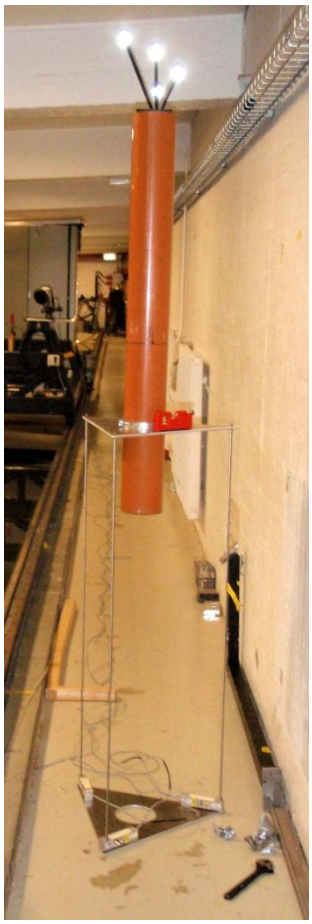

Figure 32: The model as it was originally built

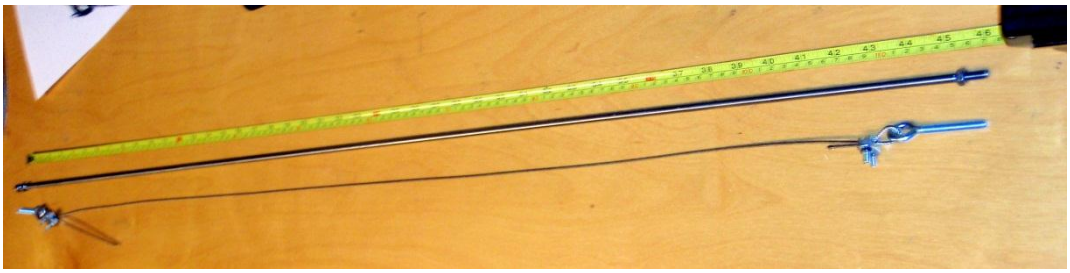

Figure 33: The original tendons together with the new tendons made of wire

In principle, it is possible to adjust the wire-length of tendons which again will make it possible to adjust the vertical position of the upper fastening point of the tendons. This could be interesting in order to see how vulnerable the design is for vertical position of tendon termination. However, this is a time consuming process to fit the length of the tendons to be as uniform as possible. Therefore the wires will in principle have constant length for the laboratory test when they first are fitted due to the time consuming process fitting them. Since time is a limiting factor in the experiment it is more favorable to adjust e.g. the draught of the column, which is a much quicker process and also can give interesting results.

The total mass of the model is 4.59 kg, which is a bit more than what was expected due to a heavy steel plate used as mooring attachment arrangement. In Table 6 specific parts of the model are shown with their respective mass and center of gravity.

Mass distribution of scaled model		
Part	**Mass**	**Center of gravity (w.r.t. bottom of column)**
Column	2.53 kg	0.575 m
Mooring steel plate	1.68 kg	0.225 m, 0.25 m ,0.275 m, 0.30 m
Positioning sensors	0.38 kg	1.15 m
Whole structure	*4.59 kg*	*0.49 m, 0.50 m, 0.51 m, 0.52 m*

Table 6: Mass distribution of scaled model

The draught have been adjusted in some of the tests (0.45 m, 0.5 m, 0.55 m and 0.6 m) and steel plate- and total center of gravity will therefore vary. Adjustments are performed by moving the column deeper and keep the length of the tendons constant. Since an elongation/abbreviation would lead to more use of time in an already tight scheme, this was considered as the best solution. The default draught is 0.5 m and is used if nothing else is mentioned.

5.2.2 Instrumentation

Following equipment was used for measurements during the test;

- Amplifier
- Real-time positioning system
- 3 force sensors
- Wave sensor
- Laptop (with Catman software installed)

How the different equipment is organized, is illustrated in Figure 34.

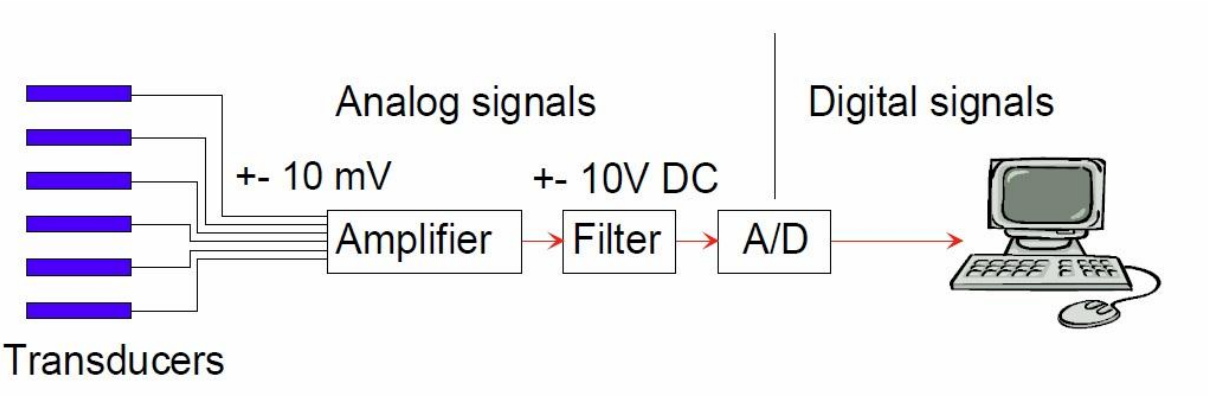

Figure 34: Overview of acqusition system for model testing (Steen S, 2011)

Transducers are used to measure the forces in the tendons, while a real-time positioning system tracks the motion of the structure in 6-dofs using optical tracking technology. A sampling frequency of 50 Hz is used for the force sensors while 25 Hz is used for the positioning sampling. Low pass filtering at 5 Hz is applied to the force signals to remove unwanted noise. The analog voltage from the transducers is low and the output is in microvolt. To amplify this signal, amplifier with the range +/- 10 volt is used. The amplifier has built-in analog to digital conversion.

The wave maker generates a wave with wanted height and period. However, it is not given that the generated wave corresponds to the theoretical wave ordered. Therefore a wave sensor is placed in the basin to track the real wave data.

The runs shown in Table 7 were executed during the laboratory test. Wave parameters presented in table are values ordered from the wave maker, and not measured values.

Test log			
Run number	**Wave height [m]**	**Wave period [s]**	**Wave heading [deg]**
Run52	0,05	0,5	0
Run53	0,05	1	0
Run54	0,08	1	0
Run55	0,1	1	0
Run56	0,1	0,8	0
Run57	0,15	1	0
Run58	0,15	1,2	0
Run59	0,15	1,5	0
Run60	0,18	1	0
Run61	0,05	0,5	60
Run62	0,05	1	60
Run63	0,08	1	60
Run64	0,1	1	60
Run65	0,1	0,8	60
Run66	0,15	1	60
Run67	0,15	1,2	60

Run68	0,15	1,5	60
Run69	0,18	1	60
Run70	0,05	0,5	90
Run71	0,05	1	90
Run72	0,08	1	90
Run73	0,1	1	90
Run74	0,1	0,8	90
Run75	0,15	1	90
Run76	0,15	1,2	90
Run77	0,15	1,5	90
Run78	0,18	1	90
Run79	0,15	1	0 (Draught 0.55 m)
Run80	0,15	1,2	0 (Draught 0.55 m)
Run81	0,15	1,5	0 (Draught 0.55 m)
Run82	0,18	1	0 (Draught 0.55 m)
Run83	0,15	1	0 (Draught 0.60 m)
Run84	0,15	1,2	0 (Draught 0.60 m)
Run85	0,15	1,5	0 (Draught 0.60 m)
Run86	0,18	1	0 (Draught 0.60 m)
Run87	0,15	1	0 (Draught 0.45 m)
Run88	0,15	1,2	0 (Draught 0.45 m)
Run89	0,15	1,5	0 (Draught 0.45 m)

Table 7: Test log for rebuilt model

5.3 Data analysis

Figure 35: Calibration of force sensor

5.3.1 Calibration

Before any tests are performed, a calibration of the different sensors needs to be executed. This is an important part of a laboratory test in order to get good results. It is done by exposing the sensors for a known physical value, and see what output value this leads to. When this is done several times a correlation to the physical value and the output voltage can be obtained.

For the force sensors known loads are applied and further is a correlation found. The calibrations are done by fixing the sensors and load them with incremental larger weights. Figure 35 show how the force sensor is calibrated. In Figure 36, the results from the calibration for the force sensor can be seen. The red marks, represent the measured points during the calibration while the blue line is a linear regression between the

points. On the graph we can see that the load leads to a negative output value and indicates that the load is applied in the negative direction. The linear regression equation gives the correlation factor, which later can be put into the software with the unit [N/V]. Multiplied with the output [V] this gives the force [N].

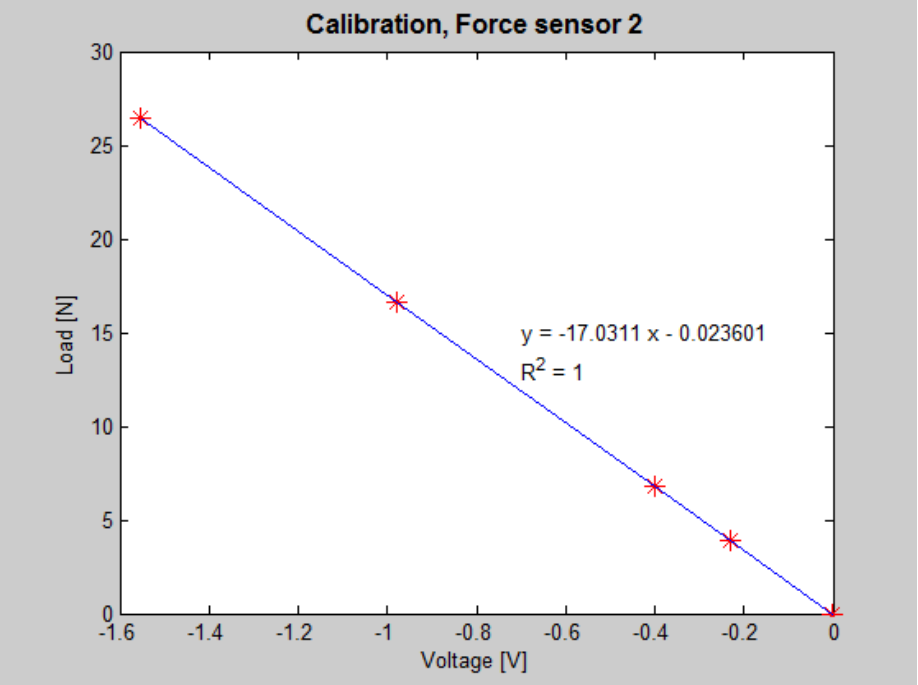

Figure 36: Regression of calibration measurements for force sensor

When it comes to the wave sensor, the principle is the same. The wave sensor is submerged to a number of known depths while the output value is tracked. Logged values are plotted and using a linear regression the correlation factor is obtained. This can be seen in Figure 37. The correlation factor from the wave sensor is given the unit [m/V] and multiplied with the output voltage gives wave elevation in [m].

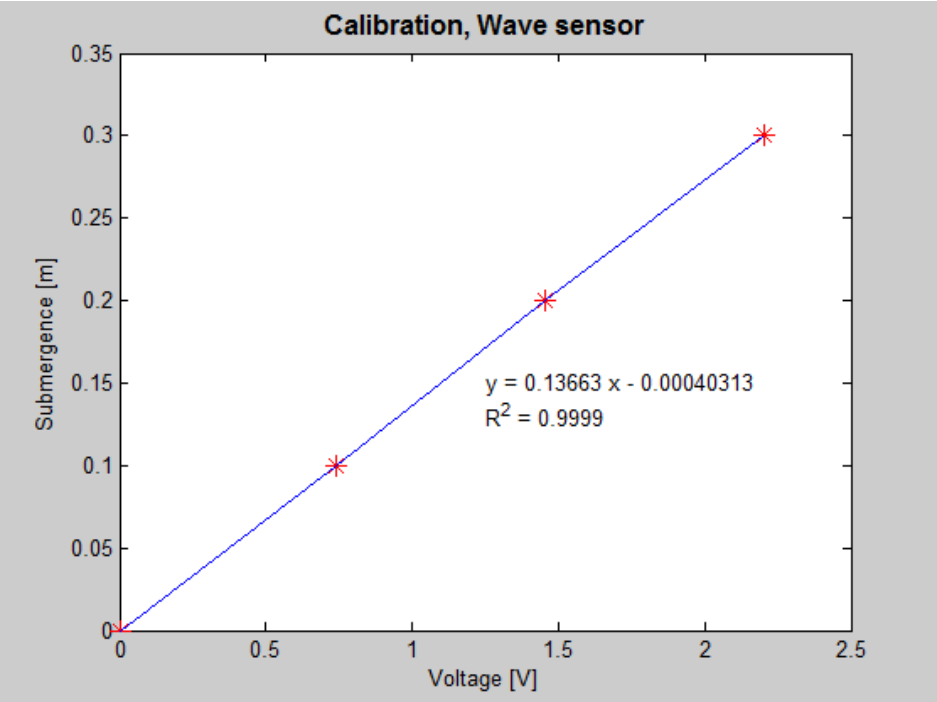

Figure 37: Regression of calibration measurements for wave sensor

A summary of correlation factors are listed in Table 8.

Correlation factors for sensors	
Force sensor tendon 1	-17.025 [N/V]
Force sensor tendon 2	-17.031 [N/V]
Force sensor tendon 3	-17.016 [N/V]
Wave sensor	0.137 [m/V]

Table 8: Correlation factors from calibration

5.3.2 Decay test

Decay tests are performed to decide the damping and eigenperiods in different directions for the structure. Decay tests are executed for the horizontal degrees of freedom (surge, sway and yaw). In this section methods used for finding damping and eigenperiods are presented.

The eigenperiod is found by generating spectra from the motion in the respectively directions. This was done by Fast Fourier Transform (FFT) using a specter generator from (WAFO 2011). The natural frequency is the frequency where most of the energy in the spectrum is concentrated i.e. the frequency corresponding to the maximum value in the power spectrum can be taken as the natural frequency of the model for the relevant degree of freedom. This is illustrated in Figure 38.

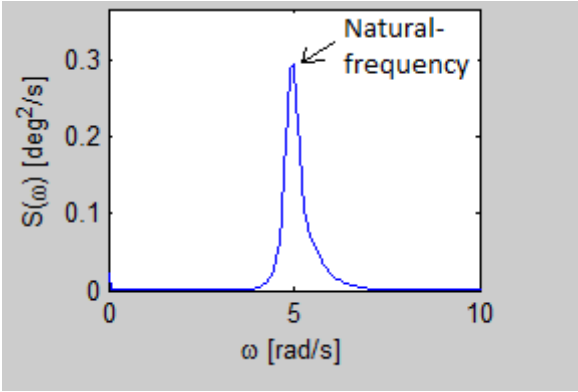

Figure 38: Finding natural frequency from specter

The damping of a vibrating structure can be grouped into structural damping, material damping and fluid damping. When a structure is vibrating in water, all three types of damping mentioned above contribute to the total damping. The different types of damping are difficult to separate from each other, but for a floating body as used in this laboratory test it is logical to assume that fluid damping gives the largest contribution. From the recorded decay test, damping ratios are found by applying the so-called log decrement. If Ui and Ui+1 are two consecutive amplitudes from the record, the damping ratio is given as (Larsen 2009):

$$\xi = \frac{1}{2\pi} \cdot \ln\left(\frac{U_i}{U_{i+1}}\right) \tag{4.11}$$

The method is illustrated in Figure 39.

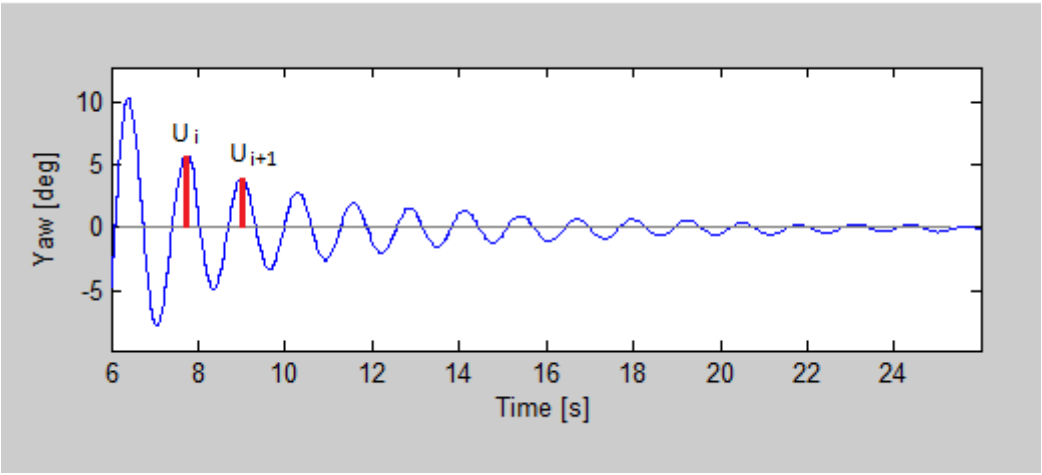

Figure 39: Finding damping ratio from decay test

6. Results

In this section results from laboratory tests and numerical calculations are presented. Results presented are basically design parameters taken from Demirbilek (1989).

For the regular waves presented, the structure is exposed to waves from different headings. The structure is exposed to waves from three different angles; zero, 60 and 90 degrees. In the laboratory test the model is rotated, hence the tendons will get a new position. In order to compare the results from the laboratory test and the numerical calculations this is also the case for the numerical model. The heading and the new position of the tendons are illustrated in Figure 40.

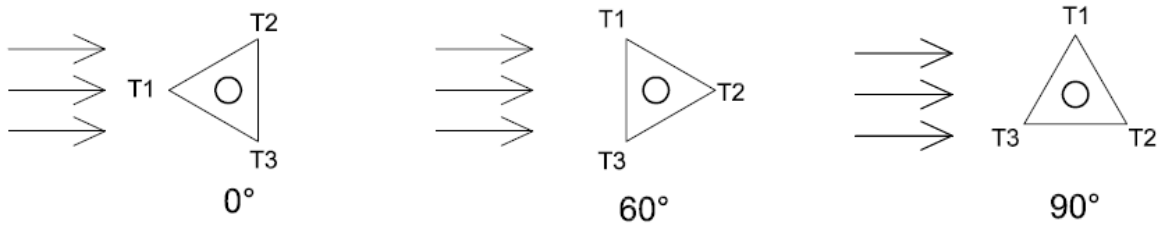

Figure 40: Different headings, and position of tendons at corresponding heading.

6.1 One degree of freedom system

The results presented in this section are based on calculations performed in Matlab. Wave heights and periods used for different cases are presented underway, but also in the top of each figure presenting results with wave generation. Wave parameters used are chosen so that numerical calculations are comparable with experimental results. It should be noted that the results in this section are presented as full scale values, while laboratory values are presented in model scale.

6.1.1 Vortex induced vibrations

VIV calculations for tendons and structure are executed for different current velocities. The velocities used in the calculations are taken as constant over the depth. VIV is a complex problem, and more thorough analysis should be performed for a final design. These calculations are meant mostly as a confirmation that VIV and VIM can occur for such structures.

Eigenfrequencies for a tendon with outer diameter 0.6 m and inner diameter 0.56 m are calculated for different eigenmodes, and shown in Table 9. The eigenperiods are the same both in-line and cross-flow.

Eigenperiods for tendons										
Eigenmode	1	2	3	4	5	6	7	8	9	10
Eigenperiod [s]	6.9	3.3	2.0	1.4	1.0	0.8	0.6	0.5	0.4	0.3

Table 9: Eigenperiods for tendons

Load periods for the tendons both in-line and cross-flow are presented in Table 10. These values are calculated from equation (3.1).

Load periods for tendons										
Current velocity [m/s]	0.2	0.4	0.6	0.8	1.0	1.2	1.4	1.6	1.8	2.0
Cross flow period [s]	15.0	7.5	5.0	3.8	3.0	2.5	2.1	1.9	1.7	1.5
In line period [s]	7.5	3.8	2.5	1.9	1.5	1.3	1.1	1.0	0.9	0.8

Table 10: Load periods for tendons at different current velocities

As seen from Table 9 and Table 10 there is danger for VIV to occur in tendons. Selected modes may be excited by certain current velocities due to coinciding vortex shedding period and eigenperiod.

The vortex shedding can also affect the motion of the structure if the vortex shedding period coincides with the eigenperiod in surge and sway. This motion is then referred to as vortex induced motion (VIM). The eigenperiod in surge and sway are 57.1 s, as presented in Table 13. Load periods from vortex shedding on the structure are shown in Table 11.

Load periods for column										
Current velocity [m/s]	0.2	0.4	0.6	0.8	1.0	1.2	1.4	1.6	1.8	2.0
Cross flow period [s]	312.5	156.3	104.2	78.1	62.5	52.1	44.6	39.1	34.7	31.3
In line period [s]	156.3	78.2	52.1	39.1	31.3	26.1	22.3	19.6	17.4	15.7

Table 11: Load periods for structure at different current velocities

Since some load periods coincide with the eigenfrequencies it is possible to experience VIM for a structure with given dimensions.

As mentioned, there will be a danger of both VIV and VIM to occur. VIV suppression, for example helical streaks, could be a way to adjust the vortex shedding frequency outside the eigenfrequency range and hence reduce the risk of resonant motions.

6.1.2 Air gap

The air gap is most commonly used for deck clearance on platforms. In this thesis the air gap is referred to as the distance from the lowest point on the rotor to the water surface. This distance will be on the smallest when the wave is at its maximum, and the rotor is rotated such that one blade points directly downwards. Due to small heave motions, this contribution is neglected when the air gap is calculated. If results from the coming section show otherwise this is a contribution that needs to be included. The air gap hence is calculated from the formula below;

$$Airgap = H_{nacelle} - \frac{1}{2}D_{rotor} - \frac{1}{2}H_{wave} \tag{6.1}$$

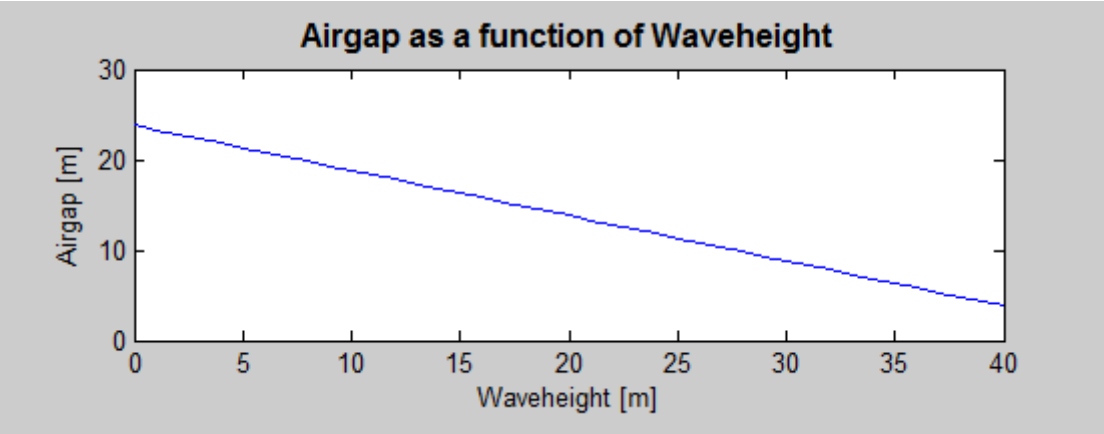

Figure 41: Air gap as a function of wave height

As seen from Figure 41, the air gap decreases as the waves are gets larger, which is expected. For a wave height of 40 m the air gap is about 4 m which should be sufficient since a 1000 year sea state corresponds to a maximum wave height of 33.6 m according to calculations in section 4.2.1.

6.1.3 System charachteristics

The pretension in tendons will be the net buoyancy force at a given draught divided by number of tendons. In the numerical calculations the total weight increase or decrease as the draught is adjusted, because the submerged column needs to be elongated or shortened. This is done in order to keep the nacelle 65 m above mean water level regardless of draught. When the pretension values from the numerical model are to be compared to the model test pretensions, there will however be a difference since the scaled model has a constant weight at all draughts. The different pretensions for the numerical model can be seen in Table 12.

Pretension and moment capacities in the numerical model				
Draught [m]	**Pretension [N]**	**Mom. Cap 0° [Nm]**	**Mom. Cap 60° [Nm]**	**Mom. Cap 90° [Nm]**
45	3.87 e6	+/- 1.11 e8	+/- 1.11 e8	+/- 0.97 e8
50	5.18 e6	+/- 1.49 e8	+/- 1.49 e8	+/- 1.30 e8
55	6.49 e6	+/- 1.87 e8	+/- 1.87 e8	+/- 1.62 e8
60	7.80 e6	+/- 2.25 e8	+/- 2.25 e8	+/- 1.95 e8

Table 12: Pretension and moment capacity for numerical model at different draughts

Eigenfrequencies for a draught of 50 m together with eigenperiods are presented for six degrees of freedom in Table 13.

System characteristics for numerical model		
Degree of freedom	**Eigenfrequency [rad/s]**	**Eigenperiod [s]**
Surge	0.11	57.12
Sway	0.11	57.12
Heave	6.25	1.00
Roll	2.24	2.80
Pitch	2.24	2.80
Yaw	0.25	25.13

Table 13: System characteristics for numerical model

As seen from table, all eigenfrequencies except Yaw are outside the first order wave frequency loading range according to theory. The Yaw values are therefore causing some concern. This structure is not taking much loading in the Yaw motion, but the parameter should nevertheless be looked carefully after.

6.1.4 Wave height = 10 m, Period = 10 s

This section will thorough investigate how forces, motions and overturning moment behaves for a wave with height 10 m and period 10 s. Three different wave headings are investigated, and the mentioned parameters are discussed for each of them in order to find possible unfavorable heading.

Heading = 0 degrees

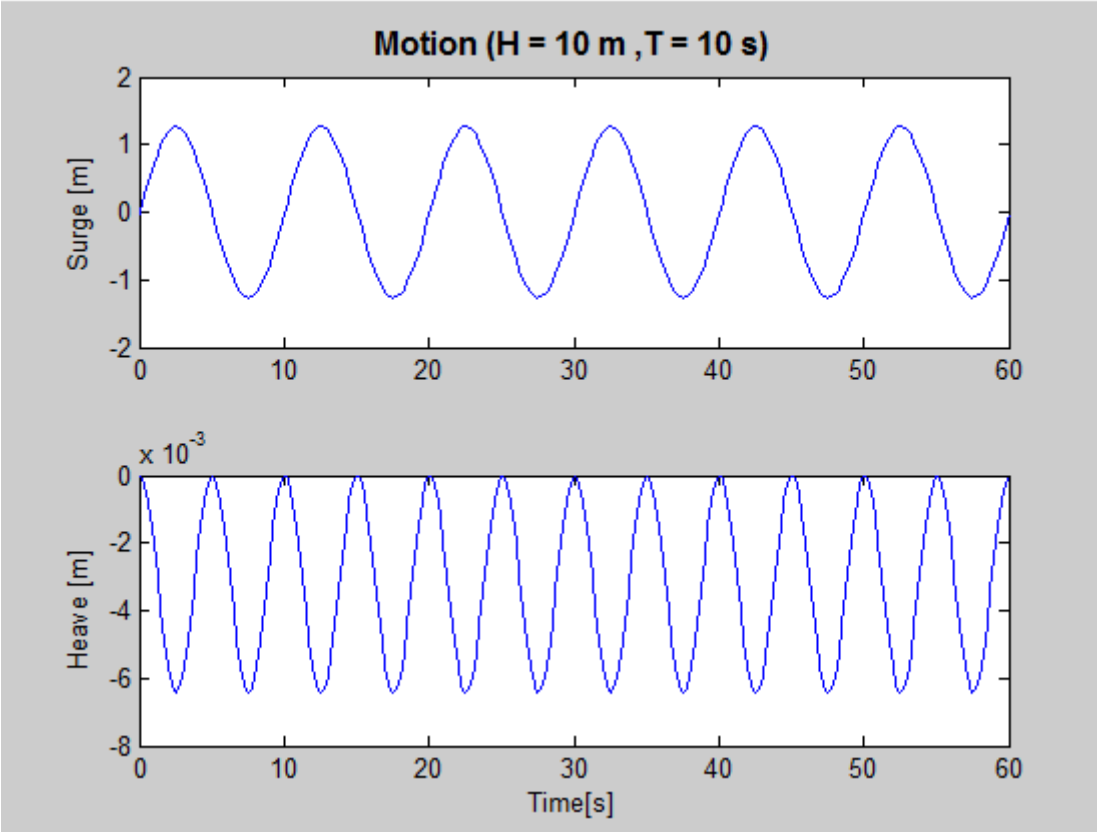

Figure 42: Motion of numerical model, H=10 m, T= 10 s, Heading = 0 deg.

In Figure 42 motion in Surge and Heave for the numerical model is shown. The Surge motion is calculated from the one degree of freedom theory presented in Section. 0. As seen the structures displacement amplitude is approximately 1.2 m in both positive and negative direction. The motion is symmetrical around the x-axis.

Heave motion is calculated on the basis that the tendons have constant length, and the Surge motion hence will generate a set down. The heave motion will never be positive since the tendons are defined such that no elongation occurs. As seen from graph, set down has twice the frequency of surge motion. This can be explained by that set down is generated on both negative and positive motion amplitudes. Due to relative small Surge amplitudes, Heave amplitudes are very small.

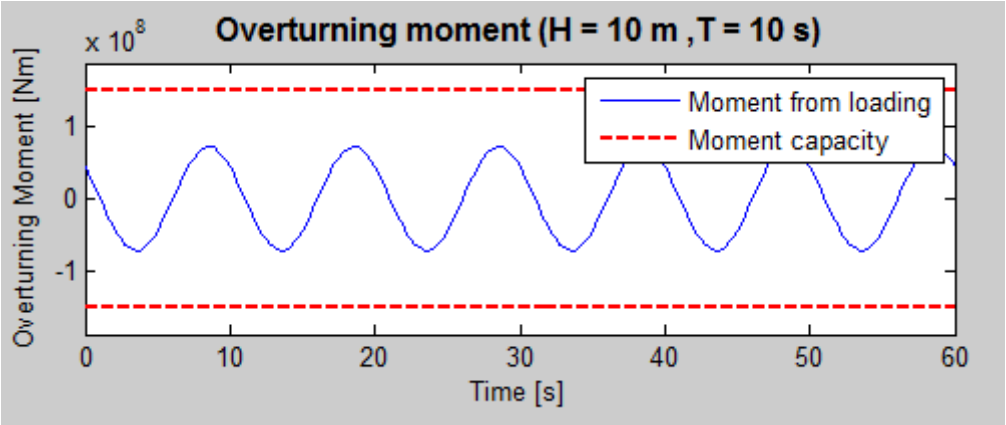

Figure 43: Overturning moment for numerical model, H=10 m, T= 10 s, Heading = 0 deg.

Overturning moment for the structure is shown in Figure 43. The moment, shown in blue, is calculated from the environmental loading and the inertia forces. In red the moment capacities are shown, and represent the pretension in the system. As seen from the figure, the margin to the moment capacity from the moment curve is good. This means that for the given wave there is no risk of tendons going slack.

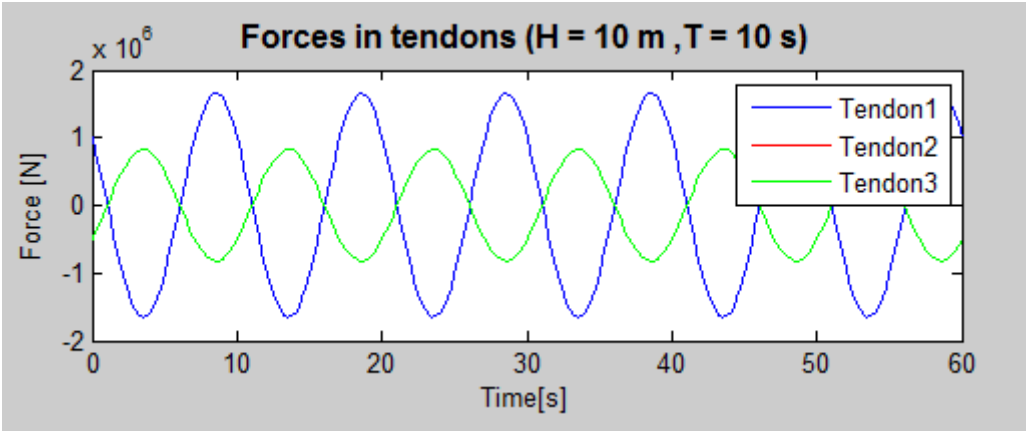

Figure 44: Forces in tendons for numerical model, H=10 m, T= 10 s, Heading = 0 deg.

Forces in tendons are shown in Figure 44. The forces are calculated from the overturning moment in Figure 43 and the moment consideration in section 4.4. The forces are, as mentioned together with the moment consideration influenced by the restrictions introduced in order to find the forces. It should be noted that the tension curve for tendon 2 is hidden behind the green line, as the tension in tendon 2 and tendon 3 are identical.

Heading = 60 degrees

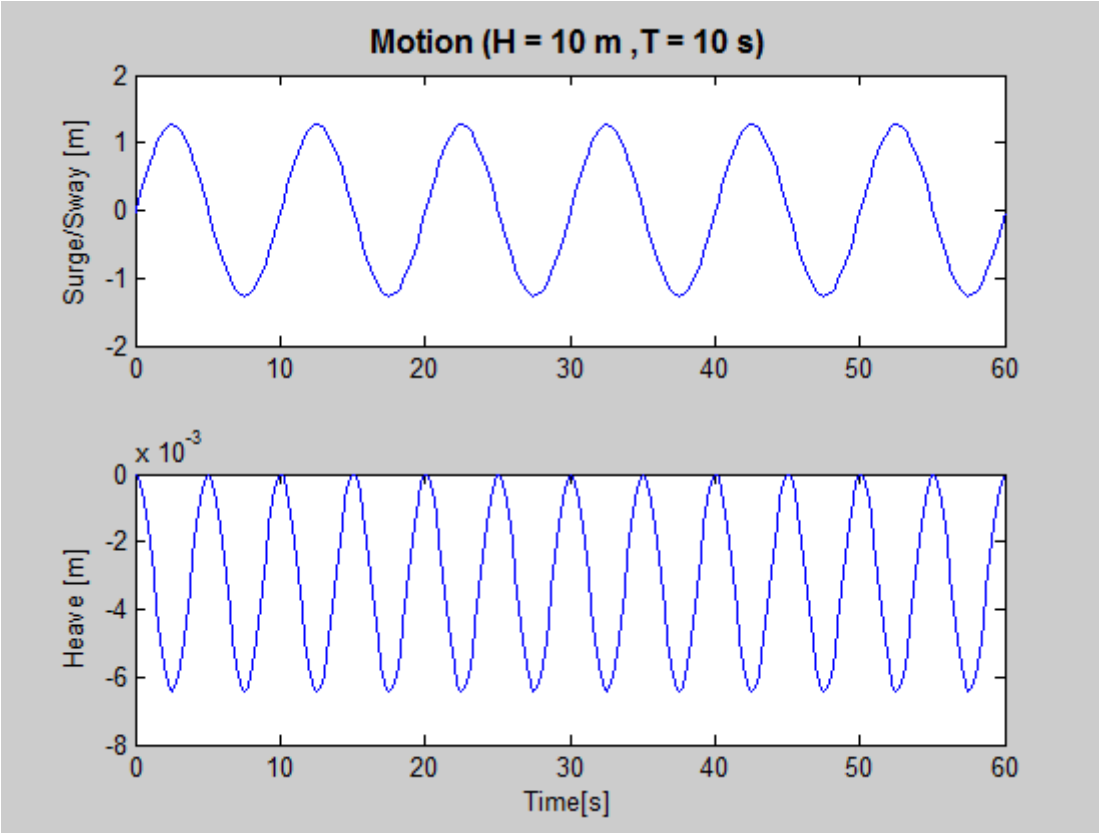

Figure 45: Motion of numerical model, H=10 m, T= 10 s, Heading = 60 deg.

Motion when the model is rotated 60 degrees is a coupled motion of Surge and Sway. This motion is presented together with the heave motion in Figure 45. The motion at this heading is identical to the motion presented in Figure 42, where the heading was zero degrees. The loading on the cylindrical column will be the same regardless of heading, and since the stiffness in these motions is identical the motion will also be the same. The Heave motion is calculated from the surge motion and will therefore be the same as for zero heading.

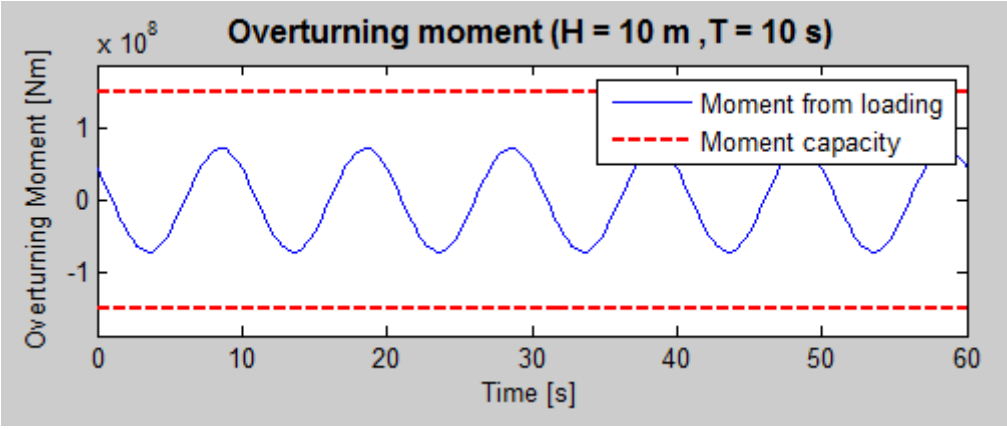

Figure 46: Overturning moment for numerical model, H=10 m, T= 10 s, Heading = 60 deg.

As mentioned above the loading on the cylindrical column will be the same for all headings. In Figure 46 the overturning moment for 60 degree heading is shown. It is seen that the moment is identical to the one presented for zero degree heading in Figure 43. The difference when it comes to heading from a moment point of view is that the moment capacity will change. In this case will however the capacity be the same as for zero degrees due to geometry.

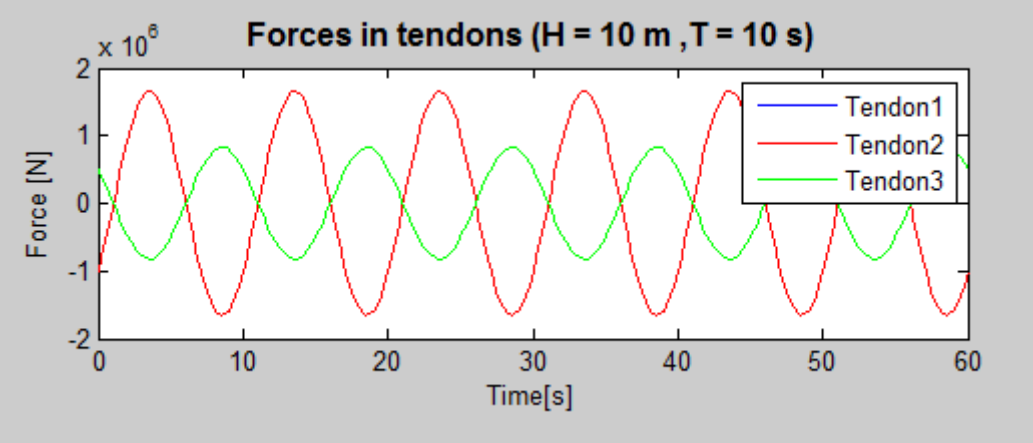

Figure 47: Forces in tendons for numerical model, H=10 m, T= 10 s, Heading = 60 deg.

Forces in tendons for 60 degree heading are shown in Figure 47. The forces in the tendons will be affected by the wave heading. The moment from environmental loading and inertia forces will not change due to the heading, but the moment is distributed differently to the tendons. This is clear in the figure above, where tendon 2 now is the one which is handling the largest loading. Tendon 2 is for this heading alone on the downstream side of structure. For this case tendon 1 will have the same tension as tendon 3 and is therefore not visible in the figure.

Heading = 90 degrees

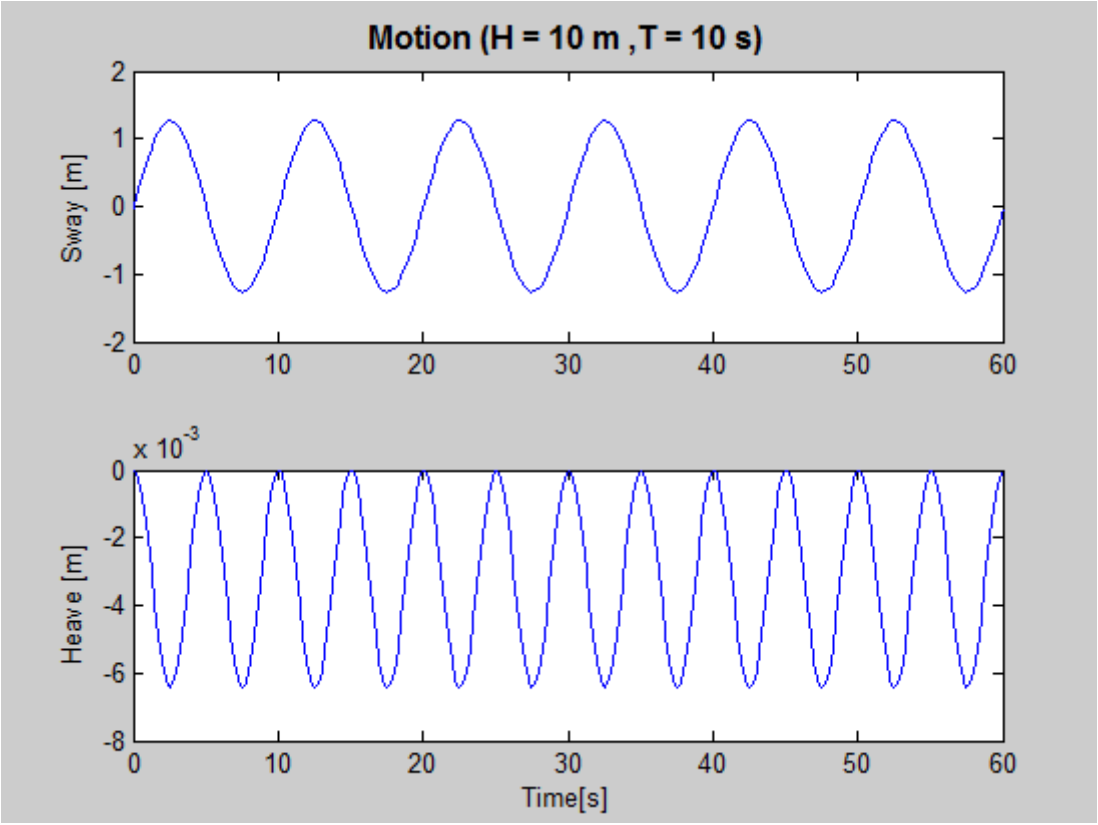

Figure 48: Motion of numerical model, H=10 m, T= 10 s, Heading = 90 deg.

Motion with wave heading 90 degrees is shown in Figure 48. Not surprisingly the Sway motion is identical to the motions presented for the other headings above. Since the loading and the stiffness is identical for all headings, the motion will also be identical.

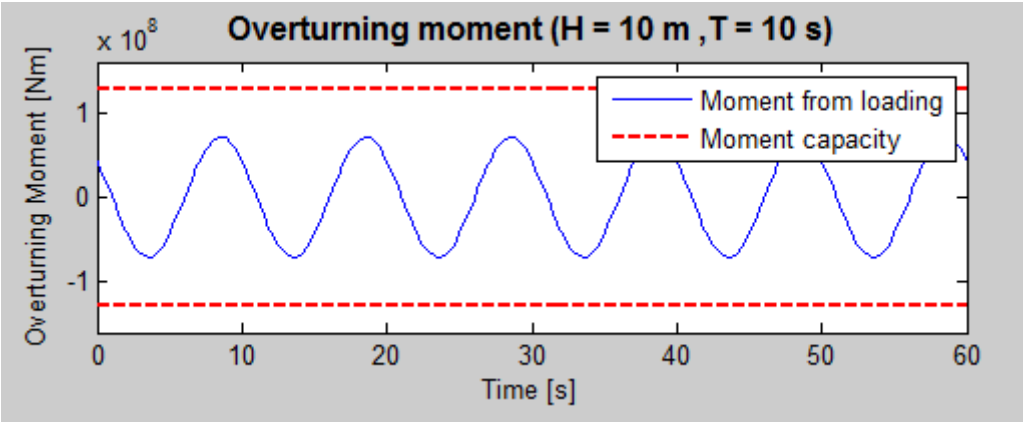

Figure 49: Overturning moment for numerical model, H=10 m, T= 10 s, Heading = 90 deg.

Overturning moment when the structure is exposed to waves with 90 degree heading is shown in Figure 49. As mentioned earlier the loading is the same for the different headings, which also is seen from this figure. However the moment capacity will not be the same for this case, as the moment axis is changed. From Figure 40 it can be seen that tendon 1 is placed in the neutral axis, and will not

contribute to any stabilizing moment. The arms to the other tendons have also changed. These changes lead to a different moment capacity. The overturning moment still have a good margin to exceed the moment capacity, but the maximum value is closer to the system's capacity.

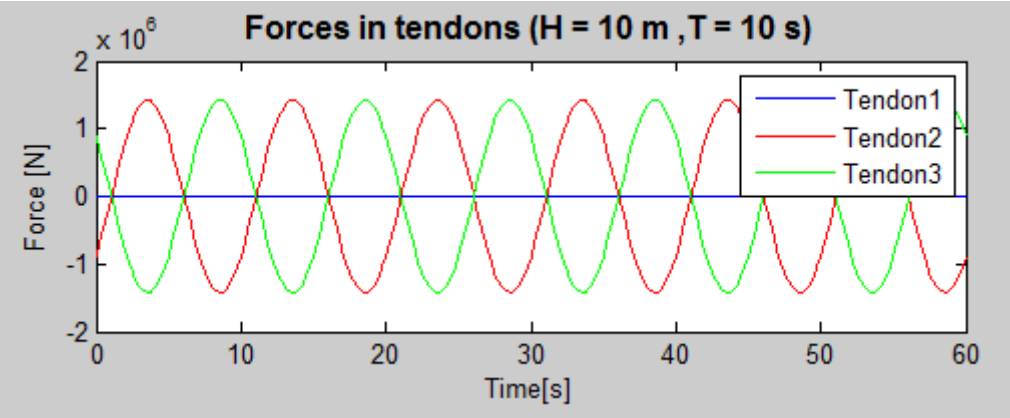

Figure 50: Forces in tendons for numerical model, H=10 m, T= 10 s, Heading = 90 deg.

90 degree heading leads to quite different tension distribution in the tendons, which is seen in Figure 50. Tendon 1 is placed in the neutral axis of rotation and hence it will have zero tension. Tendon 2 and tendon 3 will have the same moment arm and will therefore have to handle the same amount of moment. However are they stabilizing in opposite directions, and will therefore be in anti-phase.

According to numerical calculations, a wave with height 10 m and period 10 s will not be a problem for the system at investigated wave headings. 90 degree heading will lead to lowest moment capacity and the structure is therefore likely to experience slack for this heading first as the wave loading increases. It is therefore reasonable to use the 90 degree moment capacity as a check for overturning moment on the system.

The above presentation is comprehensive, and requires a lot of space. In the coming sections parameters are therefore shown as a function of wave height, period and model draught. This gives a better overview of how the parameters change.

6.1.5 Effect of wave height variation

In this section maximum values for different design parameters are presented as a function of wave height. From the previous section it could be seen that motions and overturning moment was identical for investigated headings. Maximum tendon forces occurred for zero and 60 degree heading. Results in this section are presented for zero degree heading, and all waves used have period 10 s.

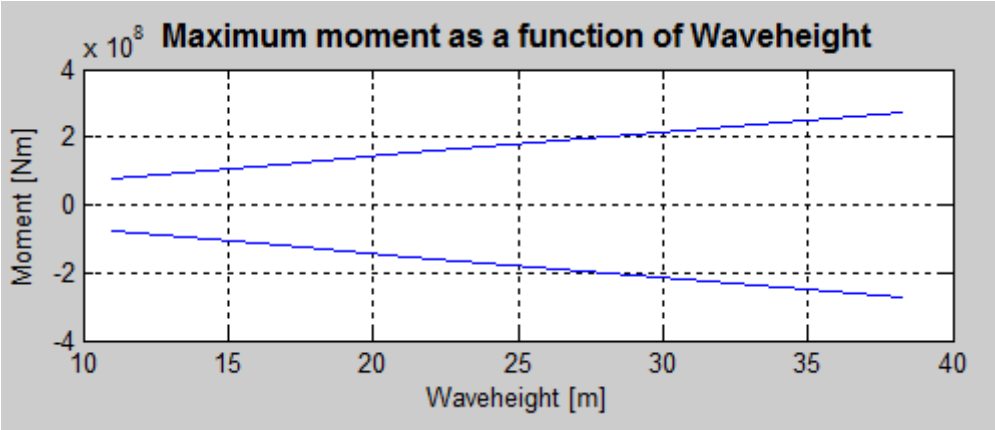

Figure 51: Maximum moment as a function of wave heigth (T=10 s)

As the wave height increase the moment will also increase, as illustrated in Figure 51. If we compare the values with the moment capacities in Table 12, it is seen that the moment capacity for 90 degree heading at 50 m draught is 1.3e8 Nm, which is exceeded by a wave with approximately 18 m wave height. If the draught is increased to 60 m, the moment capacity is 1.95e8 Nm, and the structure can sustain waves up to 27 m. The moment capacity is solely based on the pretension, which means that a sufficient pretension is crucial for a feasible design.

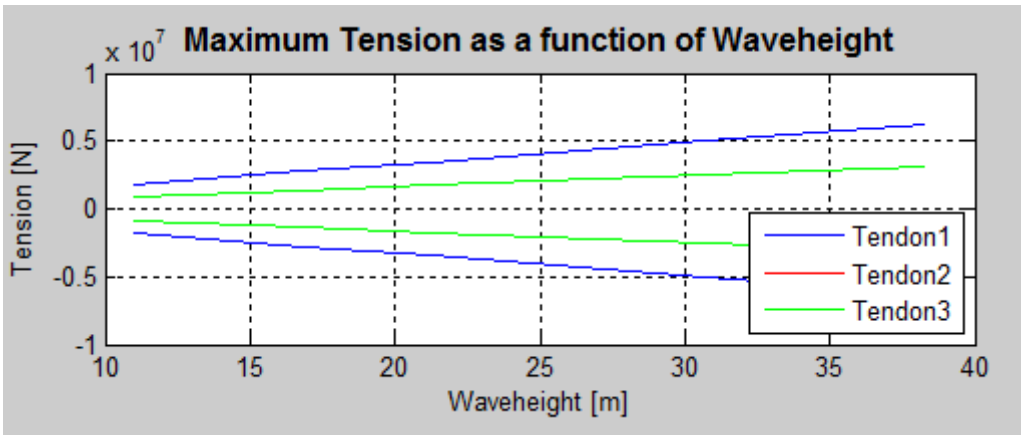

Figure 52: Maximum tension as a function of wave heigth (T=10 s)

Maximum forces in tendons as wave height increases are shown in Figure 52. The forces are calculated from the overturning moment and will therefore increase linearly as the moment increase. As mentioned for the moment, tendons will go slack for larger wave heights depending on the pretension in the system. If the tendons go slack snatch loading would most probable occur, but this effect is not included in these calculations and will therefore not be illustrated in the figure.

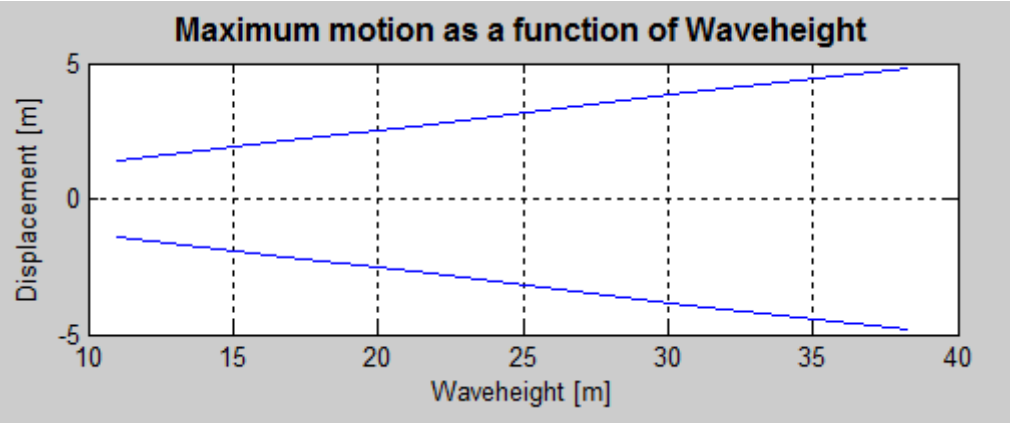

Figure 53: Maximum motion as a function of wave heigth (T=10 s)

Figure 53 show the motion in the wave direction as a function of wave height. The maximum motion amplitudes are very modest as they for a 37 m high wave is about 5 m. For comparison the diameter of the larger column is 12.5 m. Small surge motions will also lead to very small set down values.

Summarized, larger wave height will lead to increased motion, overturning moment and forces. The system will go slack for the larger waves, and it may therefore be necessary to do changes to the system in order to get a feasible design. As mentioned in section 4.1, the VCG is adjusted higher to represent the experimental model better, which also most probable lead to larger overturning moment on the structure. The horizontal motions are small and the set down at this stage can therefore be neglected.

6.1.6 Effect of wave period variation

Since wave height variations in the previous section used the same wave period, it is interesting to investigate how changes in period will affect the system. The parameters presented will be symmetrical around the horizontal axis, and in order to illustrate the variation clearer, only positive values are shown. In these calculations, wave height 30 m is used.

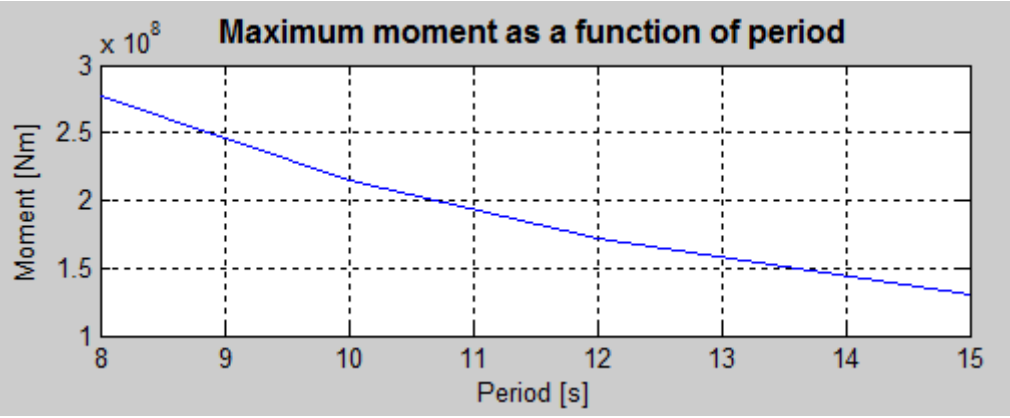

Figure 54: Maximum moment as a function of period (H=30 s)

The moment as a function of wave period is shown in Figure 54. The particle acceleration in a wave decreases as the period gets larger. The structure is mass dominated, and the forces on the structure will hence decrease as the period increase. Reducing environmental forces will again lead to decreased overturning moment. Tendon forces are calculated from the overturning moment and will

therefore also decrease as the period increases. It was seen from previous section that the forces were directly dependent on the moment for the numerical model. The forces are therefore not illustrated in this section.

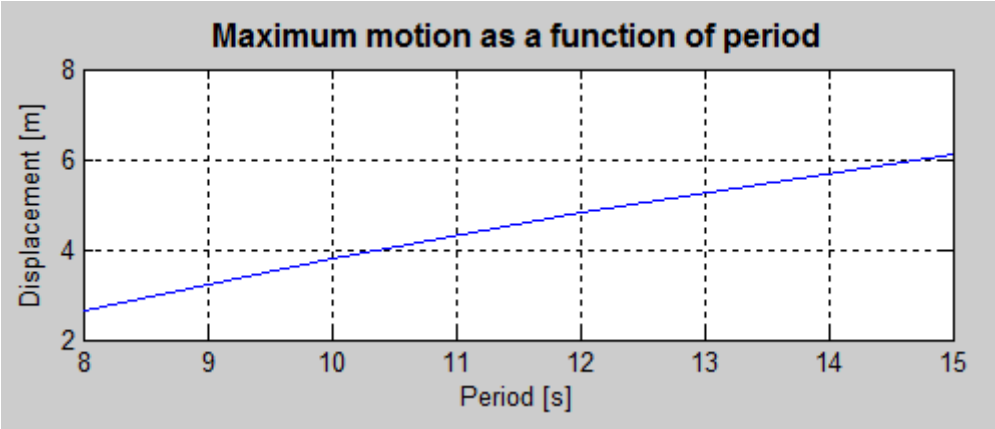

Figure 55: Maximum motion as a function of period (H=30 m)

Figure 55 show maximum motion amplitudes as a function of wave height. The motion increases as the length of the wave increases. This means that the structure follow the wave, probably due to the low stiffness in the wave propagation direction. When taking the moment decrease into consideration this means that the structure moves more without contributing to higher overturning moment from inertia forces.

Summarized, larger wave period leads to lower overturning moment, but larger horizontal motion. The motion still is not large, and a large set down will thus not be experienced. The overturning moment will therefore be the governing design parameter, and the system is most likely to go slack for a low wave period.

6.1.7 Vertical position of mooring configuration

Overturning moment is affected by the length of resultant arm both for inertia forces and environmental loading. These arms are represented by the distance from the point of attack to moment of rotation at the mooring configuration. A variation of the vertical position of tendon termination will show where an ideal position will be with respect to the mentioned contributions.

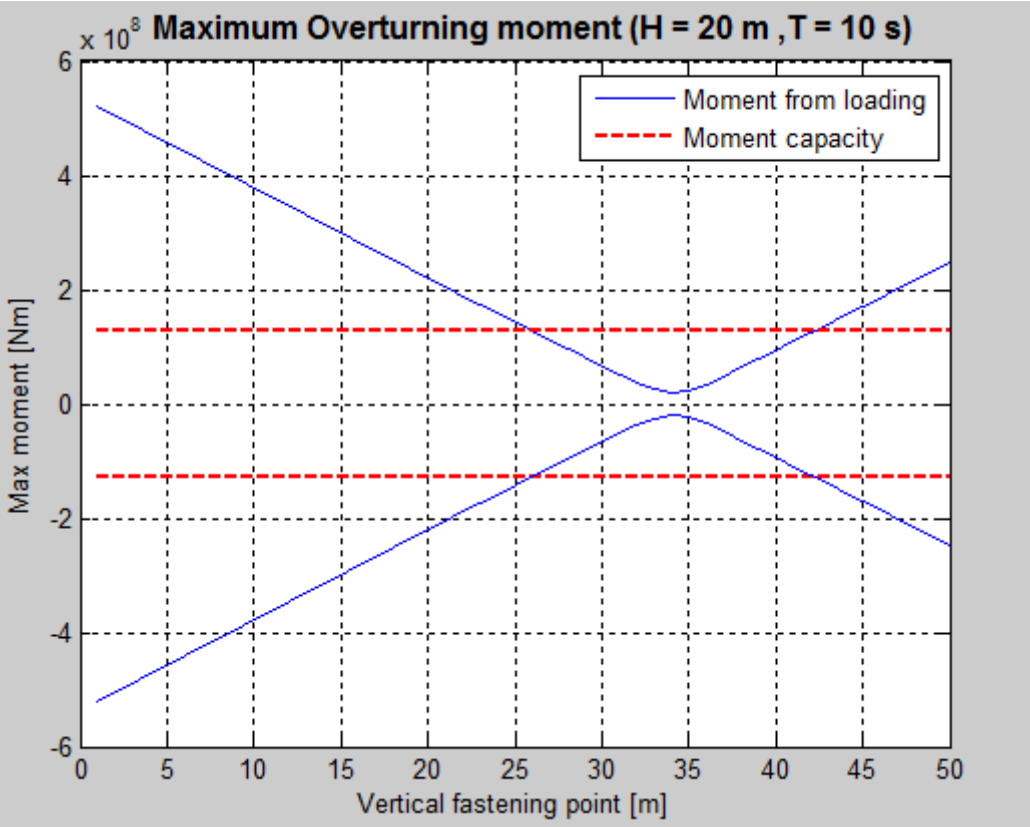

Figure 56: Maximum overturning moment as a function of vertical fastening point (H=20 m, T=10 s)

Figure 56 show the maximum overturning moment on the full scale structure for a 20 m high wave with period 10 s and zero degree heading. The parameter on the horizontal axis represents the distance from the lower end of the column to the position of the configuration where the tendons are fastened. The upper blue line represents the maximum positive overturning moment, while the lower blue line represents the maximum negative moment. The moment capacity is defined with a draught of 50 m and represents the moment capacity for 90 degree heading, seeing this as the limiting factor. It should be noted that the vertical center of gravity is constant for these calculations which might not be the real case. The center of gravity would most likely be higher as the mooring configuration is moved upwards. On the other hand, the VCG is already adjusted higher than the basis in order to fit the scaled model better. The results are therefore likely to represent the system fairly well.

As seen it is vital for the design to avoid a low fastening point due to a very large overturning moment which leads to tendons going slack, and further generates huge snatch loading in tendons. For the given wave, it is seen that a fastening point between approximately 25 m and 43 m will be sufficient to sustain the moment. The absolute lowest moment occurs when the fastening point is 34 m above the base, i.e. somewhat higher than the position used in this thesis. However, something not taken into consideration in these calculations is the effect of the configuration getting closer to the surface. A final mooring design will probably consist of a truss work which will contribute to drag forces from large particle velocities at a high fastening point. In order to decide a final vertical position is it therefore necessary to make a detailed scaled model, and run tests where this

parameter is adjusted. An alternative may be to make a detailed numerical model which is run in suitable advanced software.

6.2 Laboratory test

Results presented in this section are only results from the rebuilt model, seeing that results from the original model are useless. Tendons used in the original model was overly stiff, hence is the results from those tests not representative for the actual system. Raw log files from the experiment are enclosed in appendix D.

In the following several results are presented. The section starts with pretension- and eigenfrequency investigations for selected degrees of freedom. A regular wave series are presented where the model is exposed to regular waves with different heading. This presentation is quite detailed in order to get an overview of how the structure behaves. The wave used in these tests represents the full scale wave used for the numerical calculations in section 6.1.4. Further different draughts are investigated in order to see how sensitive the system is for the pretension parameter. Maximum motion, tension and moment are also presented as a function of wave height and period. It could also be interesting to vary the vertical position of the tendon termination. Due to the initial problems with the model this was not possible to carry through.

Wave heights presented in the following are higher than the waves presented in the test log. This because the wave maker seems badly calibrated. The maximum possible wave height is said to be 0.25 m (NTNU 2011), but in the laboratory test executed larger waves are generated. The values used in the following calculations are measured by a wave sensor, and should therefore represent the actual wave parameters.

6.2.1 Pretension

For a system of this type, the pretension is likely to be a very important parameter which affects the motion of the system and the system characteristics in form of eigenperiods in different dofs.

A pretension check was executed after the model was rebuilt, and is illustrated in Figure 57. The test was carried out by letting the model find its equilibrium position, and further force the tendons slack by pushing the model deeper in the water. As seen from the equilibrium force in the first part of the time series all of the tendon forces are zero, which is because the sensors are zeroed before the test. The pretension will therefore be presented as a negative value in the last part of the time series.

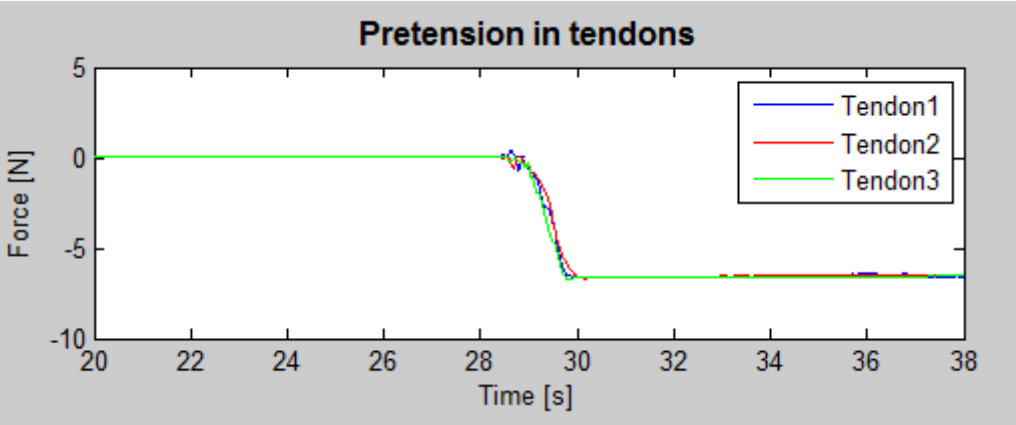

Figure 57: Pretension check in laboratory test

It may be difficult to find an accurate value from Figure 57, but when using Matlab the pretension values are found to be about 6.6 N. in Table 14 the accurate values found, are presented together with the corresponding full scale value.

Pretension in tendons (Draught=0.5 m)		
	Test-value	**Full scale value**
Tendon 1	6.64 N	6.81e6 N
Tendon 2	6.60 N	6.77e6 N
Tendon 3	6.66 N	6.83e6 N

Table 14: Result from pretension test in experiment

To get a comparative value it is possible to obtain theoretical values for the model, and see if the measured pretension values are reasonable. This can be done by finding the net buoyancy at a given draught, and further divide on number of tendons. The same model weight is used for all draughts and it is further assumed that all tendons are equally loaded. The estimates are simple displacement calculations based on dimensions presented in section 5.2.1.

In Table 15 the theoretical pretensions are presented for different draughts.

Theoretical pretension values for different draughts	
Draught	**Pretension**
0.45 m	3.05 N
0.5 m	5.05 N
0.55 m	7.06 N
0.6 m	9.07 N

Table 15: Pretension for scaled model for different draughts

As seen from Table 15 and Table 14, the test values are approximately 1.5 N larger than the theoretical values. In the calculations are however not the buoyancy from the mooring plate included. Another reason may be that the sensors in the pretension test show a larger negative load value because they are loaded by the tendon weight when the model is pushed downwards.

In calculations and conclusions with respect to feasibility of the design, theoretical pretension values are recommended to use as they are conservative. In Table 16 theoretical pretension values are presented together with moment capacities at different headings.

Moment capacity for different draughts				
Draught [m]	**Pretension [N]**	**Mom. Cap 0° [Nm]**	**Mom. Cap 60° [Nm]**	**Mom. Cap 90° [Nm]**
0.45	3.05	+/- 0.88	+/- 0.88	+/- 0.76
0.50	5.05	+/- 1.46	+/- 1.46	+/- 1.26
0.55	7.06	+/- 2.04	+/- 2.04	+/- 1.77
0.60	9.07	+/- 2.62	+/- 2.62	+/- 2.27

Table 16: Moment capacity for different draughts

6.2.2 Decay tests

Decay tests for surge, sway and yaw are executed. The objective with a decay test is to find the eigenperiod and damping of the system.

Surge- and sway motion

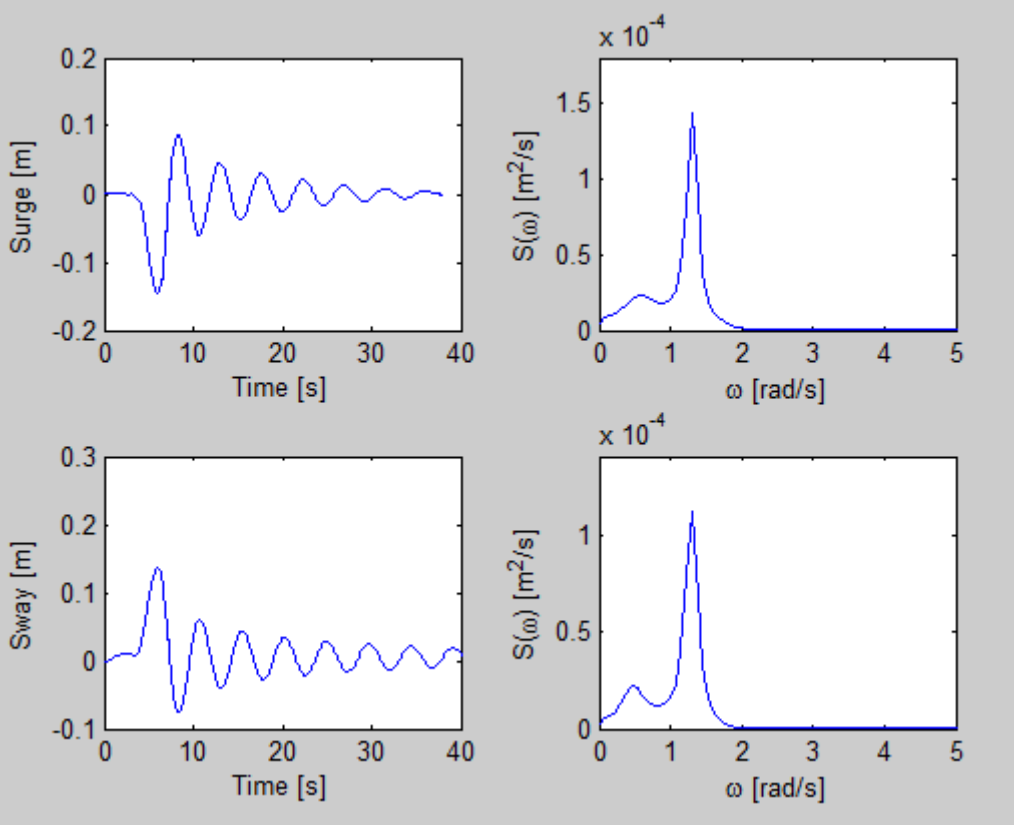

Figure 58: Decay tests in Surge- and Sway motion

In Figure 58 decay tests for surge and sway together with power spectra are shown. The shape of the motion implies that this is an undercritical damped system. The damping ratios are found to be approximately 0.1 for both motions.

According to Larsen (2009) the damped eigenperiod for an undercritical system will be quite similar to the actual eigenperiod of the system, thus can the eigenperiod be taken as the damped eigenperiod. From the spectra plots, it can be seen that the eigenfrequency for both Surge and Sway motion is 1.3 rad/s, which corresponds to an eigenperiod of 4.8 s.

From the theoretical calculations it was expected that the values for Surge and Sway were similar, which is verified by these tests. The value 4.8 s corresponds to a full scale value of 48 s, which is about 20 seconds smaller than the theoretical value (57 s). This may be due to the fact that the weight of the model is checked in dry condition, and that the buoyancy from the mooring plate is not included. The actual pretension of the system is about 1.5 N larger than the theoretical pretension, and for a model with such a small weight this will be a percentage that actually can be of importance.

Yaw motion

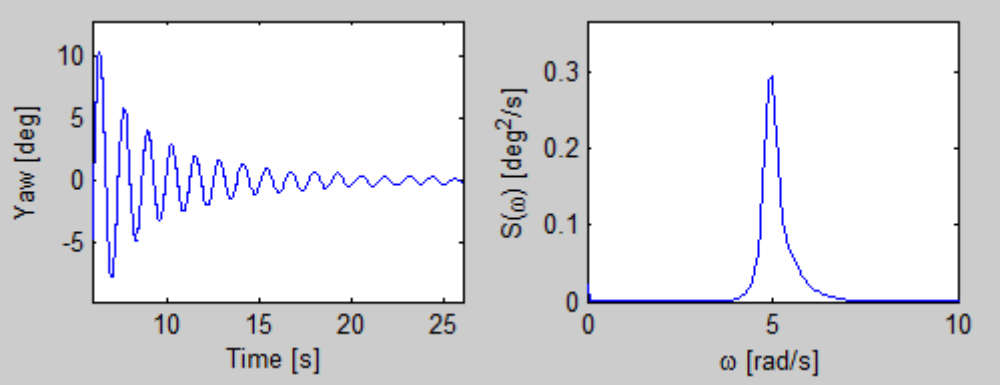

Figure 59: Decay test in Yaw motion

Decay test for Yaw motion is shown in Figure 59. As for Surge and Sway, the Yaw motion has the motion characteristics of an undercritical damped system. From the figure the damping ratio is found to be approximately 0.06.

The eigenfrequency in Yaw is 4.98 rad/s, corresponding to a period of 1.26 s. In full scale the related value is 12.6 s. As for Surge and Sway values the Yaw period is lower than the theoretical (25 s). This may support the statement that the model has larger pretension than the full scale model and hence is stiffer. As mentioned for the full scale model the eigenfrequency in yaw is in the first order load frequency range. Due to little loading in Yaw for a cylindrical structure this is not necessarily fatal for the design. The final mooring arrangement may lead to periodic drag loading in Yaw, and should be taken into consideration for the final design.

An overview of the obtained values can be found in Table 17.

Result from decay tests			
Degree of freedom	**Eigenfrequency [rad/s]**	**Eigenperiod [s]**	**Damping ratio, ξ**
Surge	1.30	4.83	0.096
Sway	1.30	4.83	0.098
Yaw	4.98	1.26	0.058

Table 17: Results from decay tests

6.2.3 Wave height = 0.1 m, Period = 1 s

Below results from regular wave series are presented. This section should represent the scaled wave of the one used for the numerical calculations in section 6.1.4. The discussion in the coming text will be quite detailed, in order to detect specific trends with the system. As one will see from the figures, different time intervals are presented. When the position measurements were post-processed,

glitches in the time series were discovered. This may be due to the optical sensors lose the reference points on the structure or alternatively it could be a software problem. The software was updated, but no improvement was discovered. Since the wave is regular the motion and forces also will be regular and hence a part of the time series will nevertheless give sufficient information.

Heading = 0 degrees;
The model is headed zero degrees, and exposed to a wave with height 0.1 m and period 1 s.

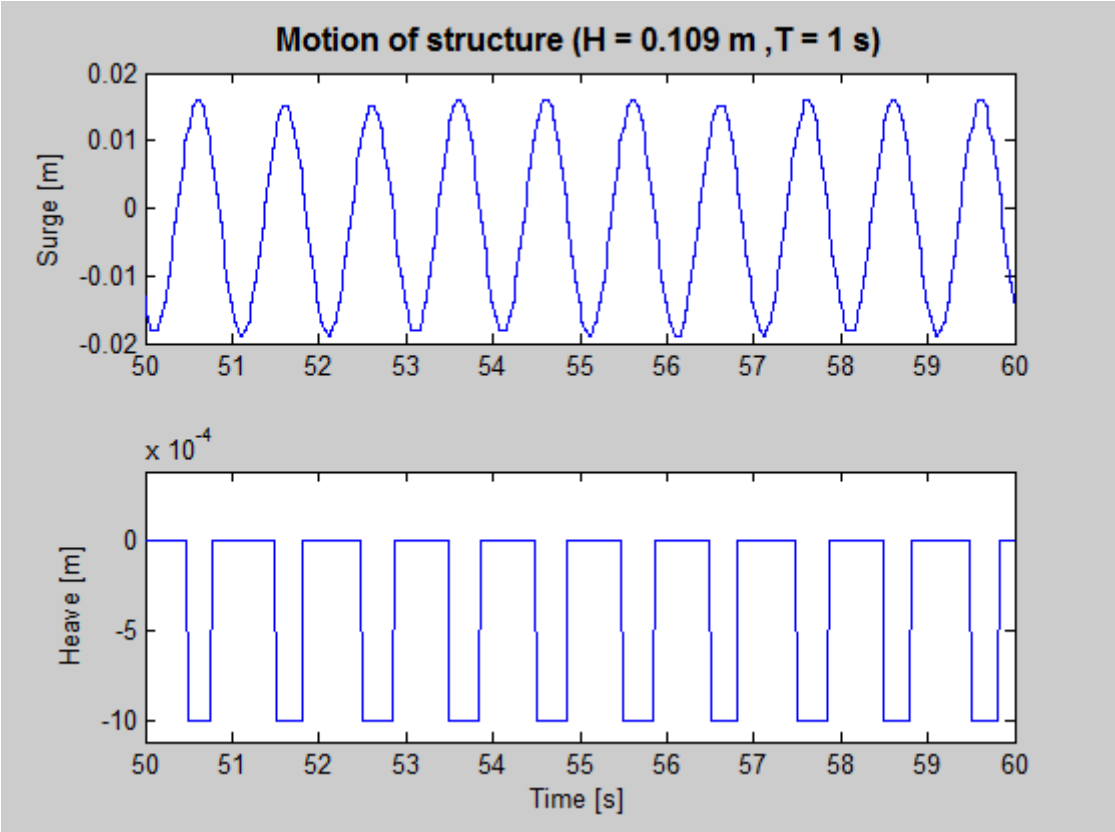

Figure 60: Motion of scaled model, H=0.1 m, T= 1 s, Heading = 0 deg.

Motion of the structure in surge and heave is shown in Figure 60. As seen from figure, the structure gets larger negative amplitudes than positive. The structure moves a bit due to the wave loading and obtains equilibrium a bit from the initial equilibrium position. Further the motion is harmonic and without any chaotic behavior. If we compare the motion with the numerical model the motion amplitudes are a bit higher for the experiment.

The heave motion from the figure seems quite strange. The time series have been checked, and the plot is illustrating the measured values. Since it is very small values that are measured, the strange shape is most likely that the sensors have problems with measuring such small values. A heave motion with half the period of surge motion would be expected due to set down which occur at maximum positive and negative motion amplitude, as for the numerical calculations. This is however not the case here, most probably due to measuring problems.

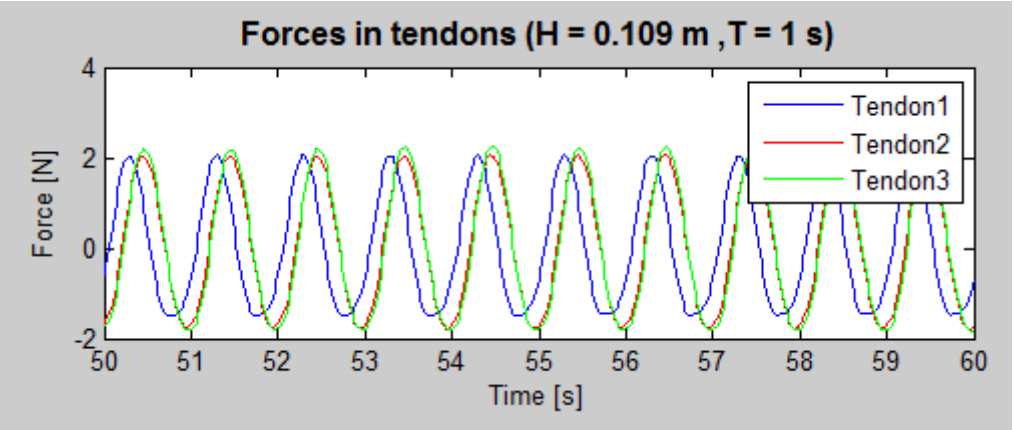

Figure 61: Forces in tendons for scaled model, H=0.1 m, T= 1 s, Heading = 0 deg.

Forces in tendons for the same wave are shown in Figure 61. The forces are shown without the pretension, as the force sensors are zeroed with regular intervals. As expected Tendon 1 is loaded before Tendon 2 and Tendon 3 which is loaded at the same time .The amplitude values are quite similar for all the three tendons, which is slightly unexpected. From the wave theory, we know that the acceleration in the wave, hence the mass force have a maximum value in the same order of magnitude both on upstream and downstream side of the structure in a wave period. In addition we have the inertia moment due to the structure motion, which also will lead to an equal force on the upstream and downstream side of the structure. In theory these contributions would lead to an overturning moment that the tendons need to resist. Since the tendons on the downstream side of the structure can share this loading it would be expected that they had half the loading, and in anti-phase, with tendon 1 which is obviously not the case here.

As the motion of the model was observed during the test, it could be spotted that the model after moving to its maximum negative position had a yank motion when it started to move in the positive direction again. This quick motion may have generated amplified forces, and could possible explain that the tension in tendon 2 and 3 is not half of tendon 1. A movie-file where the model is exposed to larger wave and the mentioned motion is conspicuous can be seen in appendix D.

A reason to the unexpected shape might also be that the model is loaded somewhere around the mooring plate, which leads to little overturning moment. However, the moment due to the inertia forces and the motion should still have been possible to spot from the time series. Another reason may be that there are pressure forces acting on the mooring plate.

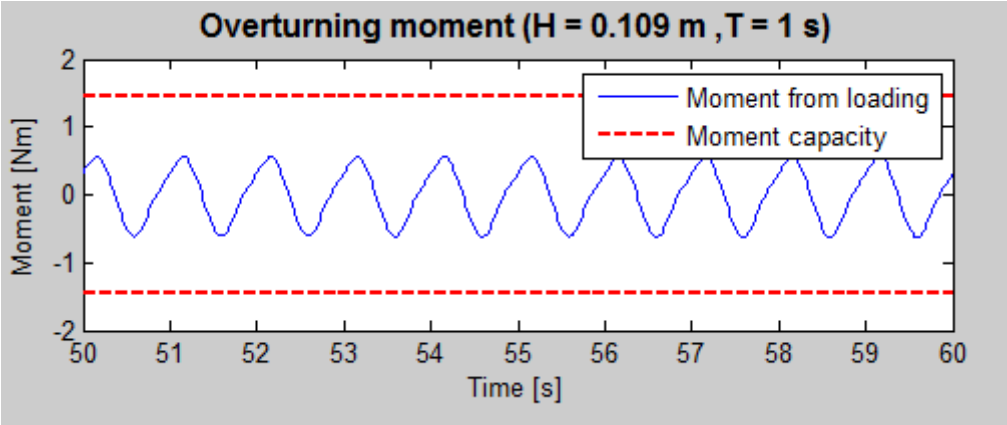

Figure 62: Overturning moment for scaled model, H=0.1 m, T= 1 s, Heading = 0 deg.

In Figure 62 the overturning moment on the structure is shown. The moment value is calculated from the measured forces using the moment equation in section 4.4. The red lines are moment capacities, and we can see that for this sea state the margin is good when it comes to danger of tendons going slack.

When comparing this moment with the moment from the numerical model, they are quite similar despite the differences discovered for the forces. This may show that there are forces acting on the structure, which not necessarily contribute to the overturning moment, but still loads the tendons.

Heading = 60 degrees;
The model now is rotated 60 degrees, while the model is exposed to a wave with the same parameters. As we can see from the heading of Figure 63, there are small differences in wave height, but the differences are so small that the conditions can be compared as equal.

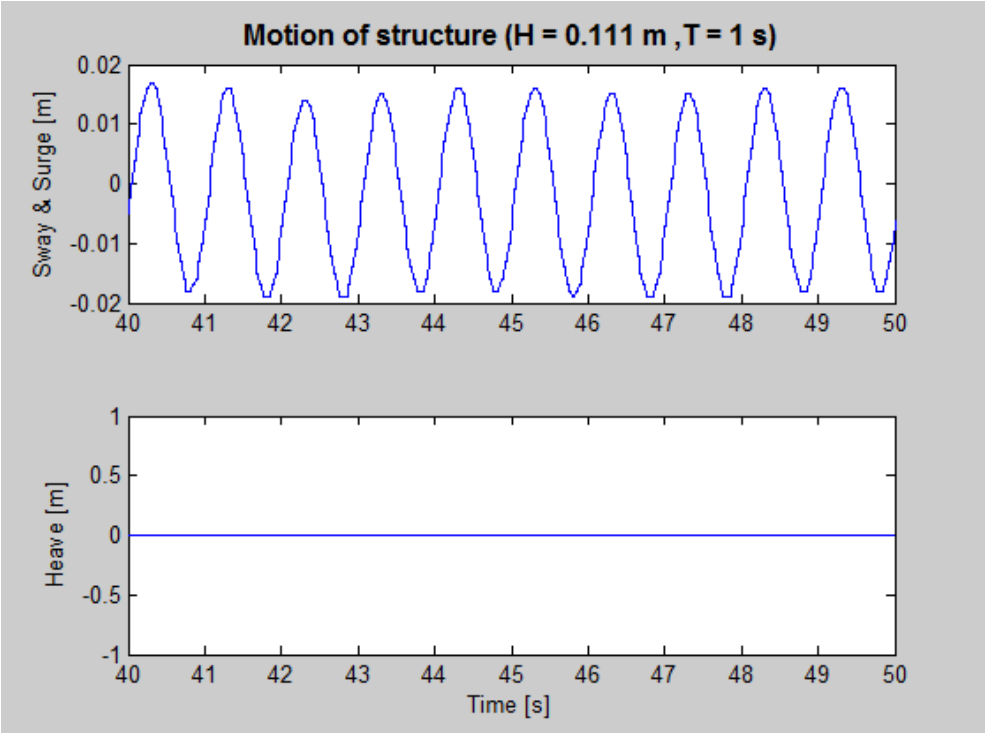

Figure 63: Motion of scaled model, H=0.1 m, T= 1 s, Heading = 60 deg.

The motion of the structure can be seen in Figure 63. The horizontal motion for this heading is coupled motion in Surge and Sway. It is seen that the motion is very like the motion at zero degree heading. This is not surprising, since we from the decay tests found that stiffness is identical in Surge and Sway. If the possible effect from the mooring plate is ignored, the loading will also be the same. As for zero degree heading, the structure is also for this heading oscillating around a position a bit from zero.

The heave motion in this case is zero the whole time interval. If this is the real case or a measuring problem is uncertain. The mentioned glitches that occurred in the position measurements occurred at the same time for all motions. If the measuring problem in heave was due to glitches, also the surge motion would be affected, which is not the case. Therefore it is likely that the motions are very small, and the sensors have problem tracking the motion in heave.

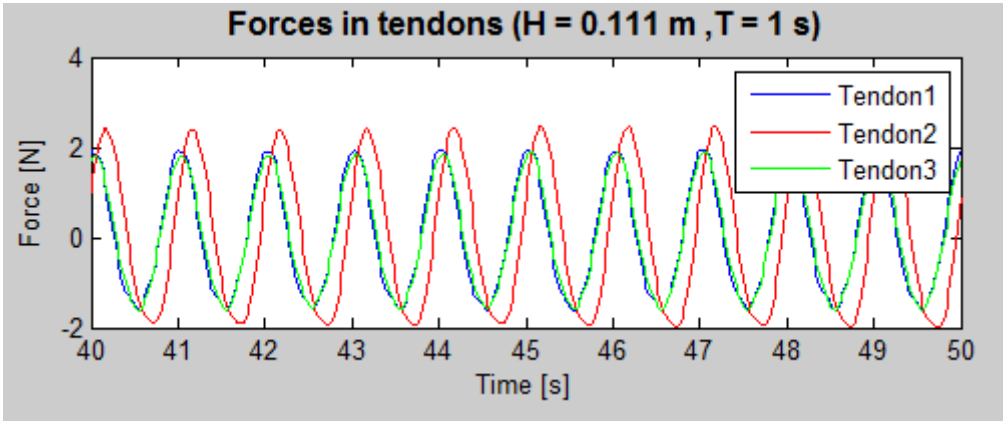

Figure 64: Forces in tendons for scaled model, H=0.1 m, T= 1 s, Heading = 60 deg.

In Figure 64 the forces for 60 degree heading are shown. Compared to zero degree heading this is a more expected shape of the force distribution. The tendon which is alone on one side of the structure (in this case Tendon 2) gets more loading than the two on the opposite side. If we compare the force in tendon 2 from this run with the tendon 1 in the zero degree heading, it can be seen that tendon 2 in this case is more loaded even though they in principle should have to handle the same overturning moment. This may indicate that there will be larger forces on the downstream side of the structure which may be due to the yank motion mentioned earlier.

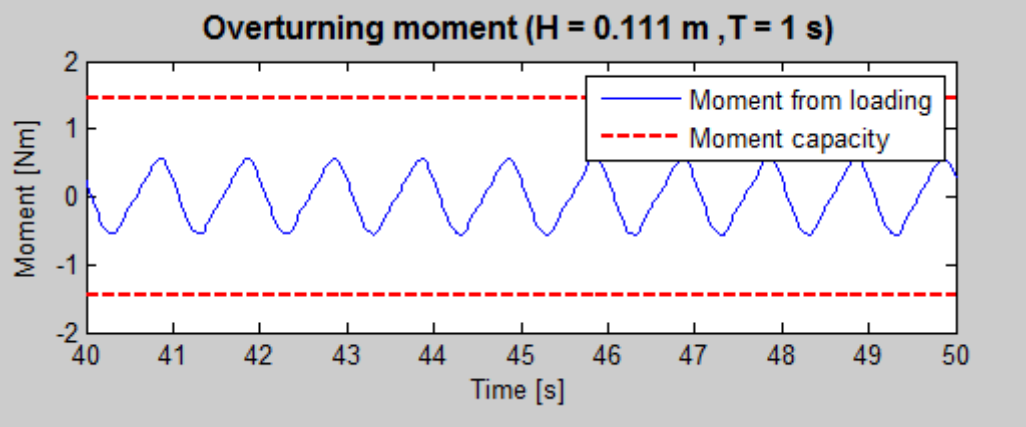

Figure 65: Overturning moment for scaled model, H=0.1 m, T= 1 s, Heading = 60 deg.

Overturning moment for 60 degree heading is shown in Figure 65. Compared to zero degree heading the moment is very similar, which is in accordance to the theory. The moment at all headings should in principle be the same when exposed to the same wave. The moment capacity in this case is equal to moment capacity in zero degree heading due to geometry. We can still see that there are good margin to tendons going slack.

Heading = 90 degrees;

The model is once again rotated, and the heading is now 90 degrees. The same wave as for the other headings are ordered from the wave maker, but the heading in Figure 66 show that there are small differences.

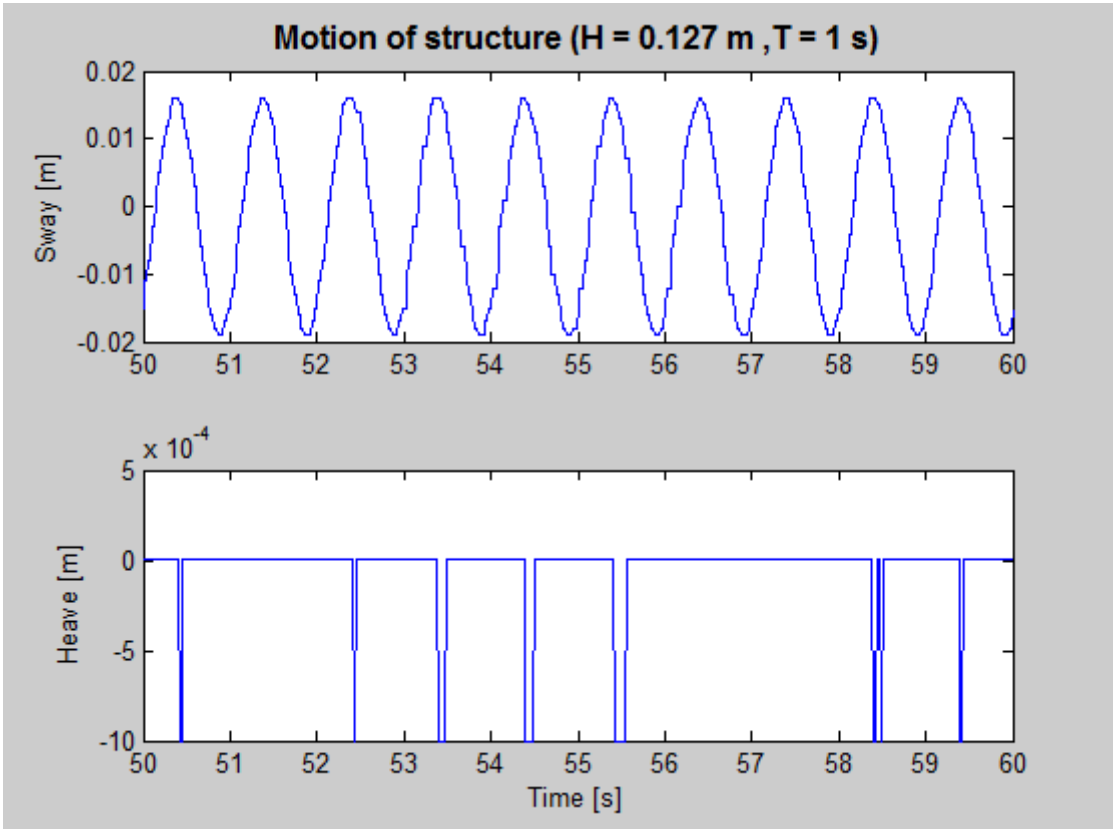

Figure 66: Motion of scaled model, H=0.1 m, T= 1 s, Heading = 90 deg.

The model motions when rotated 90 degrees are shown in Figure 66. Not surprisingly the motion in sway is very similar to the structures motion for zero-, and 60 degree heading, which can be explained by the same stiffness for these motions.

The registered heave motion still is somewhat odd. The measured motions are very small and the motions are therefore disregarded.

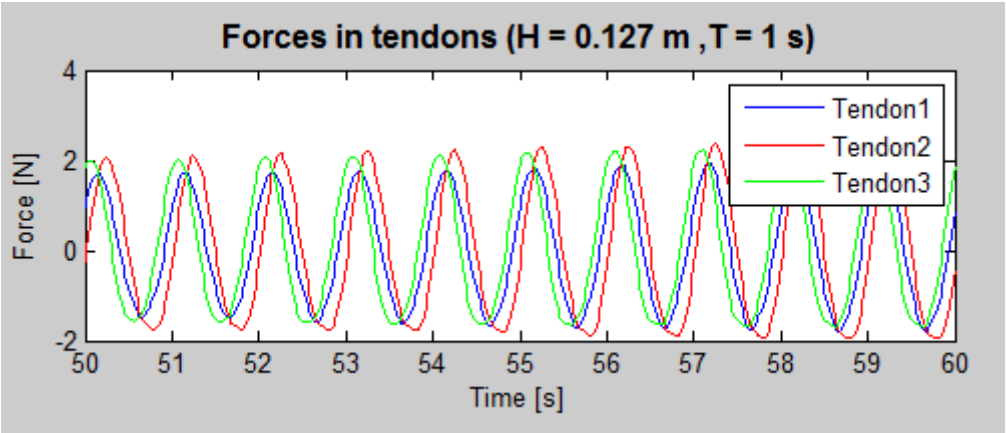

Figure 67: Forces in tendons for scaled model, H=0.1 m, T= 1 s, Heading = 90 deg.

Tendon forces for 90 degree heading are shown in Figure 67. It can still be seen that the trend with largest load at the downstream tendon still applies, which also in this case is tendon 2. At this heading tendon 1 is placed at the axis of rotation for the overturning moment. From the theory this

should lead to zero force in this tendon as long as the model keep the heading angle. The yaw angle for the same time interval is shown in Figure 68.

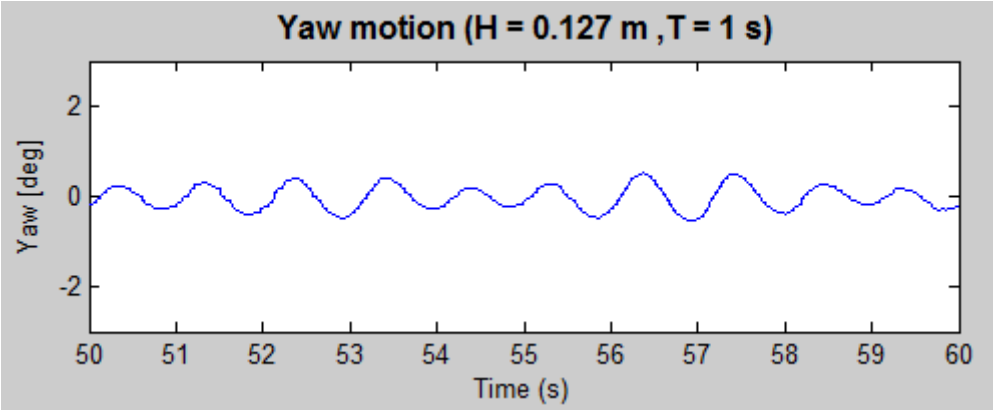

Figure 68: Yaw motion for scaled model, H=0.1 m, T= 1 s, Heading = 90 deg.

As we can see from the Yaw motion, there is no large rotation in the time series and tendon 1 should therefore in theory be minimally loaded. This means that there are forces which do not contribute to the moment that are loading tendon 1. This may also explain the unexpected force distribution at the other headings.

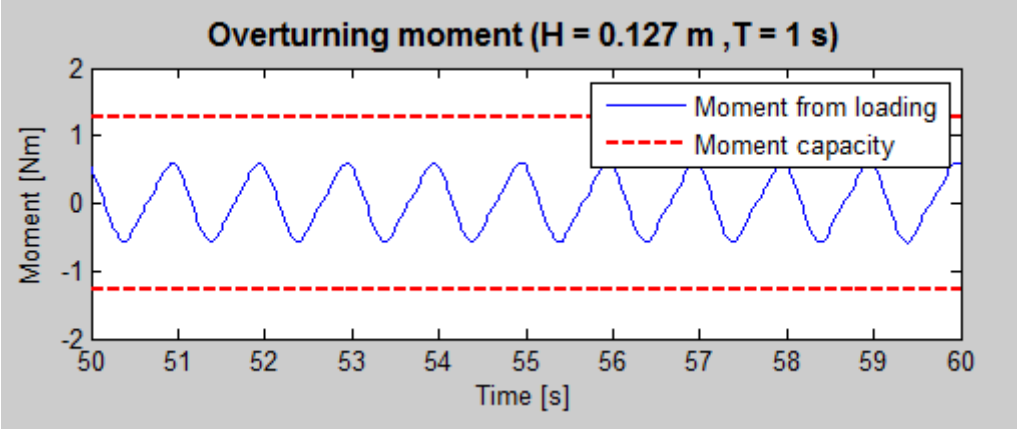

Figure 69: Overturning moment for scaled model, H=0.1 m, T= 1 s, Heading = 90 deg.

Figure 69 show the overturning moment for the 90 degree heading. According to the defined coordinate system this will correspond to overturning moment in roll motion. In the calculation of this moment the contribution from tendon 1 is omitted since the moment arm around the rotational axis is zero. However the moment is quite similar to the moment at zero-, and 60 degree heading. For this case the moment capacities are a bit smaller since the moment arms are different and there are only two tendons contributing to withstand the moment.

Three headings are now investigated for the same wave. The most surprising with the measured data is the behavior of the forces. It was expected that the forces on the upstream tendons would be in anti-phase with downstream tendons and vice versa. The forces order of magnitude is also for many situations larger than expected. The forces in all three tendons seem to be loaded in a magnitude which is larger than the most loaded tendon from the numerical calculations. The overturning moment is calculated from the forces, and the magnitude of the moment is quite similar to the

numerical calculations. The motion, especially the negative amplitudes are larger than the numerical results. Therefore, it may look like the model is loaded more than expected, and that this loading leads to an offset which loads all tendons almost at the same time. The scaled model is stiffer than the numerical model, as seen from eigenperiods, and it is therefore likely that the forces acting on the structure are larger in real life.

6.2.4 Effect of wave height variation

Different wave heights are generated in order to see how the model reacts to waves with larger height. In this section design parameters are shown as a function of wave height. All waves in this section have period 1 s.

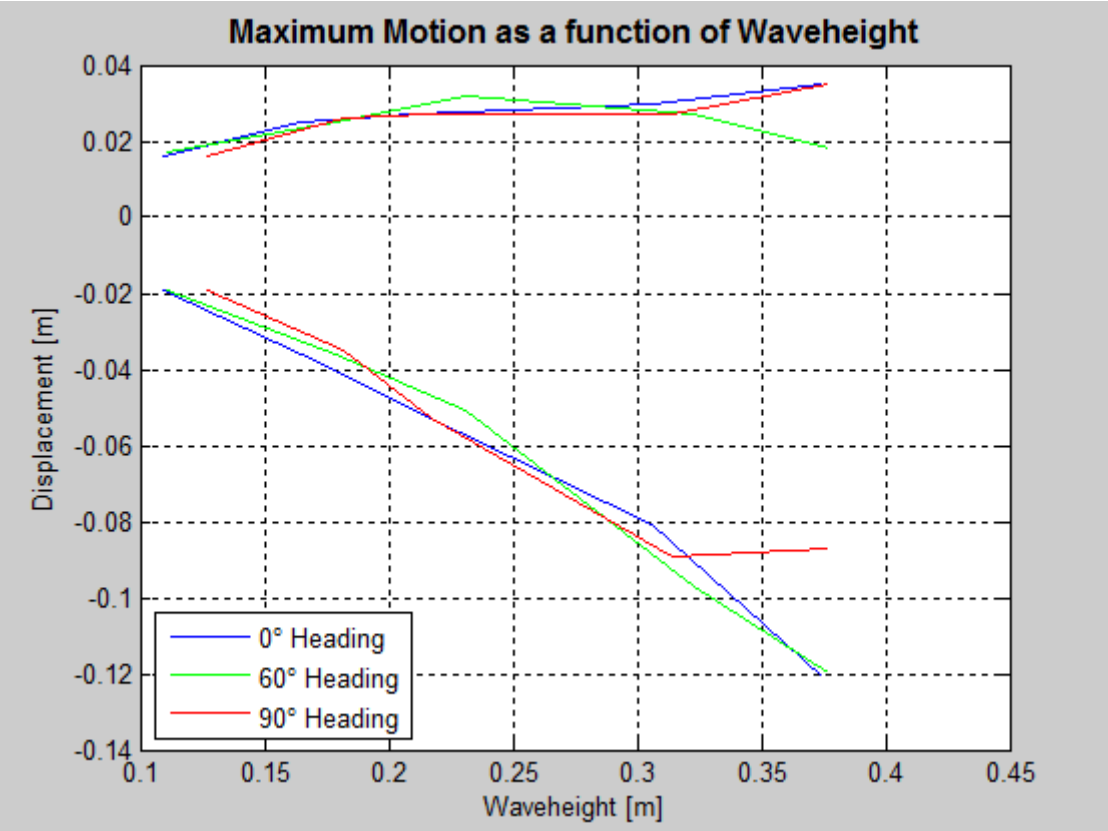

Figure 70: Maximum motion as a function of wave height for all headings (T=1 s)

In Figure 70 motion in the wave direction is presented for zero, 60 and 90 degree heading. It can be seen that the motion gets larger as wave height increases, and that the model gets larger offset from the origin in larger waves. The motion is virtually alike for all headings, which again confirm that the stiffness in the different directions is the same.

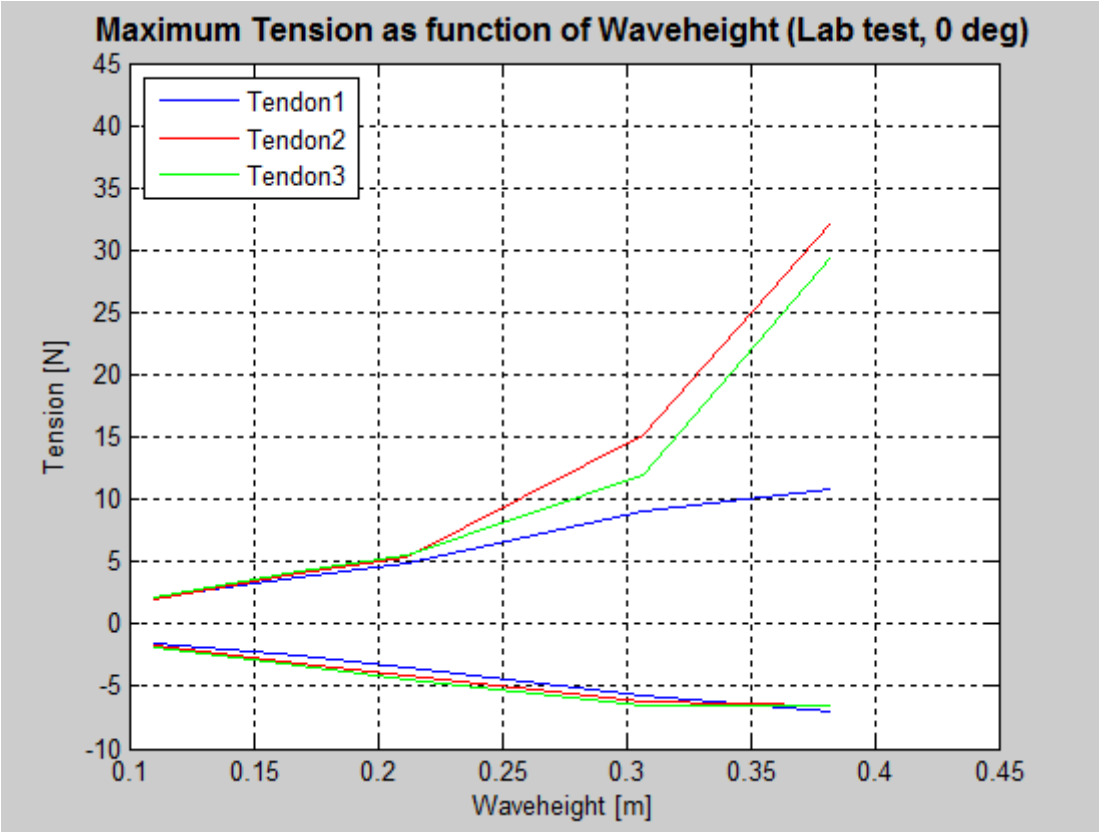

Figure 71: Maximum tendon tension as a function of wave height for zero degree heading (T=1 s).

Figure 71 show maximum tension in tendons for zero degree heading. The trend mentioned in section 6.2.3, that largest loading occur at the downstream tendons is more conspicuous in this figure. Downstream tendons (tendon 2 & 3) are loaded three times as much as the upstream tendon (tendon 1).The rapidly increased tension can be explained by that larger waves lead to snatch loading. These snatch loads would most likely be fatal for the tendons since they are very large. However, the figure is helpful because it confirms that the model get a yank-motion which lead to large load on the downstream side.

The negative load amplitudes do not get the same behavior since a wire is not capable of taking forces in compression. The forces will therefore converge to the negative pretension value, and maybe somewhat more since the sensors are loaded by the tendon weight when they go slack. The fact that all the tendons have the same minimum value may indicate that all the tendons go slack for the largest waves.

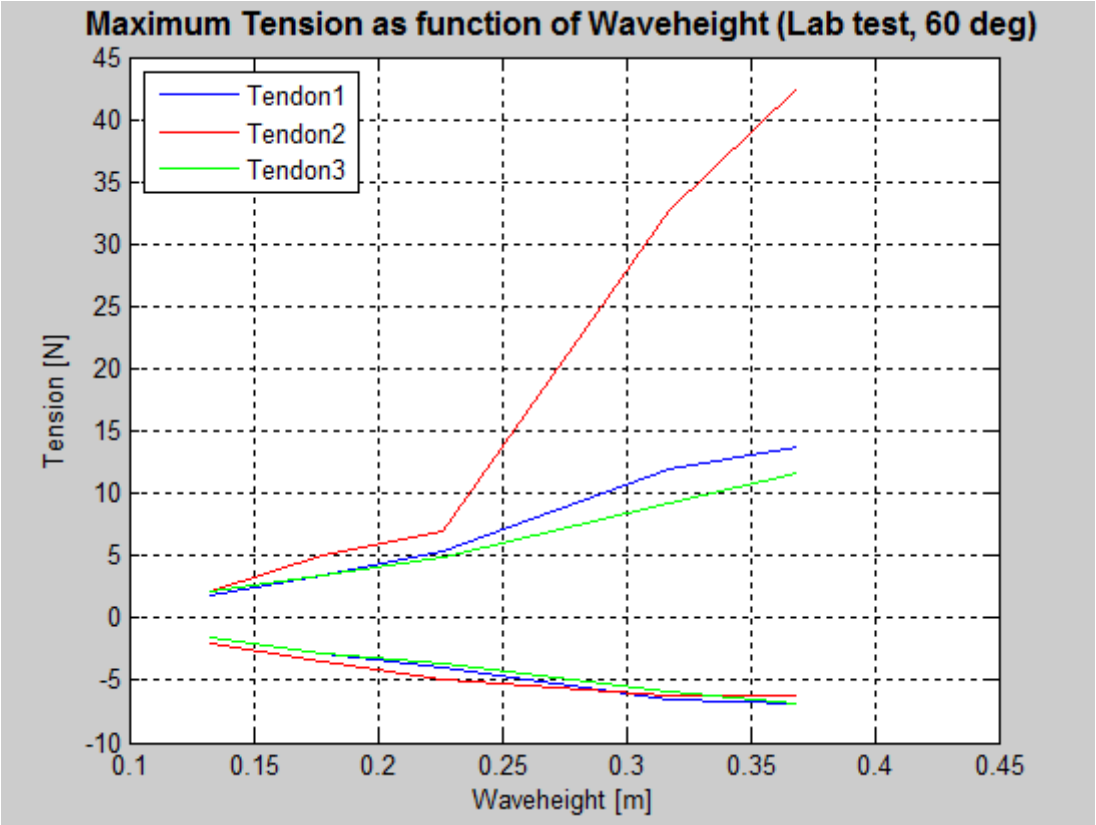

Figure 72: Maximum tendon tension as a function of wave height for 60 degree heading (T=1 s).

Figure 72 show maximum amplitude values for tension with 60 degree heading. As mentioned for zero-degree heading the largest forces will occur on the downstream tendon. Tendon 2 for this heading is alone on the downstream side of the model. It is seen that the snatch loads are even higher in this tendon than for zero degree heading which is explained that yank-motion is taken by one tendon instead of two. Tendon 1 have about the same loading as for zero-degree heading despite that the forces on the upstream side is taken by two tendons.

The negative amplitudes have the same magnitude of loading as for zero degree heading.

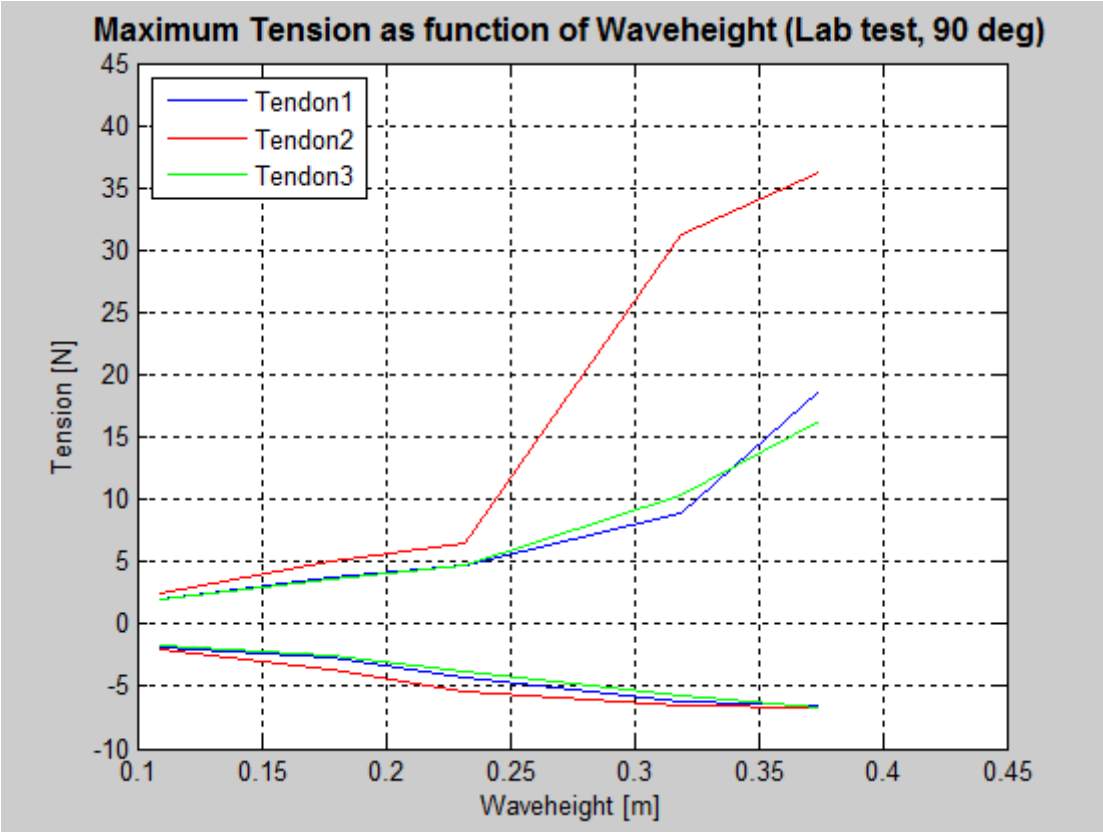

Figure 73: Maximum tendon tension as a function of wave height for 90 degree heading (T=1 s).

In Figure 73 maximum amplitude values for the tendons are shown for 90 degree heading. It should be noted that for the largest waves at this heading the structure had a quite chaotic motion which generated rotation as the snatch loading occurred. The forces will therefore most probable not represent the theory as good as for a less chaotic motion. This may explain the large loading in tendon 1 despite its position in the center of rotation. It can however still be seen that the downstream tendon (tendon 2), get the largest loading.

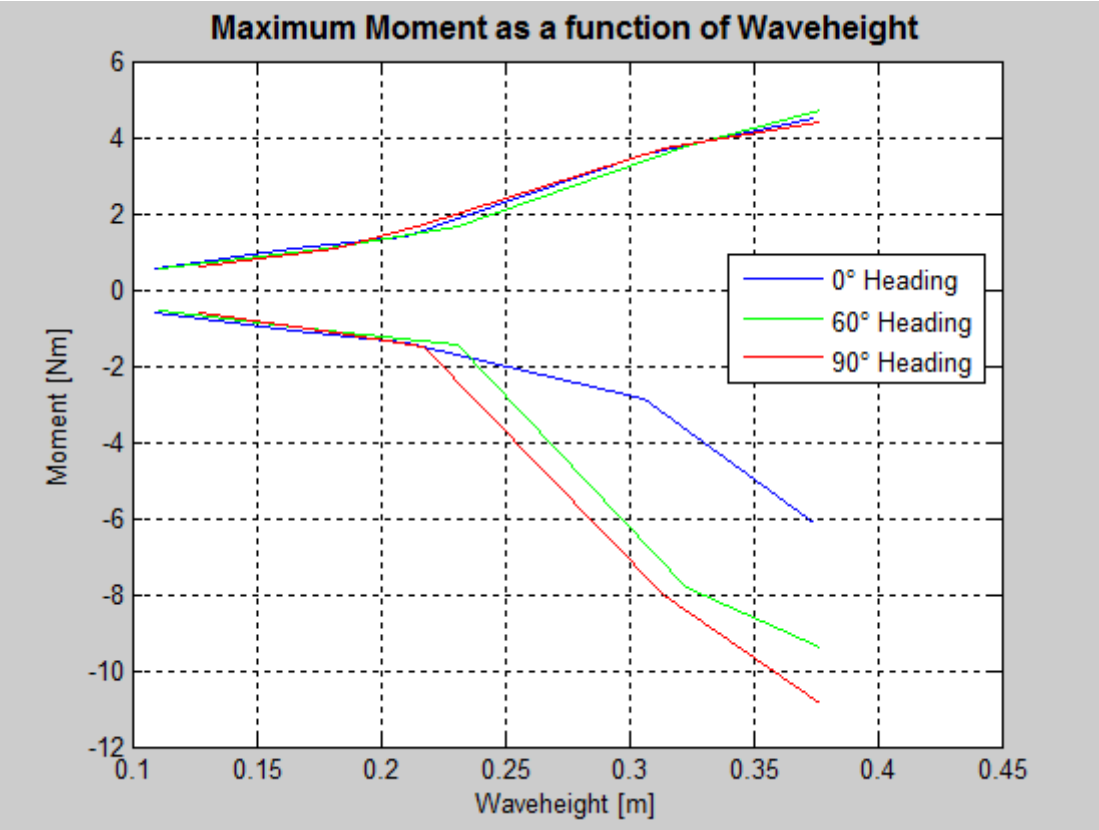

Figure 74: Maximum moment as a function of wave height for all headings (T=1 s).

In Figure 74 maximum moment amplitudes are shown for all headings. The moments are as mentioned calculated from the forces, and it can be seen that the snatch loads from the tendon forces leads to a large negative moment. This would not necessarily represent the overturning moment due to loading on the model. It should be mentioned that the moment capacity is +/- 1.26 Nm for 90 degree heading when the draught is 0.5 m. From the figure it is seen that the moment capacities are exceeded for the largest waves. The moment capacity is exceeded when the wave height is approximately 0.19 m which is too low for a design wave. This means that the pretension in the system is to low, or that the vertical center of gravity is too high. Investigations with variation in draught and hence the pretension are performed later in the report.

It is clear from this section that larger wave height leads to increased motion, tendon forces and overturning moment on the model. The results are somewhat limited since the largest waves led to a quite chaotic behavior due to tendons going slack during the tests. From the results presented above it is certain that a larger pretension is needed if the mooring design is to be implemented for a full scale structure.

6.2.5 Effect of wave period variation

As shown in section 4.2.1, wave loading will change as the wave period change. In this section the same wave height is used while variation is done to the period. Unfortunately limited number of variations is executed due to limited time. All waves in this section have 0.3 m wave height.

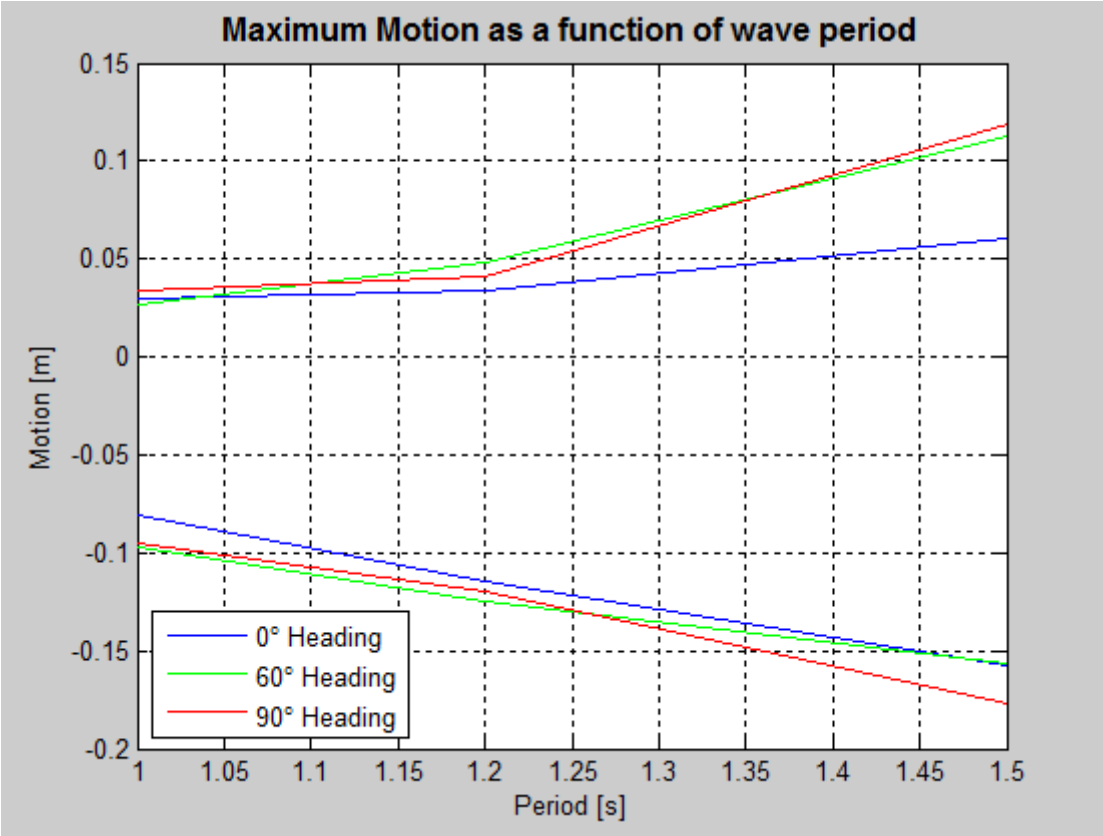

Figure 75: Maximum amplitude for motion as a function of wave period (H=0.3)

Figure 75 show the motion of the model as a function of wave period. The graph is based on three runs with period from 1 s to 1.5 s. It is seen that the motion amplitude increases both in positive and negative direction for increasing wave period which also was the case for the numerical model. The motion may however be explained by that the stiffness in the wave direction is quite low for a tension leg structure, and the model therefore follow the wave as it gets longer with increased period.

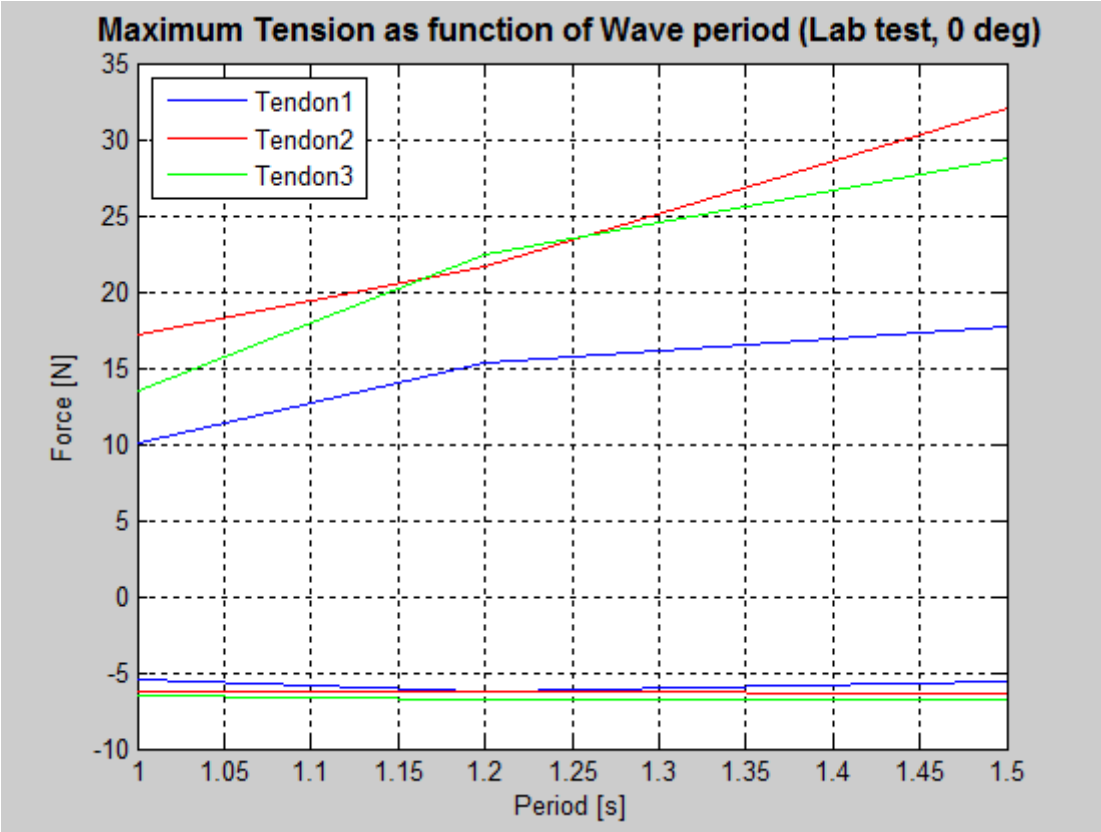

Figure 76: Maximum tendon tension as a function of wave period (H=0.3)

Figure 76 show the maximum tension amplitudes for zero degree heading. Since the plot is based on few points is it unfortunately not easy to draw a conclusion from the figure, but it is seen that the forces increase for larger wave periods. The magnitude of the forces is large and represent snatch loading in the tendons. Ideally this period variation should have been executed for smaller waves where snatch loads didn't occur. Due to problems with higher waves than wanted from the wave maker, this was discovered too late and there was not enough time to perform the tests again.

However, it can be concluded that the motion gets larger with longer waves which again lead to larger forces in the tendons. The overturning moment is calculated from the forces, and will also increase with larger period. This is not according to theory, and the reliability of the measurements should be considered since they represent snatch loading.

6.2.6 Effect of variation in draught

In this section the model is exposed to waves with zero degree heading while the draught is varied from 0.45 m to 0.60 m. Length of tendons are kept constant; hence the position of the tendon termination is half the draught above bottom of structure for all draughts. Different draughts, corresponding theoretical pretension and moment capacities for three wave headings were presented in Table 16 and are used as reference values for this section. A variation in draught will affect the natural frequencies of the model, but these are not discussed any further in this section.

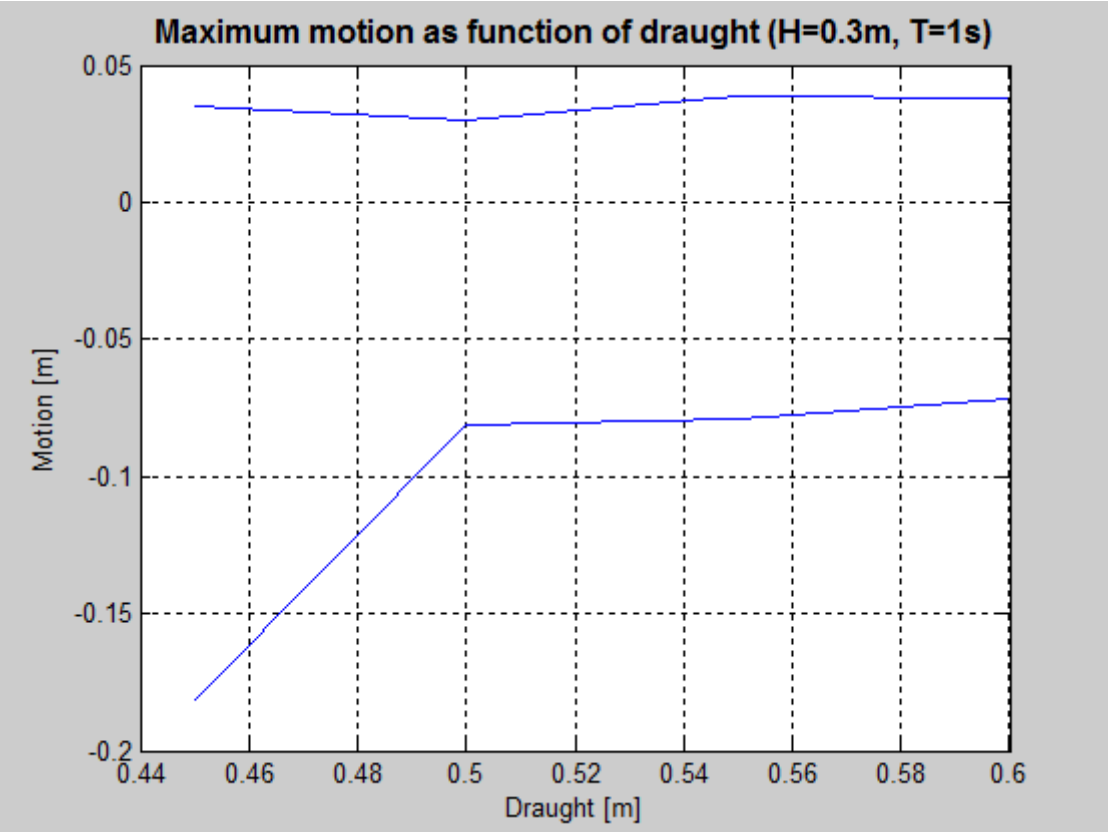

Figure 77: Maximum amplitude for motion as a function of draught (Heading=0 deg)

Figure 77 show motion in the wave direction as a function of draught. A wave with height 0.3 m, period 1 s and heading zero degrees are used. As the system gets stiffer the negative motion amplitude will get smaller. As the draught is increased from 0.45 m to 0.5 m the negative motion amplitude is approximately halved. As the draught is increased further the motion is about the same. The pretension for the smallest draught is very low, and could not be used for a final design. The motion of the model at this draught was observed to experience a rotational pitching motion due to low pretension, and the measured motion is therefore likely to be a combination of translational and rotational motion.

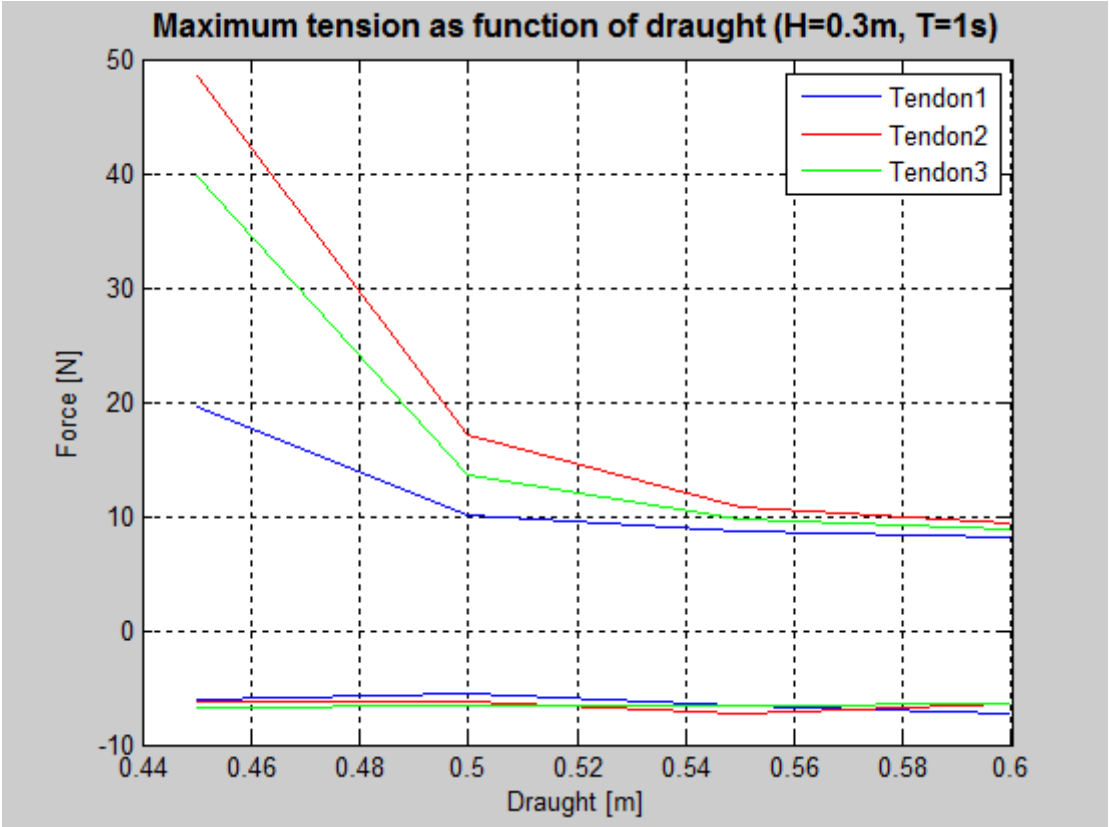

Figure 78: Maximum tendon tension as a function of draught (Heading=0 deg)

In Figure 78 tension in all tendons as a function of draught for zero degree heading is presented. It can be seen that the positive amplitude values are decreasing as the draught and hence the pretension increases. This is explained by that the tendons are exposed to less snatch-loading as the structure get stiffer and the moment capacity increases. This means; if this mooring system is to be implemented the pretension need to correspond to a value in the order of magnitude as the largest draughts in this test.

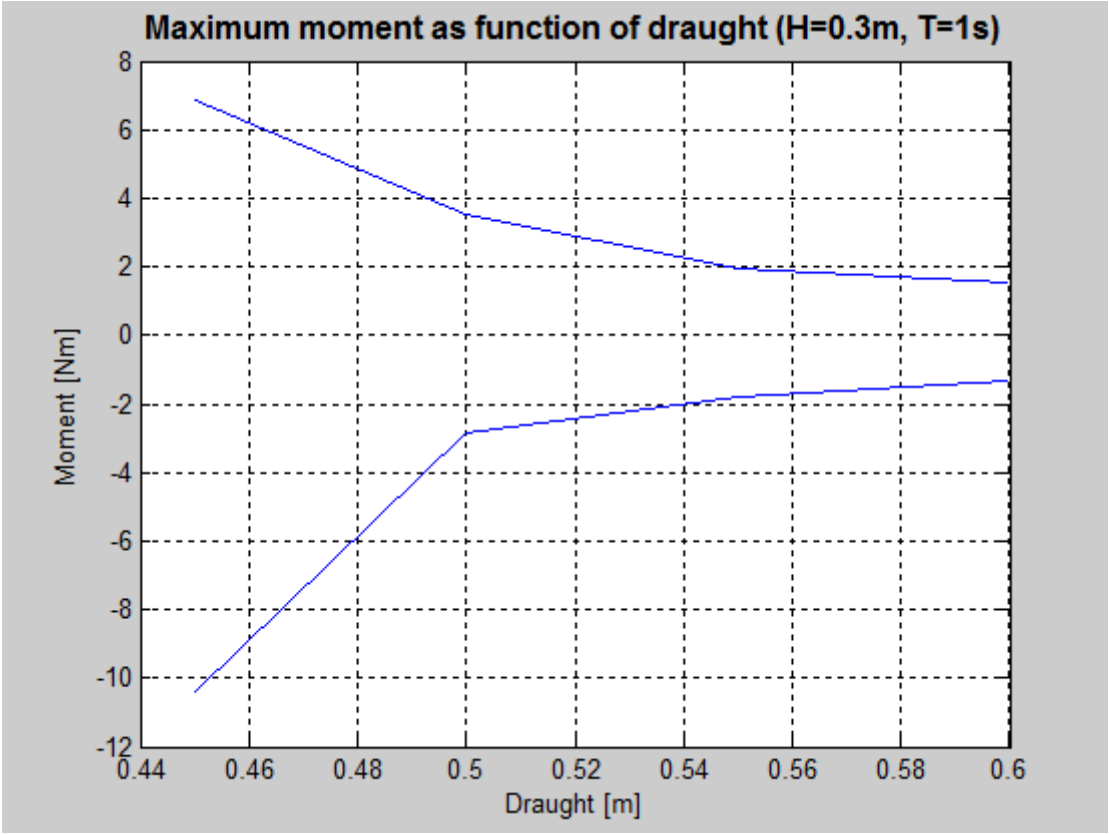

Figure 79: Maximum moment as a function of draught (Heading=0 deg)

In Figure 79 maximum moment as a function of draught is shown. The moment decreases as forces in Figure 78 decreases. This is not surprisingly since the moment is calculated from the forces. It is seen that the moment is oscillating more around the horizontal axis as the draught increases. This means that the moment is more according to theory where the structure is loaded equally on the up- and downstream side of the column as snatch loading disappears. From moment capacities presented in Table 16 it can be seen that the largest draught and hence the largest pretension have an appurtenant moment capacity of +/-2.27 Nm at 90 degree heading. From Figure 79 this is sufficient to withstand the maximum overturning moment. As mentioned for the forces, it is necessary with a pretension corresponding to one of the largest draughts in order to get a feasible design.

6.2.7 Uncertainties

All laboratory tests are associated with uncertainties, and there is no such thing as a perfect measurement. The main focus when executing an experiment is however to be aware of these uncertainties and try to minimize the effect of them. In this section uncertainties in the laboratory test is presented, some more important than others.

One of the more important uncertainties in this experiment is the heading of the model. Since the understanding of the measured forces is based on the position of the tendons this is of great importance. The model was placed manually and aligned by eye. There is therefore no guarantee that the model is positioned entirely with the correct angle. In this experiment motions are taken as deviation from the original heading angle/position. Placing the model at the measuring systems

origin is a potentially time consuming operation, but with more time available it could have given useful data, especially when it comes to heading.

The calibration is another potential uncertainty that can give consequences. The positioning system is not calibrated at all, and the measurements are taken with the understanding that values are correct. The calibration of the force sensors is done in a way which leads to little uncertainty since the sensors are fixed and the applied load is checked with weight. The largest uncertainty when it comes to the sensors is probably the wave sensor. It was calibrated by manually submerging it to different depths as the output was tracked. And if the submergence is wrong will also the correlation factor be wrong. The regression in Figure 37 show however that the points are quite linear, which implies a good calibration.

When the sensors are calibrated and ready to use the measurements should lead to little uncertainties. In this experiment are the force sensors submerged, which means that they are most likely exposed to a temperature different from the calibration temperature. In order to keep the water level constant the test facility also were constantly refilled which may have affected the sensors if the incoming water have a low temperature. To minimize this effect are however the sensors zeroed with regular intervals.

The wave height presented in the top of the figures is taken as the height of the largest wave crest in the time interval subtracting the wave trough. This will be correct provided the height of the waves in the time interval is equal. The time intervals are looked into manually and no large deviations have been found and this will hence only lead to small deviations.

The Marine Cybernetics laboratory is stated to be 1.5 m deep. According to Wahl (2011), this is not entirely correct since the bottom is built with a small angle. The basin is shallowest at the wave maker where the depth is 1.41 m. The depth increases from the wave maker and at the middle (20 m from wave maker) the depth is 1.53 m. This means that any bottom fixed structure will get a small heal angle. In the experiment executed in this thesis the varying depth may however affect the tendon forces as the model moves towards shallower or deeper water due to change in water depth and hence pretension.

7. Conclusion and further work

7.1 Conclusion

The objective of this thesis was to investigate the feasibility of tension leg anchoring for floating wind turbines. Throughout the report results for tendon forces, overturning moment and motion using numerical and experimental analysis are presented and discussed.

According to numerical moment calculations tendons, with a draught of 50 m, will go slack for a wave height of 18 m and period 10 s. This is not a particular large maximum wave in the North Sea, and implies that the design is not well suited for an area with such harsh conditions. Calculations show however that with increased draught and hence larger pretension the structure is able to sustain larger waves. A pretension of 7.8 MN, corresponding 60 m draught, makes the structure maintainable in up to 27 m high waves with 10 s period. According to earlier calculations this is about a 10-year wave for the northern part of the North Sea, and hence is the value too low to represent for example the ULS-criteria for annual exceeding probability (10^{-2}). The vertical center of gravity is adjusted for the numerical model to fit the experimental model with a center of gravity approximately in the water level. This adjustment leads to larger overturning moment from inertia forces. A final design will most certain have a lower center of gravity due to heaviest column at the lower part of the structure and weight from the mooring arrangement. Position of the mooring attachment arrangement is also an important parameter since the overturning moment can be minimized with optimal vertical position. The optimal position calculated in this thesis is 34 m above the structures base. A possible effect of getting closer to the surface is not taken into consideration. The structures motion in the horizontal direction has proven to be modest, which again leads to small vertical motions in case of set down. The air gap of the structure is safe even for a 10^{-4} annual exceeding probability wave.

In the laboratory test overturning moment is calculated from measured tendon forces. The behavior of the forces is somewhat different than expected, as the clear force distribution due to overturning moment fail to appear. The forces in different tendons are quite similar in order of magnitude and the phases are surprisingly equal. The experimental moment analysis show that tendons with model draught 0.5 m will go slack when the wave height is approximately 0.19 m and period equal to 1 s. Measurements of the forces also show that snatch loading occur for waves larger than 0.19 m, and this is represented as exponentially growth in the measurements. In order to minimize snatch loading pretension is increased by larger draught. The draught is only increased for the zero degree heading, however it is shown that overturning moment is quite similar for all headings as long as snatch loading not occur. With larger draught the snatch loading disappears and moment calculations show that the overturning moment from a wave with height 0.3 m and period 1 s is lower than the moment capacity for 0.6 m draught. This means the structure is maintainable in higher waves if the pretension is increased and hence is the pretension crucial for the concept.

The calculations from the numerical model coincide fairly well with the experimental results for the overturning moment. Motion in the wave direction is somewhat larger for the experimental model, and especially at negative motion amplitudes. The forces have shown to be difficult to recreate in the numerical model due unknown reasons. The mooring plate used in the lab test may be of importance. For the numerical model it is difficult to find the individual tendon forces due to number

of unknowns in the moment equation. Amplitude values for the most loaded tendon from the numerical calculations are almost in the same order of magnitude compared to experimental measurements. The difference in forces and similarity in overturning moment implies that the experimental model is loaded by forces that not contribute to the overturning moment, but still load the tendons. In the experiment a massive plate was used as mooring attachment arrangement, and loading on this plate may explain the strange behavior.

When it comes to the feasibility of tension leg anchoring for floating wind turbines, the latest calculations show that with sufficient pretension, the model can survive quite large waves without tendons going slack. The design used in this thesis also has a relatively high vertical center of gravity which makes the concept less optimized. With a reasonable center of gravity and with sufficient pretension it is likely that tension leg anchoring is feasible for floating wind turbines.

7.2 Further work

From the calculations executed in this thesis, one can see that there are many variables affecting the feasibility of the concept. Numerical calculations show that the pretension and vertical position of tendon termination are parameters important to withstand the overturning moment from environmental loading. It is also likely that the vertical center of gravity is of large importance since the overturning moment from inertia forces gets larger as the VCGs distance to the tendon termination increases. Two of these parameters are directly dependent on the structures weight in magnitude and distribution. At this stage masses are only estimated using simple calculations.

The structure may need adjustments in order to minimize bending moments and stresses from loading and motions, or maybe the structure is oversized and hence is too heavy. If the structure is modeled in software which also takes structural properties into account, it is possible to find a more optimized weight using finite element method analysis. Then also mooring attachment arrangement can be dimensioned, and a total weight of the structure can be found. Example of software may be the Sesam package, developed by DNV. In such software also hydrodynamic analysis can be executed, and with a detailed model also good results are normally obtained.

When a suitable design is found and tested numerically, it is advised to execute laboratory tests where a detailed scaled model including detailed mooring arrangement is tested in irregular wave series with spectra containing design sea states.

References

Books and articles:

Demirbilek Z. (1989) *Tension leg platform – A state of the art review*, American society of civil engineers.

DNV (2007) *Environmental conditions and environmental loads*, Recommended practice -C205, Det norske veritas, april 2007

Estaban M.D. Et. Al (2010) *Review Why offshore wind energy?,* Universidad Politécnica de Madrid, C/Profesor Aranguren S/N, 28040, Spain.

Faltinsen O.M. (1990) *Sea loads on ships and offshore structures*, Cambridge university press, 1990.

Fanchi, J.R. (2005) Energy in the 21st Century. River Edge, NJ, USA; World scientific Publishing Company.

Fox R. W, Mcdonald A. T., Pritchard P. J. (2004) – *Introduction to Fluid Mechanics*. Sixth edition, John Wiley & sons, USA.

Hansen, M. O. L. (2008) – *Aerodynamics of wind turbines*. Second edition, Erathscan, UK.

Haver S. (2009) *Prediction of characteristic response for design purposes*. Lecture notes TMR4195 – Design of offshore structures. Norwegian University of Science and Technology, 2009.

Haver S. (2010) *Wind loads, Lecture notes TMR4195 – Design of offshore structures*. Norwegian University of Science and Technology.

Karimirad M. & Moan T. (2010) *Effect of Aerodynamic and Hydrodynamic Damping on Dynamic response of a Spar Type Floating Wind Turbine*.

Larsen C.M. (2009) *Marin Dynamikk*, Lecture notes in TMR4180, Norwegian University of Science and Technology.

Larsen C.M (2011) *Tension leg anchor system*. Internal document, University of Science and Technology.

Moan T. (2004) *Vol.1 Design procedures and criteria*. Lecture notes TMR4195 – Design of offshore structures. Norwegian University of Science and Technology.

Myrhaug D. (2007*) Uregelmessig sjø*, Lecture notes in TMR4180, Norwegian University of Science and Technology.

Myrhaug D. & Kjeldsen S. (1986) *Steepness and asymmetry of extreme waves and the highest waves in deep water.*

Pettersen B. (2007) *Marin teknikk 3 – Hydrodynamikk*, lecture notes in TMR4247, Norwegian University of Science and Technology, 2007.

Steen S. & Aarsnes J.V. (2010) *Experimental Methods in Marine Hydrodynamics*, Lecture notes in TMR7, Norwegian University if Science and Technology

Conversations:
Fylling I. (2010) Introductory meeting for project thesis 03.09.2010 at Tyholt, Trondheim.

Haver, S. (2011) Personal communication.

Wahl, T. (2010) Personal communication.

Internet reference:
NTNU (2011), Norwegian University of Science and Technology. Available from: http://www.ntnu.no/imt/lab/kybernetikk. [Accessed 15.02.2011]

Offshorewind.net (2011), North American Offshore Wind Project Information. Available from: http://offshorewind.net/Other_Pages/Turbine-Foundations.html. [Accessed 17.01.2011]

Steen, S (2011), Lecture notes in TMR7, Norwegian University if Science and Technology. Available from: http://www.ivt.ntnu.no/imt/courses/tmr7/lecture/Instrumentation.pdf . [Accessed 15.02.2011]

WAFO (2011), Wave Analysis for Fatigue and Oceanography. Toolbox for Matlab. Available from: http://www.maths.lth.se/matstat/wafo/. [Accessed 20.02.2011]

Appendices

Appendix A - Matlab script for Numerical model

```
clc
clear
close all

%%
%-------------------------------------------------------------------
% NUMERICAL MODEL. ZERO DEGREE HEADING
%-------------------------------------------------------------------

%% Input parameters

% Physical input parameters
rho_w=1025; % Density of sea water
rho_s=7850; % Density of steel
Cm=1; % Mass coefficient
g=9.81; %Gravity acceleration

% Input parameters for environment
h=150; % water depth
T=15; % Wave period
H=30; % Wave height

% Input parameters for body
o_diameter1=12.5; % Outer diameter of submerged coloumn
i_diameter1=12.2; % Inner diameter of submerged coloumn
o_diameter2=6; % Outer diameter of coloumn above sea level
i_diameter2=5.7; % Inner diameter of coloumn above sea level
draught=50; % Draught of coloumn
height=draught+65; % Total height of coloumn
A_cross1=(pi/4)*((o_diameter1^2)-(i_diameter1^2)); % Cross sectional area of submerged coloumn
A_cross2=(pi/4)*((o_diameter2^2)-(i_diameter2^2)); % Cross sectional area of coloumn above sea
level
B=(pi/4)*(o_diameter1^2)*draught*rho_w; % Bouancy of submerged body
a=50; % Distance between tethers (side in triangle)

% Input parameters for mooring system
n_tendons=3; % Number of tendons
Dy_tendon=0.6; % Tendon outer diameter
Di_tendon=0.56; % Tendon inner diameter
A_tendon=(pi/4)*((Dy_tendon^2)-(Di_tendon^2)); % Cross-sectional area for tendon
fastening_point=draught/2; %Vertical position of fastening point (from bottom of structure)
length_tendon=h-draught+fastening_point; % Length of tendon
E=2.1e11; %Youngs modulus for steel

 %% Wave- and force calculations
lamda1=(g/(2*pi))*(T^2); % Wave length

% While loop to find the wavelength corresponding to period and height
dummy=1;
while dummy>=0.01
   lamda=(g/(2*pi))*(T^2)*tanh(((2*pi)/lamda1)*h);
```

```
    dummy=abs(lamda-lamda1);
    lamda1=lamda;
end

zeta_a=H/2; % Wave amplitude
omega=(2*pi)/T; % Wave frequency
k=(2*pi)/lamda; % Wave number
Z=0:-1:-h; % Depth coordinate vector
t=0:0.25:6*T; % Time vector
ax=(omega^2)*zeta_a*(((cosh((k*Z)+(k*h)))/(sinh(k*h)))'*cos(omega*t); % Particle acceleration in
the wave over the depth
wave_profile=zeta_a*sin(omega*t);

z=0:1:draught; % Integration vector over the body
ax_constr=zeros(length(z),length(t)); %Particle acceleration in the wave over the submerged body

% For-loop to assign correct acceleration from wave to the right depth of body:
for i=1:length(z)
    for j=1:length(t)
        ax_constr(i,j)=ax(i,j);
    end
end

dF=rho_w*((1/4)*pi*o_diameter1^2)*Cm*ax_constr; %Load matrix. (Depth and time varying)

% For-loop to integrate the wave-loading over the body
for i=1:length(t)
    Mass_force(i)=trapz(z,dF(:,i));
end

%% Finding coefficients for the equation of motion

% Weight and inertia forces
weight_coloumn1=(A_cross1*(draught+5)*rho_s); %Weigth of material in submerged coloumn
weight_coloumn2=A_cross2*(height-(draught+5))*rho_s; %Weigth of material in coloumn above sea
level
weight_nacelle=138e3; % Weight of nacelle
weight_adjusted=0.75565e6; % Due to a heavier model than expected
m=weight_coloumn1+weight_coloumn2+weight_nacelle+weight_adjusted; %Structural mass
added_mass=(pi/4)*(o_diameter1^2)*draught*rho_w; %Added mass in surge. Taken as the weight
of the displaced water

% Stiffness
Tension=((B-m)/n_tendons)*g; % Tension force

% Eigenperiod in Surge
k_1=n_tendons*Tension/length_tendon; % Stiffness in surge motion
m_1=m+added_mass; % Mass in surge motion
omega_1=sqrt(k_1/m_1); % Eigenfrequency in surge
T_1=(2*pi)/omega_1; % Eigenperiod in surge
```

```
% Damping
ksi=0.1; % Damping ratio assumed to be 10%

%% Solving the equation of motion
 P_0=max(Mass_force); % Load amplitude
beta=omega/omega_1; % Frequency ratio

C1=(P_0/k_1)*((1-beta.^2)./((1-beta.^2).^2+(2*ksi*beta).^2)); % constant 1
C2=(P_0/k_1)*((2*ksi*beta)./((1-beta.^2).^2+(2*ksi*beta).^2)); % constant 2

R=sqrt(C1^2+C2^2);
Teta=atan(-C2/C1);
DLF=1/sqrt((1-beta^2)^2+(2*ksi*beta^2));

u=R*sin(omega*t-Teta);
u_dot=R*cos(omega*t-Teta)*omega;
u_dot_dot=R*sin(omega*t-Teta)*-omega^2;

%% Setdown calculations in Surge
% Assuming no elongation in the tendons when the structure sets down

Setdown=length_tendon-sqrt((length_tendon^2)-(abs(u).^2));

%% Plotting mass force together with displacement, velocity and acceleration
% of construction.
subplot(2,1,1)
plot(t,u)
ylabel('Surge [m]')
title(['Motion (H = ' num2str(H) ' m ,T = '...
      num2str(T) ' s)'], 'FontSize', 12, 'FontWeight'...
     ,'bold')
subplot(2,1,2)
plot(t,Setdown*-1)
ylabel('Heave [m]')
xlabel('Time[s]')

%% Overturning moment calculation in pitch

% For-loop to calculate the point of attack for wave
for i=1:length(z)-1
   a_wave1(i,1)=(ax_constr(i,1)-((ax_constr(i,1)-ax_constr(i+1,1))...
      *(1/2)))*(z(i+1)-z(i))*(z(i+1)-((z(2)-z(1))*(1/2)));

   a_wave2(i,1)=(ax_constr(i,1)-((ax_constr(i,1)-ax_constr(i+1,1))...
      *(1/2)))*(z(i+1)-z(i));
end

% Center of gravity for the turbine included added mass (from bottom of structure)
 VCG_dry=49; % Measured vertical center of gravity from scaled model
VCG_wet=((m*VCG_dry)+(added_mass*draught/2))/(m+added_mass);
```

```
a_u_t=sqrt(3)*a/3; % Arm Upweather Tendon
a_d_t=sqrt(3)*a/6; % Arm Downweather Tendon
a_mass=VCG_wet-fastening_point; % Arm to mass from rotation point
a_wave=draught-(sum(a_wave1)/sum(a_wave2))-fastening_point; % Point of attack for wave from
rotation point

Moment=(Mass_force*a_wave)+(m_1*u_dot_dot*a_mass);

% Defining the moment from the tension legs
delta_elong2=Moment/(((E*A_tendon)/length_tendon)*(a_d_t-(2*(a_u_t^2)/a_d_t)));
delta_tension2=((E*A_tendon)/length_tendon)*delta_elong2;

delta_elong1=(a_u_t/a_d_t)*delta_elong2;
delta_tension1=((E*A_tendon)/length_tendon)*delta_elong1;

upper_limit=ones(1,length(t))*2*(Tension)*a_d_t; %2*(Tension+delta_tension2)*a_d_t;
lower_limit=ones(1,length(t))*(-Tension)*a_u_t; %(-Tension+delta_tension1)*a_u_t;

figure
subplot(2,1,1)
plot(t,Moment)
hold on
plot(t,upper_limit,'--r','linewidth',1.5)
legend('Moment from loading','Moment capacity')
hold on
plot(t,lower_limit,'--r','linewidth',1.5)
xlabel('Time [s]')
ylabel('Overturning Moment [Nm]')
ylim([(lower_limit(1)*1.25) (upper_limit(1)*1.25)])
title(['Overturning moment (H = ' num2str(H) ' m ,T = '...
      num2str(T) ' s)'], 'FontSize', 12, 'FontWeight'...
     ,'bold')

%% Eigenperiod in Heave
k_3=(n_tendons*(E*A_tendon)/length_tendon); % Stiffness in heave motion
m_3=m; % Mass in heave motion
omega_3=sqrt(k_3/m_3); % Eigenfrequency in heave
T_3=(2*pi)/omega_3; % Eigenperiod in heave

%% Eigenperiod in Roll

k_4=(2*((a/2)^2)*((E*A_tendon)/length_tendon)); % Stiffness in roll motion
m_4=(m*(VCG_dry^2))+(added_mass*((draught/2)^2)); % inertia moment in roll included added
mass
omega_4=sqrt(k_4/m_4); % Eigenfrequency in roll
T_4=(2*pi)/omega_4; % Eigenperiod in roll

%% Eigenperiod in Pitch

k_5=((a_u_t^2)*(E*A_tendon)/length_tendon)+(2*(a_d_t^2)*...
   (E*A_tendon)/length_tendon); % Stiffness in pitch motion
```

```
m_5=(m*(VCG_dry^2))+(added_mass*((draught/2)^2)); % inertia moment in pitch included added
mass
omega_5=sqrt(k_5/m_5); % Eigenfrequency in pitch
T_5=(2*pi)/omega_5; % Eigenperiod in pitch

%% Eigenperiod in Yaw
k_6=(Tension*n_tendons/length_tendon)*a;        % Stiffness in yaw
m_6=m*((o_diameter2/2)+(((o_diameter1/2)-(o_diameter2/2))/(2)))^2;      % Inertia moment in yaw
omega_6=sqrt(k_6./m_6);                  % Eigenfrequencies in yaw
T_6=(2*pi./omega_6);                % Eigenperiod in yaw

%% Calculating and plotting forces in tendons
Tendon1=(-Moment./(-a_u_t-a_d_t));
Tendon2=-Tendon1./2;
Tendon3=-Tendon1./2;

figure
subplot(2,1,1)
plot(t,Tendon1)
xlabel('Time[s]')
ylabel('Force [N]')
title(['Forces in tendons (H = ' num2str(H) ' m ,T = '...
      num2str(T) ' s)'], 'FontSize', 12, 'FontWeight'...
     ,'bold')
hold on
plot(t,Tendon2,'r')
hold on
plot(t,Tendon3,'g')
legend('Tendon1','Tendon2','Tendon3')
```

```
clc
clear
close all


%%
%-----------------------------------------------------------------
% NUMERICAL MODEL. SIXTY DEGREE HEADING
%-----------------------------------------------------------------

%% Input parameters

% Physical input parameters
rho_w=1025; % Density of sea water
rho_s=7850; % Density of steel
Cm=1; % Mass coefficient
g=9.81; %Gravity acceleration

% Input parameters for environment
h=150; % water depth
T=10; % Wave period
H=10; % Wave height

% Input parameters for body
o_diameter1=12.5; % Outer diameter of submerged coloumn
i_diameter1=12.2; % Inner diameter of submerged coloumn
o_diameter2=6; % Outer diameter of coloumn above sea level
i_diameter2=5.7; % Inner diameter of coloumn above sea level
draught=50; % Draught of coloumn
height=draught+65; % Total height of coloumn
A_cross1=(pi/4)*((o_diameter1^2)-(i_diameter1^2)); % Cross sectional area of submerged coloumn
A_cross2=(pi/4)*((o_diameter2^2)-(i_diameter2^2)); % Cross sectional area of coloumn above sea
level
B=(pi/4)*(o_diameter1^2)*draught*rho_w; % Bouancy of submerged body
a=50; % Distance between tethers (side in triangle)

% Input parameters for mooring system
n_tendons=3; % Number of tendons
D_tendon=0.5; % Tendon diameter
A_tendon=(pi/4)*D_tendon^2; % Cross-sectional area for tendon
fastening_point=draught/2; %Vertical position of fastening point (from bottom of structure)
length_tendon=h-draught+fastening_point; % Length of tendon
E=2.1e11; %Youngs modulus for steel


%% Wave- and force calculations

lamda1=(g/(2*pi))*(T^2); % Wave length

% While loop to find the wavelength corresponding to period and height
dummy=1;
```

```
while dummy>=0.01
   lamda=(g/(2*pi))*(T^2)*tanh(((2*pi)/lamda1)*h);
   dummy=abs(lamda-lamda1);
   lamda1=lamda;
end

zeta_a=H/2; % Wave amplitude
omega=(2*pi)/T; % Wave frequency
k=(2*pi)/lamda; % Wave number
Z=0:-1:-h; % Depth coordinate vector
t=0:0.25:6*T; % Time vector
ax=(omega^2)*zeta_a*(((cosh((k*Z)+(k*h))))/(sinh(k*h)))'*cos(omega*t); % Particle acceleration in
the wave over the depth
wave_profile=zeta_a*sin(omega*t);

z=0:1:draught; % Integration vector over the body
ax_constr=zeros(length(z),length(t)); %Particle acceleration in the wave over the submerged body

% For-loop to assign correct acceleration from wave to the right depth of body:
for i=1:length(z)
   for j=1:length(t)
      ax_constr(i,j)=ax(i,j);
   end
end


dF=rho_w*((1/4)*pi*o_diameter1^2)*Cm*ax_constr; %Load matrix. (Depth and time varying)

% For-loop to integrate the wave-loading over the body
for i=1:length(t)
   Mass_force(i)=trapz(z,dF(:,i));
end

%% Finding coefficients for the equation of motion

% Weight and inertia forces
weight_coloumn1=(A_cross1*(draught+5)*rho_s); %Weigth of material in submerged coloumn
weight_coloumn2=A_cross2*(height-(draught+5))*rho_s; %Weigth of material in coloumn above sea
level
weight_nacelle=138e3; % Weight of nacelle
weight_adjusted=0.75565e6; % Due to a heavier model than expected
m=weight_coloumn1+weight_coloumn2+weight_nacelle+weight_adjusted; %Structural mass
added_mass=(pi/4)*(o_diameter1^2)*draught*rho_w; %Added mass in surge. Taken as the weight
of the displaced water

% Stiffness
Tension=((B-m)/n_tendons)*g; % Tension force

% Eigenperiod in Surge
k_1=n_tendons*Tension/length_tendon; % Stiffness in surge motion
m_1=m+added_mass; % Mass in surge motion
```

```
omega_1=sqrt(k_1/m_1); % Eigenfrequency in surge
T_1=(2*pi)/omega_1; % Eigenperiod in surge


% Damping
ksi=0.1; % Damping ratio assumed to be 10%

%% Solving the equation of motion

P_0=max(Mass_force); % Load amplitude
beta=omega/omega_1; % Frequency ratio

C1=(P_0/k_1)*((1-beta.^2)./((1-beta.^2).^2+(2*ksi*beta).^2)); % constant 1
C2=(P_0/k_1)*((2*ksi*beta)./((1-beta.^2).^2+(2*ksi*beta).^2)); % constant 2

R=sqrt(C1^2+C2^2);
Teta=atan(-C2/C1);
DLF=1/sqrt((1-beta^2)^2+(2*ksi*beta^2));

u=R*sin(omega*t-Teta);
u_dot=R*cos(omega*t-Teta)*omega;
u_dot_dot=R*sin(omega*t-Teta)*-omega^2;

%% Setdown calculations in Surge
% Assuming no elongation in the tendons when the structure sets down

Setdown=length_tendon-sqrt((length_tendon^2)-(abs(u).^2));

%% Plotting mass force together with displacement, velocity and acceleration
% of construction.
subplot(2,1,1)
plot(t,u)
ylabel('Surge/Sway [m]')
title(['Motion (H = ' num2str(H) ' m ,T = '...
      num2str(T) ' s)'], 'FontSize', 12, 'FontWeight'...
     ,'bold')
subplot(2,1,2)
plot(t,Setdown*-1)
ylabel('Heave [m]')
xlabel('Time[s]')


%% Overturning moment calculation in pitch

% For-loop to calculate the point of attack for wave
for i=1:length(z)-1
   a_wave1(i,1)=(ax_constr(i,1)-((ax_constr(i,1)-ax_constr(i+1,1))...
      *(1/2)))*(z(i+1)-z(i))*(z(i+1)-((z(2)-z(1))*(1/2)));

   a_wave2(i,1)=(ax_constr(i,1)-((ax_constr(i,1)-ax_constr(i+1,1))...
      *(1/2)))*(z(i+1)-z(i));
```

```
end

% Center of gravity for the turbine included added mass (from bottom of structure)

VCG_dry=49; % Measured vertical center of gravity from scaled model
VCG_wet=((m*VCG_dry)+(added_mass*draught/2))/(m+added_mass);

a_u_t=sqrt(3)*a/3; % Arm Upweather Tendon
a_d_t=sqrt(3)*a/6; % Arm Downweather Tendon
a_mass=VCG_wet-fastening_point; % Arm to mass from rotation point
a_wave=draught-(sum(a_wave1)/sum(a_wave2))-fastening_point; % Point of attack for wave from
rotation point

Moment=(Mass_force*a_wave)+(m_1*u_dot_dot*a_mass);

% Defining the moment from the tension legs
delta_elong2=Moment/(((E*A_tendon)/length_tendon)*(a_d_t-(2*(a_u_t^2)/a_d_t)));
delta_tension2=((E*A_tendon)/length_tendon)*delta_elong2;

delta_elong1=(a_u_t/a_d_t)*delta_elong2;
delta_tension1=((E*A_tendon)/length_tendon)*delta_elong1;

upper_limit=ones(1,length(t))*2*(Tension)*a_d_t; %2*(Tension+delta_tension2)*a_d_t;
lower_limit=ones(1,length(t))*(-Tension)*a_u_t; %(-Tension+delta_tension1)*a_u_t;

figure
subplot(2,1,1)
plot(t,Moment)
hold on
plot(t,upper_limit,'--r','linewidth',1.5)
legend('Moment from loading','Moment capacity')
hold on
plot(t,lower_limit,'--r','linewidth',1.5)
xlabel('Time [s]')
ylabel('Overturning Moment [Nm]')
ylim([(lower_limit(1)*1.25) (upper_limit(1)*1.25)])
title(['Overturning moment (H = ' num2str(H) ' m ,T = '...
      num2str(T) ' s)'], 'FontSize', 12, 'FontWeight'...
     ,'bold')



%% Eigenperiod in Heave
k_3=(n_tendons*(E*A_tendon)/length_tendon); % Stiffness in heave motion
m_3=m; % Mass in heave motion
omega_3=sqrt(k_3/m_3); % Eigenfrequency in heave
T_3=(2*pi)/omega_3; % Eigenperiod in heave

%% Eigenperiod in Roll

k_4=(2*(a/2)*(E*A_tendon)/length_tendon); % Stiffness in surge motion
```

```
m_4=(m+added_mass)*a_mass^2; % inertia moment in pitch included added mass
omega_4=sqrt(k_4/m_4); % Eigenfrequency in pitch
T_4=(2*pi)/omega_4; % Eigenperiod in pitch

%% Eigenperiod in Pitch

k_5=(a_u_t*(E*A_tendon)/length_tendon)+(2*a_d_t*...
   (E*A_tendon)/length_tendon); % Stiffness in surge motion
m_5=(m+added_mass)*a_mass^2; % inertia moment in pitch included added mass
omega_5=sqrt(k_5/m_5); % Eigenfrequency in pitch
T_5=(2*pi)/omega_5; % Eigenperiod in pitch

%% Calculating and plotting forces in tendons
Tendon2=(Moment./(-a_u_t-a_d_t));
Tendon1=-Tendon2./2;
Tendon3=-Tendon2./2;

figure
subplot(2,1,1)
plot(t,Tendon1)
xlabel('Time[s]')
ylabel('Force [N]')
title(['Forces in tendons (H = ' num2str(H) ' m ,T = '...
      num2str(T) ' s)'], 'FontSize', 12, 'FontWeight'...
     ,'bold')
hold on
plot(t,Tendon2,'r')
hold on
plot(t,Tendon3,'g')
legend('Tendon1','Tendon2','Tendon3')
```

```
clc
clear
close all


%%
%-----------------------------------------------------------------
% NUMERICAL MODEL. NINETY DEGREE HEADING
%-----------------------------------------------------------------

%% Input parameters

% Physical input parameters
rho_w=1025; % Density of sea water
rho_s=7850; % Density of steel
Cm=1; % Mass coefficient
g=9.81; %Gravity acceleration

% Input parameters for environment
h=150; % water depth
T=10; % Wave period
H=10; % Wave height

% Input parameters for body
o_diameter1=12.5; % Outer diameter of submerged coloumn
i_diameter1=12.2; % Inner diameter of submerged coloumn
o_diameter2=6; % Outer diameter of coloumn above sea level
i_diameter2=5.7; % Inner diameter of coloumn above sea level
draught=50; % Draught of coloumn
height=draught+65; % Total height of coloumn
A_cross1=(pi/4)*((o_diameter1^2)-(i_diameter1^2)); % Cross sectional area of submerged coloumn
A_cross2=(pi/4)*((o_diameter2^2)-(i_diameter2^2)); % Cross sectional area of coloumn above sea
level
B=(pi/4)*(o_diameter1^2)*draught*rho_w; % Bouancy of submerged body
a=50; % Distance between tethers (side in triangle)

% Input parameters for mooring system
n_tendons=3; % Number of tendons
D_tendon=0.5; % Tendon diameter
A_tendon=(pi/4)*D_tendon^2; % Cross-sectional area for tendon
fastening_point=draught/2; %Vertical position of fastening point (from bottom of structure)
length_tendon=h-draught+fastening_point; % Length of tendon
E=2.1e11; %Youngs modulus for steel


%% Wave- and force calculations

lamda1=(g/(2*pi))*(T^2); % Wave length

% While loop to find the wavelength corresponding to period and height
dummy=1;
```

```
while dummy>=0.01
   lamda=(g/(2*pi))*(T^2)*tanh(((2*pi)/lamda1)*h);
   dummy=abs(lamda-lamda1);
   lamda1=lamda;
end

zeta_a=H/2; % Wave amplitude
omega=(2*pi)/T; % Wave frequency
k=(2*pi)/lamda; % Wave number
Z=0:-1:-h; % Depth coordinate vector
t=0:0.25:6*T; % Time vector
ax=(omega^2)*zeta_a*(((cosh((k*Z)+(k*h))))/(sinh(k*h)))'*cos(omega*t); % Particle acceleration in
the wave over the depth
wave_profile=zeta_a*sin(omega*t);

z=0:1:draught; % Integration vector over the body
ax_constr=zeros(length(z),length(t)); %Particle acceleration in the wave over the submerged body

% For-loop to assign correct acceleration from wave to the right depth of body:
for i=1:length(z)
   for j=1:length(t)
      ax_constr(i,j)=ax(i,j);
   end
end


dF=rho_w*((1/4)*pi*o_diameter1^2)*Cm*ax_constr; %Load matrix. (Depth and time varying)

% For-loop to integrate the wave-loading over the body
for i=1:length(t)
   Mass_force(i)=trapz(z,dF(:,i));
end

%% Finding coefficients for the equation of motion

% Weight and inertia forces
weight_coloumn1=(A_cross1*(draught+5)*rho_s); %Weigth of material in submerged coloumn
weight_coloumn2=A_cross2*(height-(draught+5))*rho_s; %Weigth of material in coloumn above sea
level
weight_nacelle=138e3; % Weight of nacelle
weight_adjusted=0.75565e6; % Due to a heavier model than expected
m=weight_coloumn1+weight_coloumn2+weight_nacelle+weight_adjusted; %Structural mass
added_mass=(pi/4)*(o_diameter1^2)*draught*rho_w; %Added mass in surge. Taken as the weight
of the displaced water

% Stiffness
Tension=((B-m)/n_tendons)*g; % Tension force

% Eigenperiod in Surge
k_1=n_tendons*Tension/length_tendon; % Stiffness in surge motion
m_1=m+added_mass; % Mass in surge motion
```

```
omega_1=sqrt(k_1/m_1); % Eigenfrequency in surge
T_1=(2*pi)/omega_1; % Eigenperiod in surge


% Damping
ksi=0.1; % Damping ratio assumed to be 10%

%% Solving the equation of motion

P_0=max(Mass_force); % Load amplitude
beta=omega/omega_1; % Frequency ratio

C1=(P_0/k_1)*((1-beta.^2)./((1-beta.^2).^2+(2*ksi*beta).^2)); % constant 1
C2=(P_0/k_1)*((2*ksi*beta)./((1-beta.^2).^2+(2*ksi*beta).^2)); % constant 2

R=sqrt(C1^2+C2^2);
Teta=atan(-C2/C1);
DLF=1/sqrt((1-beta^2)^2+(2*ksi*beta^2));

u=R*sin(omega*t-Teta);
u_dot=R*cos(omega*t-Teta)*omega;
u_dot_dot=R*sin(omega*t-Teta)*-omega^2;

%% Setdown calculations in Surge
% Assuming no elongation in the tendons when the structure sets down

Setdown=length_tendon-sqrt((length_tendon^2)-(abs(u).^2));

%% Plotting mass force together with displacement, velocity and acceleration
% of construction.
subplot(2,1,1)
plot(t,u)
ylabel('Sway [m]')
title(['Motion (H = ' num2str(H) ' m ,T = '...
      num2str(T) ' s)'], 'FontSize', 12, 'FontWeight'...
     ,'bold')
subplot(2,1,2)
plot(t,Setdown*-1)
ylabel('Heave [m]')
xlabel('Time[s]')


%% Overturning moment calculation in pitch

% For-loop to calculate the point of attack for wave
for i=1:length(z)-1
   a_wave1(i,1)=(ax_constr(i,1)-((ax_constr(i,1)-ax_constr(i+1,1))...
      *(1/2)))*(z(i+1)-z(i))*(z(i+1)-((z(2)-z(1))*(1/2)));

   a_wave2(i,1)=(ax_constr(i,1)-((ax_constr(i,1)-ax_constr(i+1,1))...
      *(1/2)))*(z(i+1)-z(i));
```

```
end

% Center of gravity for the turbine included added mass (from bottom of structure)
%{
VCG_dry=(((weight_nacelle*height)+(weight_coloumn1*draught/2)+...
   (weight_coloumn2*(draught+((height-draught)/2))))/(weight_nacelle+weight_coloumn1+...
   weight_coloumn2));
%}

VCG_dry=49; % Measured vertical center of gravity from scaled model
VCG_wet=((m*VCG_dry)+(added_mass*draught/2))/(m+added_mass);

a_u_t=sqrt(3)*a/3; % Arm Upweather Tendon
a_d_t=sqrt(3)*a/6; % Arm Downweather Tendon
a_mass=VCG_wet-fastening_point; % Arm to mass from rotation point
a_wave=draught-(sum(a_wave1)/sum(a_wave2))-fastening_point; % Point of attack for wave from
rotation point

Moment=(Mass_force*a_wave)+(m_1*u_dot_dot*a_mass);

% Defining the moment from the tension legs
delta_elong2=Moment/(((E*A_tendon)/length_tendon)*(a_d_t-(2*(a_u_t^2)/a_d_t)));
delta_tension2=((E*A_tendon)/length_tendon)*delta_elong2;

delta_elong1=(a_u_t/a_d_t)*delta_elong2;
delta_tension1=((E*A_tendon)/length_tendon)*delta_elong1;

upper_limit=ones(1,length(t))*(Tension)*(a/2); %2*(Tension+delta_tension2)*a_d_t;
lower_limit=ones(1,length(t))*(-Tension)*(a/2); %(-Tension+delta_tension1)*a_u_t;

figure
subplot(2,1,1)
plot(t,Moment)
hold on
plot(t,upper_limit,'--r','linewidth',1.5)
legend('Moment from loading','Moment capacity')
hold on
plot(t,lower_limit,'--r','linewidth',1.5)
xlabel('Time [s]')
ylabel('Overturning Moment [Nm]')
ylim([(lower_limit(1)*1.25) (upper_limit(1)*1.25)])
title(['Overturning moment (H = ' num2str(H) ' m ,T = '...
      num2str(T) ' s)'], 'FontSize', 12, 'FontWeight'...
     ,'bold')



%% Eigenperiod in Heave
k_3=(n_tendons*(E*A_tendon)/length_tendon); % Stiffness in heave motion
m_3=m; % Mass in heave motion
omega_3=sqrt(k_3/m_3); % Eigenfrequency in heave
```

```
T_3=(2*pi)/omega_3; % Eigenperiod in heave

%% Eigenperiod in Roll

k_4=(2*(a/2)*(E*A_tendon)/length_tendon); % Stiffness in surge motion
m_4=(m+added_mass)*a_mass^2; % inertia moment in pitch included added mass
omega_4=sqrt(k_4/m_4); % Eigenfrequency in pitch
T_4=(2*pi)/omega_4; % Eigenperiod in pitch

%% Eigenperiod in Pitch

k_5=(a_u_t*(E*A_tendon)/length_tendon)+(2*a_d_t*...
   (E*A_tendon)/length_tendon); % Stiffness in surge motion
m_5=(m+added_mass)*a_mass^2; % inertia moment in pitch included added mass
omega_5=sqrt(k_5/m_5); % Eigenfrequency in pitch
T_5=(2*pi)/omega_5; % Eigenperiod in pitch

%% Calculating and plotting forces in tendons
Tendon1=Moment*0;
Tendon2=-Moment./a;
Tendon3=-Tendon2;

figure
subplot(2,1,1)
plot(t,Tendon1)
xlabel('Time[s]')
ylabel('Force [N]')
title(['Forces in tendons (H = ' num2str(H) ' m ,T = '...
      num2str(T) ' s)'], 'FontSize', 12, 'FontWeight'...
     ,'bold')
hold on
plot(t,Tendon2,'r')
hold on
plot(t,Tendon3,'g')
legend('Tendon1','Tendon2','Tendon3')
```

Appendix B - Model test specification

Introduction

A Model test with a tension legged floating windmill is to be carried out. The full scale floating wind turbine is intended to have a 2.3 MW turbine installed.

The test is to be executed in the MC-lab at NTNU, Trondheim.

Objectives

The main purpose of the model test is to see how the design behaves in regular waves. And also reveal possible weaknesses with the mooring system for this type of construction. The results will also serve as verification of the theoretical and design analyses. Especially attention should be paid in the investigation of tendons going slack during the test, seeing that this is fatal for the design.

The objectives of the model tests with the floating windmill can be summarized as follows:

- Measure the tension in the mooring system.
- Measure global response, set down and maximum offset.
- Finding the overturning moment due to loading and compare with moment capacity.
- Finding eigenperiods for the structure in relevant degrees of freedom
- Verify numerical predictions of system global response, maximum offset, maximum set down, and moment capacity.

Model description

The model shall be constructed to a linear scale of 1:100.

The water depth in the model test is 1.5 m

The total test set up includes the following components:

- Cylindrical column without rotor
- Tension leg mooring system with adjustable vertical position

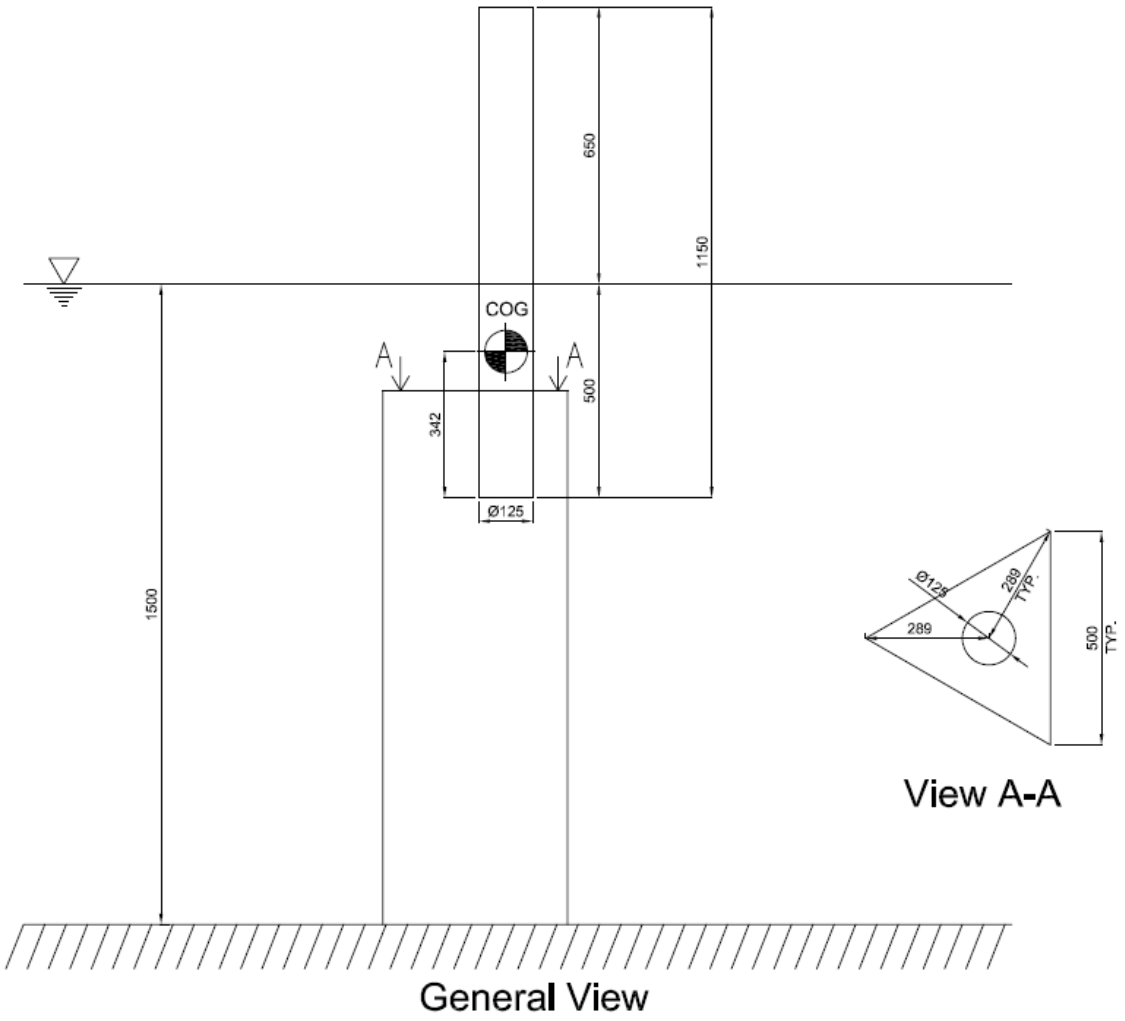

Figure 80 – Model drawing

Main data for structure

The model shall be built in accordance with the following full scale values

Parameter	Full scale value
Height above water level to center of turbine	65 m
Draught	50 m
Outer diameter of submerged body	12.5 m
Structural mass	3.95e6 kg
Buoyancy	6.29e6 kg
Vertical center of gravity (from bottom of structure)	33.5 m

The model body should be built as a uniform column with a total height of 1.15 m. Turbine and nacelle is not included in the model. However, the center of gravity is calculated with the turbine mass included.

Main data for mooring system

The mooring shall consist of 3 tension legs, organized in an equilateral triangle. The windmill column should have its center in the triangle-center-of-gravity. The pretension in each of the tendons should correspond to a full-scale tension of 7.65e6 N. The length of the tendons should be between 100 m and 150 m (The length depends on how deep the fastening point will be).

Test program

Still water tests

1. Decay test in lateral motions in order to decide natural periods for relevant degrees of freedom.
2. Heave, pitch and roll natural periods

Regular wave test

According to the information given on NTNUs home page, the wave height in the MC-lab is limited to 0.25 m. However it have been stated that in practice the maximum wave height is closer to 0.20 m. In the regular wave test, the largest waves are of most importance. Seeing that the tendons will most probable go slack in a relatively large wave compared to a small.

Waves with different heading, height and period should be carried out. In addition also draught and vertical position of tendon attachment arrangement should be varied.

If time allows, some tests with reduced water depth representing tide should be performed. A way to do this could is to decrease the water level with a level corresponding to a full scale value of for example 1 meter.

Instrumentation and data acquisition

Instrumentation

The instrumentation and measurements during the tests shall as a minimum include:

- Wave elevation at structure
- Six-degree-of-freedom motions of structure
- Forces in tension legs

Data acquisition

Data shall be sampled at a satisfactory frequency in order to observe the possible high frequency motions in pitch, roll and heave.

Appendix C - Pictures of scaled model

Column with mooring plate and motion reflectors

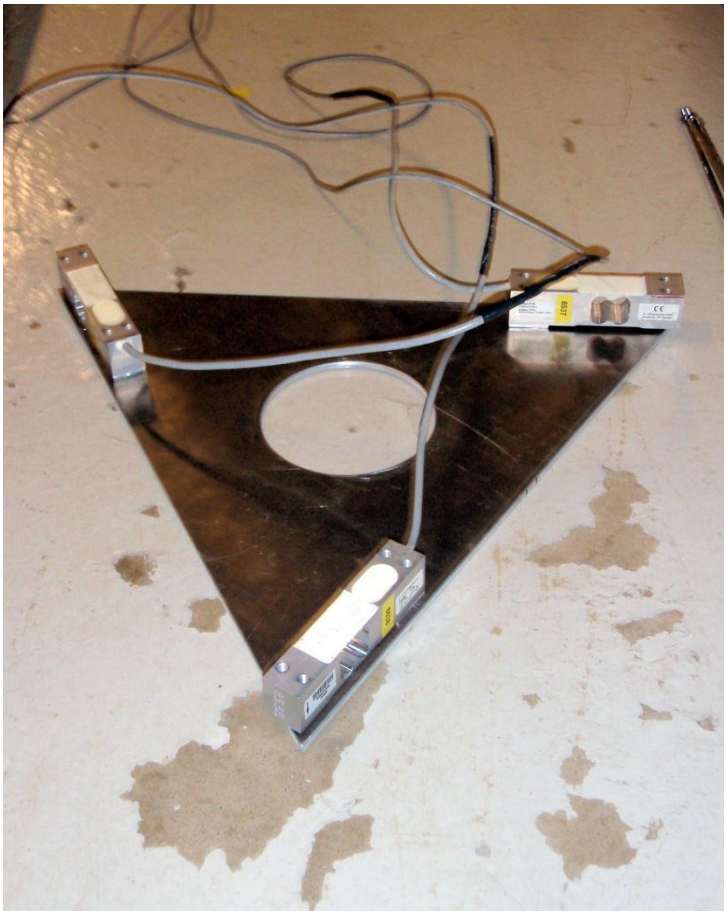

Base plate with force sensors mounted

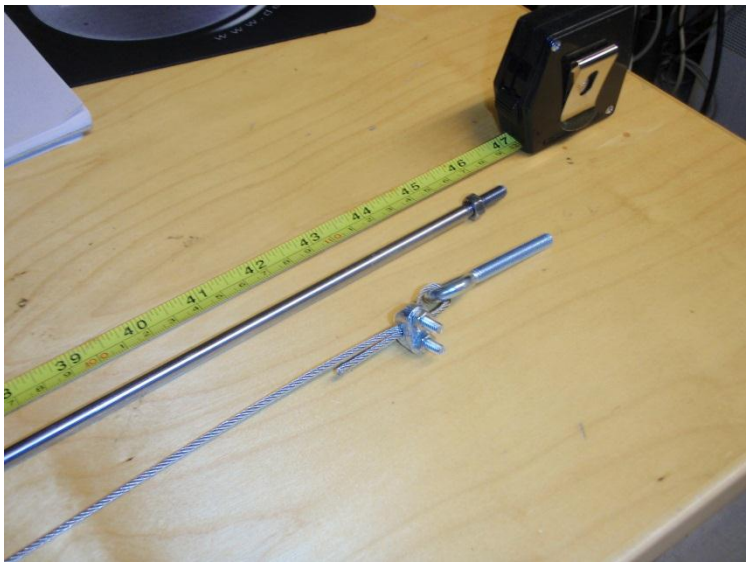

Wire tendon together with original tendon made of steel bar

Appendix D - CD

Electronic appendix is attached to the paperback and contains;

- Raw data from labarotory test
- Movie file from regular wave test
- Version of the report in .pdf - format